Novel approaches to produce radionuclides using hot atom chemistry principles

Moret, J.L.T.M.

DOI
10.4233/uuid:de78dfd6-f63b-4908-b09c-921cb7ea937e

Publication date
2020

Document Version
Final published version

Citation (APA)
Moret, J. L. T. M. (2020). *Novel approaches to produce radionuclides using hot atom chemistry principles*. [Dissertation (TU Delft), Delft University of Technology]. https://doi.org/10.4233/uuid:de78dfd6-f63b-4908-b09c-921cb7ea937e

Important note
To cite this publication, please use the final published version (if applicable).
Please check the document version above.

Novel approaches to produce radionuclides using hot atom chemistry principles

Proefschrift

Ter verkrijging van de graad van doctor
Aan de Technische Universiteit Delft,
Op gezag van de Rector Magnificus Prof. dr. ir. T.H.J.J. van der Hagen
Voorzitter van het College voor Promoties,
In het openbaar te verdedigen op
Maandag 18 mei 2020 om 15:00 uur

door

Josette Leonarda Theodora Maria MORET
Ingenieur in de (nucleaire) chemie, Technische Universiteit Delft, Nederland
Geboren te Zoetermeer, Nederland

Dit proefschrift is goedgekeurd door de promotoren.

Samenstelling promotiecommissie bestaat uit:

Rector magnificus,	Voorzitter
Prof. dr. H.T. Wolterbeek	Technische Universiteit Delft, promotor
Prof. dr. ir. J.R. van Ommen	Technische Universiteit Delft, promotor
Dr. ir. A.G. Denkova	Technische Universiteit Delft, copromotor

Onafhankelijke leden:

Prof. dr. M. Creatore	Technische Universiteit Eindhoven
Prof. dr. J.L. Kloosterman	Technische Universiteit Delft
Prof. dr. A. van de Wiel	Technische Universiteit Delft
Dr. L. Barbosa	Malincrot
Prof. dr. A. Schmidt-Ott	Technische Universiteit Delft, reserve lid

Dit onderzoek is gefinancierd door NWO-TTW en IDB Holland b.v. onder projectnummer 13306.

Keywords: ALD, hoog specifieke activiteit, nucleaire geneeskunde
Printed by: Ipskamp printing

ISBN: 978-94-6384-136-8
Een elektronische versie van dit proefschrift is verkrijgbaar op
https://repository.tudelft.nl/

Samenvatting

Radionucliden worden vaak gebruikt bij nucleair medische toepassingen. Voor een aantal ziekten is het gebruik van radionucliden de beste mogelijkheid voor diagnose of behandeling, of zelfs de enige manier. Voor deze medische toepassingen is hoog specifieke activiteit (hoge activiteit per massaeenheid) nodig. Medische radionucliden zijn over het algemeen kunstmatig geproduceerd. Ze worden geproduceerd door neutron activatie, geladen deeltjes of foton activatie of met behulp van radionuclidengeneratoren. Ziekenhuizen geven de voorkeur aan een bevoorrading 'op aanvraag'. Hiervoor kan een radionuclidegenerator uitkomst bieden. Radionuclidegeneratoren kunnen ook gebruikt worden om hoog specifieke activiteit nucliden te produceren.

Conventionele radionuclidegeneratoren zijn gebaseerd op het feit dat de moeder en dochter radionuclide verschillende elektrostatische interacties hebben met het kolom materiaal. De dochternuclide kan daardoor makkelijk van de radionuclide generator geëlueerd worden. Helaas, wanneer er gewerkt wordt met chemische identieke moeder-dochter paren (bijvoorbeeld ^{177m}Lu/^{177}Lu) zijn andere scheidingsmethodes nodig. Door gebruik te maken van 'hot atom' principes kan het mogelijk zijn deze moeder-dochter paren te scheiden. 'Hot atom' principes beschrijven de chemische effecten die optreden door nucleaire interacties of verval. Een voorbeeld van deze effecten is het breken van chemische verbindingen.

De effectieve afstand waarover deze 'hot atom' principes werken is heel erg gelimiteerd. Dit maakt het noodzakelijk hele dunne laagjes te gebruiken. Een mogelijke techniek om deze dunne laagjes aan te brengen is 'atomic layer deposition' (ALD). ALD wordt voornamelijk in de semi-conductor industrie gebruikt, maar kan door zijn veelzijdigheid ook gebruikt worden voor het maken van katalysatoren of farmaceutica. Het voordeel van ALD is dat met deze gasfase coating techniek het mogelijk is om complexe structuren van een heel dunne laag te voorzien. Deze dunne lagen zijn chemisch gebonden met het gebruikte dragermateriaal. Ook kan de hoeveelheid gedeponeerd materiaal makkelijk aangepast worden aan de toepassing doordat het ALD-proces zelflimiterend is.

In de scriptie is het gebruik van ALD voor de productie van radionucliden onderzocht. Door de veelzijdigheid van ALD kan deze techniek ook gebruikt worden voor de ontwikkeling van targets voor geladen deeltjes bestraling of verrijkingsexperimenten (hoofdstuk 2). Deze veelzijdigheid wordt geïllustreerd met een drietal casestudies, namelijk de productie van Cu-targets voor ^{64}Cu productie, de productie van ^{177}Lu met behulp van een radionuclide generator, en de productie van ^{99}Mo op drie verschillende manieren. Ook wordt beschreven hoe ALD gebruikt kan worden voor het aanpassen van de oppervlaktechemie van hoog oppervlakte deeltjes om zo hun adsorptie capaciteit voor Mo te vergroten (Hoofdstuk 3). Van de verkregen met alumina gecoate deeltjes is hun adsorptie capaciteit voor Mo bepaald en vergeleken met acid activated alumina wat in de huidige ^{99}Mo/^{99m}Tc-radionuclide generator wordt gebruikt. De adsorptiecapaciteit van de gecoate deeltjes bedraagt tweemaal die van acid activated alumina en hebben een ^{99m}Tc elutie efficiency van 55%. Verder wordt het coaten van nanodeeltjes voor de ontwikkeling van met lutetium bedekte deeltjes (hoofdstuk 4) voor een radionuclidengenerator beschreven. Het behulp van ALD kan tot 15w% Lu afgezet worden op titaanoxide deeltjes. Daarnaast heeft de gammadosis tijdens neutron activatie een invloed op de specifieke activiteit die geproduceerd kan worden (hoofdstuk 5). Door gebruik te maken van Cu(II)-phthalocyanine is aangetoond dat een verhoogde gammadosis zorgt voor meer Cu verlies en dus een lagere specifieke activiteit.

Summary

Radionuclides are often used in the field of nuclear medicine. For some deceases the use of radionuclides is the best possible care, or even the only means of diagnosis or treatment. For these medical applications high specific activity (high activity per unit of mass) is required. Commonly, medical radionuclides are man-made. They can either be produced by neutron activation, charged particle or photon activation or by means of radionuclide generator. Furthermore, hospitals prefer an 'on demand' supply. A radionuclide generator is ideal. Radionuclide generators can also be used to produce high specific activity.

Conventional radionuclide generators work with the principle that the mother and daughter radionuclide have different electrostatic interactions with the column material. This allows for easy elution of the daughter radionuclide. However, when working with chemical identical mother-daughter radionuclide pairs (e.g. ^{177m}Lu / ^{177}Lu) another separation principle is required. Utilising 'hot atom' chemical principles such a mother-daughter pairs can be separated. 'Hot atom' principles describe the chemical effects that occur due to nuclear interactions or due to decay. An example of these effects is bond rupture.

The effective range of those principles is rather limited, requiring thin layers. A possible technique to apply these thin layers is atomic layer deposition (ALD). ALD is commonly used in the semi-conductor industry, but can due to its versatility also be used in the field of catalysis or pharmaceutical. The advantage of using ALD is that this gas phase deposition technique allows for thin conformal coating of complex structured materials. Furthermore, the amount of material that can be deposited can easily be adapted to need because ALD is a self-limiting process.

In this thesis the usefulness of ALD in combination with radionuclide production is explored. Because of the versatility of ALD it can also be used to create target materials for charged particle activation and enrichment experiments (Chapter 2). This versatility is illustrated by three case studies, namely this production of targets for ^{64}Cu production, the production of ^{177}Lu by means of a radionuclide generator and the production of ^{99}Mo using three different routes. Also described is how ALD can be used to alter the surface

chemistry of high surface area materials to increase their adsorption capacity for Mo (Chapter 3). The obtained particles with an alumina coating are then tested for their adsorption capacity and compared to acid activated alumina, the current used material in ^{99}Mo/^{99m}Tc-radionuclide generators. The adsorption capacity of the obtained particles is twice that of acid activated alumina and has a ^{99m}Tc elution efficiency of 55%. Furthermore, the coating of nano-particles for the development of with Lu coated particles (Chapter 4) for the preparation of a radionuclide generator is described. ALD allows for a deposition of up to 15w% Lu. Furthermore, the gamma dose received during neutron activation has an influence on the specific activity produced (Chapter 5). Using Cu(II)-phthalocyanine as a target it is shown that an increase in gamma dose during neutron activation results in an increase in Cu release and hence a decrease in specific activity obtained.

Content

1. Introduction

Nuclear medicine

Nuclear medicine is the field of medicine that uses radionuclides for the diagnostics and treatment of patients. It accounts for over 40 million procedures annually world-wide. [1] For a number of diseases radionuclides provide the best possible or even the only way for diagnostics or treatment [2]. Commonly, the radionuclide is coupled or integrated into a larger molecule (the combination is called a radiopharmaceutical), which optimizes tumour uptake usually by recognizing certain receptors on the surface of cancer cells. In diagnostics, radionuclides provide the opportunity to non-invasively study body functions with sensitivity which can even allow detection of small metastases. In therapy, radionuclides can be used to attack metastasized tumours providing better quality of life for the patient as well as longer survival. The most common medical radionuclide is ^{99m}Tc; which is used in about 80% of all radio diagnostic procedures. Other common radionuclides include ^{18}F, ^{89}Sr, ^{125}I, ^{186}Re, ^{131}I, ^{177}Lu and ^{64}Cu [3]. In particular, the demand for ^{177}Lu is growing due to recent approval from the European Medicines Agency to use ^{177}Lu-DOTAtate in the treatment of neuroendocrine tumours [4, 5] and ^{177}Lu-PSMA in prostate cancer therapy [6]. For the application of radionuclides in diagnostics and treatment high specific activity (i.e. Becquerel per unit of mass) is required, to accumulate enough activity at the tumour necessary for a good diagnostic scan or therapeutic outcome.

Radionuclide production routes and their challenges

Commonly, medical radionuclides are man-made. They can be produced via neutron activation, by means of a radionuclide generator, or charged particle or photon activation. The majority of medical radionuclides are produced using so called nuclear research reactors. World-wide only six nuclear research reactors have the neutron flux to produce radionuclides with the medical quality required [1, 2]. This makes the medical radionuclide production fragile. Unexpected shutdowns in 2008 illustrated that a world-wide shortage of life-saving radionuclides such as ^{99m}Tc (produced by a ^{99}Mo/^{99m}Tc generator) can occur [7]. For some radionuclides, such as ^{99}Mo, alternative production methods are being developed [8, 9]. However, these methods have as disadvantage that low specific activity is obtained. To

overcome the drawback of low specific activity and to allow production of medical quality radionuclides in nuclear research reactors of lower flux, hot atom chemistry principles can be utilised. Hot atom chemistry deals with the chemical effects induced by nuclear reactions and decay [10] leading to the breaking of chemical bonds. These processes occur at the atomic level and can require strong immobilisation of the target nuclide to reduce leakage responsible for a reduction of the specific activity produced. The target nuclide can be immobilised in complexes [11, 12] or can be chemisorbed on a carrier material. In addition, the very limited range that newly produced radionuclides can travel upon effects induced by nuclear reactions or decay, require thin layers of materials. A more detailed explanation of the hot atom principles can be found in Chapter 2.

Another convenient production route is the application of radionuclide generators. These devices allow hospitals the much preferred on site and 'on demand' production of radionuclides. A radionuclide generator consists of a column material to which the mother radionuclide is immobilised. Once the daughter radionuclide is formed due to decay, the daughter can be eluted from the radionuclide generator. Commonly, the separation of mother and daughter is based on the different affinity of mother and daughter radionuclide with the column material. This way of separation is impossible when mother and daughter are chemically identical. Furthermore, high specific activity of the mother isotope is needed to load the radionuclide generator to be able to produce enough of the daughter, due to the limited capacity of the support material used in the generators. Principles of hot atom chemistry can also be used here to prepare novel radionuclide generators. In addition, improving the adsorption capacity of the column materials can provide means of utilizing low specific activity radionuclides. Also in the case of radionuclide generators processes occur on the atomic scale having limited range, therefore requiring the use of thin layers or porous substances.

Finally, the third way to produce radionuclide is by means of charged particles or photon reactions applied in accelerators or cyclotrons [2]. The targets in these cases can be gases, liquids or solids [13]. During such nuclear reactions excessive heat is produced in the target, which needs to be dissipated as efficiently as possible [14]. Especially for solid targets this can be a hurdle, and thin layers deposited on carrier materials are preferred to assure sufficient cooling [14].

Coating techniques

In all three production routes thin layers of the target elements deposited on carrier materials are beneficial. There are several techniques available to apply thin layers onto a carrier material. Examples are electroplating, wet chemistry methods such as spin coating or dipping and gas phase coating methods like chemical vapour deposition or atomic layer deposition. Electroplating is used in the preparation of cyclotron targets [13], while gas phase coating techniques are used in the semi-conductor industry [15]. Electroplating uses a current to apply a microns thick layer onto carrier s. In order for electroplating to work, the carrier material must be able to conduct electrons. Often strong acids and bases are used to make the electrolyte solution that is used to coat the carrier material [16]. Spin coating is the process in which wafers are coated with a uniform layer by spinning the wafer around. The layer thickness depends on the viscosity of the coating precursor, rotation speed and fume exhaust. The coating is in this case physiosorbed to the wafer. On the other hand, gas phase coating techniques such as atomic layer deposition (ALD) can both be used to coat wafers and particles and allows for the deposition of atomically thin conformal chemisorbed coatings, what is much wanted to be able to utilise for instance hot atom chemistry principles. Due to the nature of the ALD process complex structures and large surface areas can be coated and the amount of material deposited can be tuned. [15] Choosing the carrier material wisely will also allow for use as cyclotron targets and column material for radionuclide generators. A more detailed explanation of the ALD process can be found in Chapters 2 and 4.

Motivation

The main research objective of this thesis is to investigate novel approaches for the production of medically relevant radionuclides having high specific activity. In general, these new approaches require thin layers to be deposited on high surface area materials, providing stability as well as sufficient yield. Therefore, we focus on exploiting the potential of thin layers produced by ALD, particular in radionuclide generator driven production. Another important aspect in achieving radionuclide production based on hot atom principles is the optimal radiation field, i.e. the harsh environment in a nuclear reactor can destroy the target material making it impossible to extract the

desired radionuclide. Therefore, a small part of this work investigates the influence of irradiation conditions on the production of radionuclides making use of simple metal complexes.

Thesis outline

Chapter 2 illustrates how ALD and hot atom chemistry can benefit from each other, shown by an overview and three case studies. One of the case studies – an example where ALD can aid in the production of novel sorbent materials to be applied in ^{99}Mo/^{99m}Tc generator – is more thoroughly explored in Chapter 3. In Chapter 4, the preparation of thin layers of Lu on a carrier material using ALD, necessary for the development of a ^{177m}Lu/^{177g}Lu generator, is described. In Chapter 5, the influence of the irradiation conditions on the quality of the produced radionuclides is explored, using Cu -phthalocyanine as a model substance.

References

[1] W.N. Association, Radioisotopes in medicine, http://www.world-nuclear.org/info/non-power-nuclear-applications/radioisotopes/radioisotopes-in-medicine/, Accessed on 24 february 2015

[2] L.P. Roobol, A.v.d. Reijden, I.R. de Waard - Schaik, H. Bijwaard, Productie en gebruik van medische radio-isotopen in Nederland. Huidige situatie en toekomstverkenning, RIVM Rapport 2017-0063

[3] S. Carlson, A Glance At The History Of Nuclear Medicine, Acta Oncologica 34 (2009) 1095-1102.

[4] E.M. Agency, EPAR summary for the public: Luthetra, EMA/524726/2017

[5] B.L. Kam, J.J. Teunissen, E.P. Krenning, W.W. de Herder, S. Khan, E.I. van Vliet, D.J. Kwekkeboom, Lutetium-labelled peptides for therapy of neuroendocrine tumours, European journal of nuclear medicine and molecular imaging 39 Suppl 1 (2012) S103-112.

[6] L. Emmett, K. Willowson, J. Violet, J. Shin, A. Blanksby, J. Lee, Lutetium (177) PSMA radionuclide therapy for men with prostate cancer: a review of the current literature and discussion of practical aspects of therapy, Journal of Medical Radiation and Science 64 (2017) 52-60.

[7] IAEA, Non-HEU production technologies for molybdenum-99 and technetium-99m, IAEA, Vienna, Austria, 2013.

[8] IAEA, Alternative technologies for ^{99m}Tc generators, International atomic energy agency, Vienna, Austria, 1995.

[9] B.S. Tomar, O.M. Steinebach, B.E. Terpstra, P. Bode, H.T. Wolterbeek, Studies on production of high specific activity ^{99}Mo and ^{90}Y by Szilard Chalmers reaction, Radiochimica Acta 98 (2010) 499-506.

[10] H.K. Yoshihara, T. Sekine, Hot Atom Chemistry, Handbook of nuclear chemistry 2011, pp. 1333-1378.

[11] R. Bhardwaj, A. van der Meer, S.K. Das, M. de Bruin, J. Gascon, H.T. Wolterbeek, A.G. Denkova, P. Serra-Crespo, Separation of nuclear isomers for cancer therapeutic radionuclides based on nuclear decay after-effects, Scientific reports 7 (2017) 44242.

[12] J.W.J. van Dorp, D.S. Mahes, P. Bode, H.T. Wolterbeek, A.G. Denkova, P. Serra-Crespo, Towards the production of carrier-free $^{(99)}$Mo by neutron activation of $^{(98)}$Mo in molybdenum hexacarbonyl -Szilard-Chalmers enrichment, Applied Radiation and Isotopes 140 (2018) 138-145.
[13] W. VAALBURG, G. VAN HERK, A.M.J. PAANS, M.G. WOLDRING, Cyclotron Production Of Radioisotopes for use in Nuclear Medicine, Journal of Radioanaltical Chemistry 35 (1977) 31-35.
[14] H. Skliarova, S. Cisternino, G. Cicoria, M. Marengo, V. Palmieri, Innovative Target for Production of Technetium-99m by Biomedical Cyclotron, Molecules 24 (2018).
[15] V. Miikkulainen, M. Leskelä, M. Ritala, R.L. Puurunen, Crystallinity of inorganic films grown by atomic layer deposition: overview and general trends, Applied Physics Reviews 113 (2013).
[16] H.F. Valdovinos, R. Hernandez, S. Graves, P.A. Ellison, T.E. Barnhart, C.P. Theuer, J.W. Engle, W. Cai, R.J. Nickles, Cyclotron production and radiochemical separation of $^{(55)}$Co and $^{(58m)}$Co from $^{(54)}$Fe, $^{(58)}$Ni and $^{(57)}$Fe targets, Applied radiation and isotopes : including data, instrumentation and methods for use in agriculture, industry and medicine 130 (2017) 90-101.

2. Atomic Layer Deposition for the Production of Medical Radionuclides[1]

Abstract

Radionuclides play an important role in nuclear medicine: they find applications in diagnostics of various diseases as well as in treatment of many types of cancer. Typically, medical radionuclides are man-made, using nuclear reactors, accelerators or radionuclide generators. Depending on the production route, special targets are required allowing the production of radionuclides having high specific activity (i.e. activity per unit of mass), an important requirement for medical applications. The nuclear effects induced by these production processes happen on the atomic level and have a short effective range. Therefore, the use of atomically thin layers is beneficial. Atomic layer deposition (ALD) is a technique that can be applied to obtain targets where (atomically) thin layers of the desired nuclide are deposited. In this paper we show how ALD can be used in the production of radionuclides by discussing three different cases, namely the production of ^{64}Cu utilizing nuclear reactor targets, the production of ^{177}Lu by a radionuclide generator and the production of ^{99}Mo using the three production routes.

Keywords: ALD, radiochemistry, nuclear medicine, medical radionuclides, ^{177}Lu, ^{64}Cu, ^{99}Mo/^{99m}Tc

[1] This chapter is under review by Radiochemistry. Authors: J.L.T.M. Moret, J.R. van Ommen, H.T. Wolterbeek, A.G. Denkova

Introduction

Nuclear medicine is the field of medicine that uses radionuclide containing compounds called radiopharmaceuticals for diagnostics or treatment [1]. The use of radionuclides in nuclear medicine is not new. The first procedures were already performed in the 1930s where ^{32}P was applied in the treatment of haematological disease [2]. The use of radionuclides has since expanded, including the application of ^{131}I for the treatment of hyperthyroidism, which is still the preferred therapy of this disease today [3]. However, far out the most nuclear medical procedures are diagnostic of nature [4]. The advantages of using radiopharmaceuticals include non-invasive use, exploring bodily functions, detecting anomalies that otherwise would have been missed (e.g. metastases) and enabling targeted therapy.

The most common radionuclide used is ^{99m}Tc [5], which is applied in around 80% of the annual use of radiopharmaceuticals worldwide [1, 6]. Due to the versatile chemistry of Tc it can be incorporated in many tracer compounds. The wide spread use of ^{99m}Tc is due to its emission of a gamma photon of low energy that can be easily detected outside the body, a good half-life (6h) and the production via a radionuclide generator. While in diagnostics a few radionuclides are most often used (i.e. ^{99m}Tc and ^{18}F), in therapy different radioisotopes are applied depending on the tumour characteristics, such as ^{177}Lu, ^{64}Cu, ^{166}Ho, ^{153}Sm and ^{131}I [1, 7, 8]. The use of therapeutic radionuclides is only expected to grow [4], in particular the demand of ^{177}Lu is increasing fast, since the recent approval of the Food and Drug Administration (FDA) and European medicines agency (EMA) [9] has been granted for the application of ^{177}Lu-DOTAoctreotate in the treatment of neuroendocrine tumours.

Medical radionuclides are typically manmade [10], either by nuclear reactors, cyclotrons or radionuclide generators, each having their specific pros and cons. Nuclear reactors use neutrons for irradiation of targets and allow for a wide range of radionuclides, mostly for therapy, to be produced. However, there are only a small number of nuclear research reactors worldwide that have sufficiently high neutron flux to produce the quality and quantity needed of the medical radionuclides [1]. The dependence on only six reactors makes the supply unreliable. In some cases, such as ^{32}P, where the radionuclide is used as a last resort in patient therapy, no alternative treatments are possible [4]. Therefore, ensuring patient therapy the whole production chain should be secured, from mining of uranium, via the exploitation of nuclear reactors to the administration of the drugs [11]. Cyclotrons also allow for a variety of

radionuclides that can be produced, but usually require more complicated targets [12]. Especially, when solid targets are used, transfer of heat can be the limiting factor of producing sufficiently high specific activity and amount of activity [13]. Also, radionuclide generators can be used for the production of radionuclides. A radionuclide generator is a device in which the mother radionuclide is immobilised, which when decays leads to the formation of the desired daughter radionuclide. The daughter can then be eluted from the immobilised material provided that the mother stays attached. Most radionuclide generators work on the principle that the electrostatic interactions of mother and daughter with the column material differ; this has been so far applied for chemically different mothers and daughters like in the ^{99}Mo/^{99m}Tc radionuclide generator [5]. Radionuclide generators allow for on-site and on-demand production of radionuclides with an as high as possible specific activity (i.e. high activity per unit of mass), which is preferred by hospitals [14]. However, unwanted breakthrough of the mother or column material can occur which limits the life of such a device [1, 15, 16]. In addition, a radionuclide generator is available for just a few radionuclides.

To increase the reliability of man-made radionuclides hot atom chemistry principles can be used. Hot atom chemistry deals with the effects induced by particle (or photon) activation or decay [15] and can cause chemical bonds to break (radiochemical effects). Applying such radiochemical effects to produce neutron activation (medical) radionuclides means that production can be carried out in more reactor facilities around the world, while maintaining the quantity and quality needed even when only low neutron fluxes are available. Hot atom principles also allow to design radionuclide generators able to separate chemical identical mother and daughter radionuclides. The nature of these radiochemical effects is such that they occur at the atomic level and have limited range. Therefore, atomically thin layers are beneficial. In the production of radionuclides using charged particles and solid targets thin layers are also helpful, as they ensure better heat dissipation. One of the most promising techniques to obtain such thin layers is atomic layer deposition (ALD).

In this paper, we aim to show that atomic layer deposition can be of use in multiple ways in the production of medical radionuclides. We will provide some first experimental incentives for the application of ALD in an alternative method for copper-64 production, we will show how it can facilitate the production of a lutetium-177 radionuclide generator illustrated by some initial

experiments, and we will finally describe how ALD can be applied in depositing Mo films that can be utilized to produce molybdenum-99 based on hot atom chemistry principles. We will show this by first explaining hot atom chemistry principles and atomic layer deposition, after which their combined potential in the production of medical radionuclides is given. This potential is illustrated by the three case studies.

Hot atom chemistry

The term 'hot atom' is used to describe atoms (or nuclei) that have high kinetic energy. Hot atom chemistry refers to chemical effects that occur due to radioactive decay and particle (photon) activation, which will often lead to the breaking of chemical bonds [15]. Bond rupture can therefore be caused either by decay (delayed effects) or during activation (prompt effects). The Szilard-Chalmers effect is a specific form of bond rupture effect caused by prompt gamma emission during neutron irradiation [15]. These bond rupture effects can be utilised for the production of (medical) radionuclides. For instance, to produce high(er) specific activity or separate mother and daughter radionuclides from each other where conventional separation principles will not work (i.e. chemically alike radionuclides.)

Delayed effects

A radionuclide can either decay by alpha-, beta minus-, beta plus- emission, electron capture or internal conversion. These forms of decay are often followed by gamma ray emission [17]. During the radioactive decay energy is released. Because of conservation of momentum, this energy is shared between the formed daughter nuclide and the emitted particle [16]. The energy that the daughter receives depends on the energy of the emitted particle and can be calculated with the following equations depending on the emitted particle:

$$E_R = \frac{M_\alpha E_\alpha}{M_R} \qquad [1]$$

$$E_R = 537\frac{\bar{E}_\beta\left(1.02 + \bar{E}_\beta\right)}{M_R} \qquad [2]$$

$$E_R = 537\frac{\left(E_\gamma\right)^2}{M_R} \qquad [3]$$

in which E_R is the recoil energy given to the daughter nuclide in eV, E_γ the energy of the emitted gamma in MeV, M_α the mass of the alpha particle in u, M_R the mass of the recoiling atom in u, $\bar{E}_\beta$ the average energy of the beta particle in MeV and E_α the energy of the emitted alpha particle in eV. Equation 1 is used to calculate the recoil energy of alpha decay, Equation 2 is applied to calculate the recoil energy of both beta minus and beta plus decay, and Equation 3 shows how to calculate the recoil energy of a nucleus emitting a gamma photon. If the recoil energy of the daughter nuclide is more than the energy of the chemical bond, it will cause its release. The recoil energy of alpha emitting radionuclides is always large enough to break chemical bonds [18], while the recoil energy for delayed gamma emission is usually not. However, even nuclei that decay by internal conversion can undergo bond rupture. When a radionuclide decays via internal conversion the surplus energy of the nucleus that is emitted kicks out an inner shell electron. The vacancy that it leaves is filled with an electron from an outer shell. The energy released in this reaction kicks out more electrons, the so-called Auger electrons. This whole cascade leaves a nuclide that has lost valence electrons and hence might be freed from its chemical bond. Due to the fact that such an atom can be highly ionized Coulomb repulsion will also assist separating of the recoil atom from its environment [15, 19, 20] (Figure 1). This effect has been observed for ^{80m}Br/^{80}Br [21] and more recently for ^{177m}Lu/^{177}Lu [22].

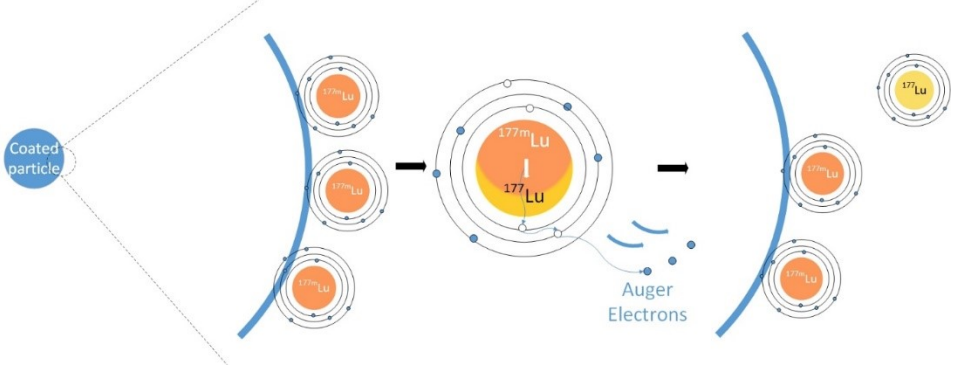

Figure 1: Graphical representation of bond rupture due to internal conversion. Upon decay an inner shell electron is kicked out. The vacancy that it leaves is filled with an electron from an outer shell. The energy that is released kicks out more electrons resulting in an Auger electron cascade. Eventually it leaves a nucleus that lost valence electrons leading often to bond rupture.

Prompt effects: Szilard-Chalmers effect

The breaking of chemical bonds can also happen during neutron activation and is a tool that can be used to produce higher specific activity of radionuclides allowing in this way for radionuclides to be produced in more nuclear reactors worldwide (i.e. nuclear reactors with low neutron flux). The first to observe this enrichment phenomenon were Szilard and Chalmers in 1934 [23]. They showed that they could collect radioactive iodine separate from the bulk of ethyl-iodine irradiated with neutrons, due to the chemical difference between the ethyl-iodine bulk and the radioactive iodine ion The emission of the prompt gamma upon neutron activation causes the nucleus to recoil according to the law of momentum conservation giving the produced atom certain amount of energy (see Equation 3). If this recoil energy is larger than the chemical bond energy (i.e. larger then 6-10 eV [18, 24]), the newly formed radionuclide will be released and if it has different chemical form than the target it often can be selectively collected. The Szilard-Chalmers effect has for instance been used to produce ^{64}Cu [25], ^{166}Ho [26], and other radioisotopes in the lanthanide series [27].

Atomic layer deposition

A possible technique to create new target or column materials is Atomic layer deposition (ALD). This is a gas phase coating technique, commonly used in the semi-conductor industry, but also finding applications in other fields such as catalysis [28], pharmaceuticals [29] and others. ALD has a number of advantages. Firstly, due to the self-limiting behaviour of ALD single layers of material can be deposited on the carrier. These single layers enable efficient escape of the product radionuclides. Secondly, ALD can be applied to obtain a uniform coating on large and/or irregular shaped surfaces. This permits easy coating of porous materials (good heat dissipation) or nano-particles (materials that can be potentially used in radionuclide generators). Thirdly, the deposited layer is chemisorbed onto the carrier material. Choosing the layer composition wisely, this allows for very stable coatings. Lastly, ALD is a process that can easily be scaled up, allowing industrial scale production of the target and or column materials.

Due to the covalent binding of the applied thin layer to the substrate material, the formed layer allows for hot atom chemistry principles to be utilised. As the precursors are in the gas phase, they can surround the substrate completely and permit uniform coating even of irregularly shaped substrates. While in the

semi-conductor industry this is ideal to coat wafers with trenches [30], this property also enables coating of particles [31] in fluidised bed reactors. In fluidised bed reactors the substrate particles are suspended in an upward gas flow behaving as if they are a liquid. Fluidised bed reactors are known for their excellent heat distribution. Moreover, they can also be operated at large scale [32, 33] and using a fluidised bed reactor for ALD processes facilitates the coating of particles with a large specific surface area [34, 35]. Due to the many choices of precursors a wide range of target materials or column materials can be synthesised. By selecting the appropriate co-reactant insoluble layers can be synthesised.

Typical ALD process

A typical ALD cycle consists of four steps. Step one is the exposure of the substrate to the first precursor enabling the first half-reaction, after which the system is purged in the second step to remove by-products and unreacted precursor. The third step is the exposure of the substrate to the co-reactant enabling the second half-reaction; again the system is purged in step four [30, 36]. As carrier and purge gas typically nitrogen is used (Figure 2). By applying multiple cycles the amount of material deposited can be tuned.

ALD differs from other deposition techniques by the self-limiting effect of the two half reactions. However, this self-limiting effect only occurs over a certain temperature range: the ALD-window [37]. Outside this ALD-window the self-limiting effect is not present. At too low reactor temperatures either precursor condensation or slow reaction kinetics can occur, while at too high reactor temperature thermal decomposition or rapid desorption of the precursor takes place (Figure 3).

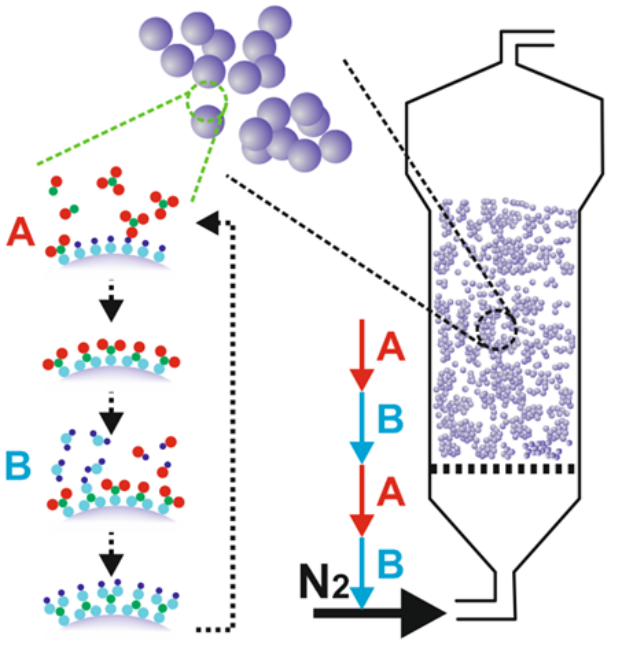

Figure 2 Schematic representation of the ALD process in a fluidised bed reactor. The substrate particles are suspended in a gas flow from below. A) Chemisorption of first precursor, followed by a purge. B) Chemisorption of co-reactant followed by a purge [31]. This represents one ALD cycle. Multiple cycles can be applied to tune the amount of material deposited.

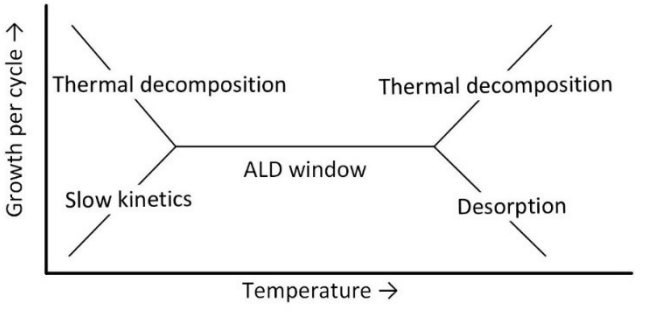

Figure 3: Graphical representation of the ALD-window as function of temperature.

Precursors and co-reactants

The precursors and co-reactants used for ALD have to be volatile to be able to get them in the vapour phase and transported to the reactor chamber. Furthermore, they have to be able to react irreversibly with the substrate surface. Also, the reaction products formed should be non-corrosive and non-

toxic [38]. However, this is not always possible and compromises have to be made.

A commonly used ALD-precursor is trimethylaluminum (TMA). This is a liquid precursor with a high vapour pressure that will react readily with the OH- or other surface groups of the used substrate. However, TMA reacts violently when coming in contact with moisture or oxygen; special care must be taken when using this precursor. Solid precursors, for example $Lu(TMHD)_3$, have a low vapour pressure. Elevated temperatures are needed to get them into the vapour phase, but too high temperatures have to be avoided to prevent decomposition of the precursor.

Depending on the precursor and the substrate either a full film or islands can be deposited on the substrate (Figure 4). The first few cycles applied to the substrate will never give a full layer, due to steric hindrance of the ligands of the precursor and or a limited number of binding sites on the surface of the substrate [36]. In case of film growth, in later cycles the holes in the coat are filled up. By contrast, in case of island growth a full coat is never formed, due to several processes including diffusion and aggregation of single atoms and diffusion and coalescence of deposited clusters. Island growth is most prominent when depositing noble metals on oxide substrates [39].

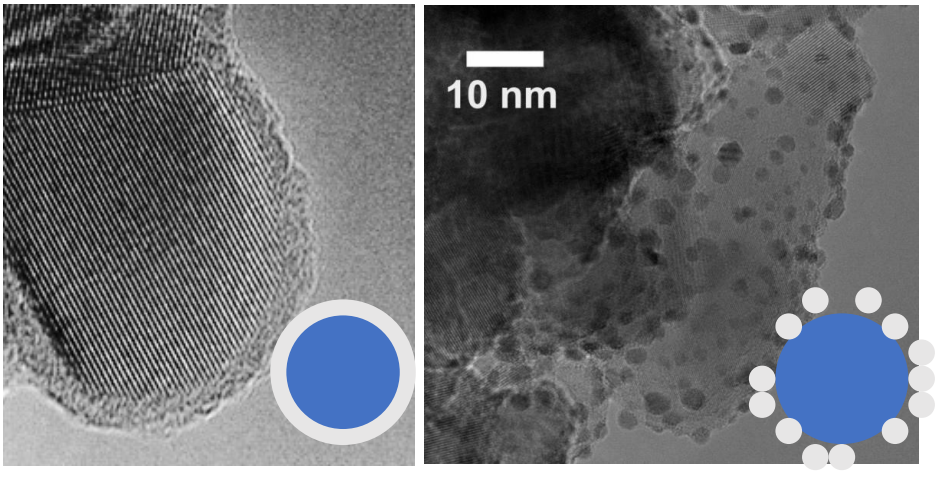

Figure 4: A) Example of a full layer: titanium oxide with an aluminium oxide layer of ~3nm, B) Example of island growth: titanium oxide nanoparticle with platinum clusters of ~2nm.

Possible nuclear medical radionuclides by ALD

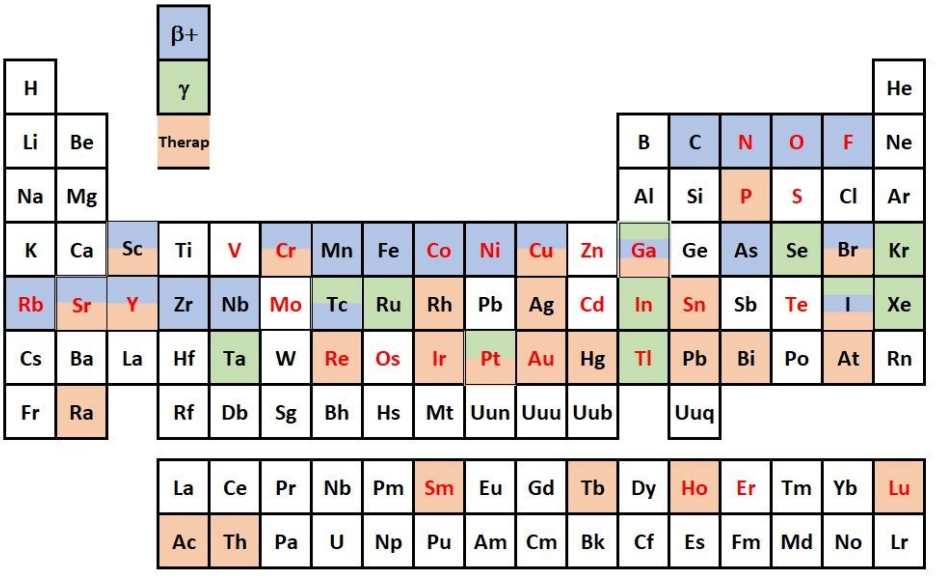

Figure 5: Periodic table containing the various elements that have medical relevant isotopes (coloured surfaces). The target elements that can be deposited using ALD are made red. Partly based on information compiled from [2, 4, 30, 40-43]

Figure 5 shows the target elements that can be deposited using ALD in the production of medical radionuclides by neutron activation and charged particle activation, respectively. More elements can be deposited using ALD [30, 41], however, those do not have medical relevant radionuclides and are therefore not shown in the figures. Some radionuclides are only relevant to function as mother radionuclide in radionuclide generators. Especially for neutron activation or radionuclide generator produced radionuclides, the required specific activity can only be achieved when no additional mass leaks from the target or column material. Therefore, for the deposited materials to be useful in the production of radionuclides, the deposited layers must be insoluble. Nitrides and fluorides are often insoluble and would be preferred compounds [44].

Case study: Copper

The trace element copper is important in several biological processes such as angiogenesis [45]. An excess of copper leads to Wilson's disease, while a deficiency leads to Menke's disease, both degenerative brain disorders. Furthermore Cu is suspected of being involved in amyloid precipitation in

Alzheimer's disease [45]. The radioisotope ^{64}Cu allows studying these biological processes [46] as well as diagnosing several types of cancer [47].

^{64}Cu can be produced using a cyclotron according to $^{63}Ni(p,n)^{64}Cu$ reaction [48] or nuclear reactors according to $^{63}Zn(n,p)^{64}Cu$ and $^{63}Cu(n,\gamma)^{64}Cu$ reactions. When irradiating copper targets with neutrons the specific activity of ^{64}Cu is usually low. However, high specific activity ^{64}Cu can be produced when utilising hot atom chemistry effects to achieve bond rupture. In order to obtain the high specific activity the non-activated Cu should remain in the bulk, while the recoiled Cu is collected. Thin copper containing layers deposited using ALD could be applied. ^{64}Cu emits several energetic prompt gammas [49] upon neutron capture, making it a very good candidate to be produced using the Szilard-Chalmers enrichment process. Commonly copper oxides are deposited with ALD. The energy of the chemical bond of Cu-O is approximately 6 eV [18], meaning that a prompt gamma energy of 900 keV is enough to break the bond (Equation 3). This theoretically leads to an activity yield of 60.7 % and a specific activity of $1.4 * 10^4$ GBq/mg.

Thin layers of a copper compound can be deposited using atomic layer deposition. Commonly copper β-dictonates are used as precursor for copper ALD [30, 41]. The advantage of using ALD is that it allows for deposition of conformal layers which are chemisorbed to the carrier material. However, the applied layer should remain undissolved, as the example will show.

We deposited a copper oxide layer on TiO_2 P25 particles using Cu(hfac) as a precursor, and H_2O as a co-reactant. The amount of Cu deposited on the particles was 4.12 w%, as determined by ICP-OES. XPS showed that the deposited Cu is Cu(II). The stability of the as deposited CuO_x on TiO_2 particles was determined in four different inorganic solvents (MilliQ, 0.9 w% NaCl, 10^{-5}M HCl and 10^{-5} M NaOH) and one organic solvent (DHE with 0.1M DEHPA). In addition, the Cu coated particles were annealed and their stability was determined in MilliQ.

The Cu loss is determined relative to the amount of Cu that was originally present on the particles. For all solvents tested the copper loss is relatively high, especially when dihexylether is used (Figure 6). This high Cu loss makes the CuO_x on TiO_2 particles not usable for enrichment purposes where only negligible Cu losses can be tolerated. The Cu on the particles is most likely Cu^{2+}, due to oxidation of the surface. Cu(II)O is less stable in water then $Cu(I)_2O$ [44]. Therefore, the remaining of the CuO_x on TiO_2 particles were

annealed in H_2 at 300°C for 1h to reduce the Cu on the particles and the stability of the particles was determined again. Unfortunately, the stability of the particles remained poor (Figure 6). This finding agrees with the XPS results, showing that the Cu remained Cu(II)O, hence the reduction did not work. Therefore, these particles are unsuitable for use for enrichment purposes. A possible solution would be to prepare Cu-particles with a Cu nitride layer, which is insoluble in water [44]. The deposition of copper nitride layers has been reported in literature by for instance Z. Li et al [50] who used copper(I) N,N'-di-sec-butylacetamidinate vapor as precursor and ammonia as co-reactant.

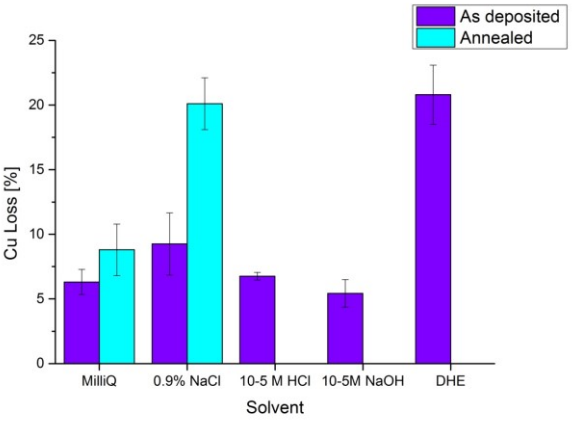

Figure 6: Relative Cu loss from the CuOx on TiO2 particles as deposited and annealed for the different solvents tested. Error bares are based on n=3

Case study: Lutetium radionuclide generator

Lutetium-177 (^{177}Lu) is a radionuclide of growing importance in the field of nuclear medicine. With a half-life of 6.7 days and emitting both a β^- (E_{max} = 0.5MeV) and low energetic γ (113 and 208 keV) [51], ^{177}Lu is ideal for the treatment and diagnostics of various cancers. Already in 2001, Breeman et al. [52] started their pioneer work on the use of somatostatin analogues, such as octreotate, in combination with ^{177}Lu for peptide receptor radionuclide therapy (PRRT) for the treatment of (metastasised) tumours. In September 2017, the European Medicines Agency (EMA) approved using ^{177}Lu-DOTAoctreotate as a radiopharmaceutical [9]. Furthermore, the use of ^{177}Lu in combination with prostate-specific membrane antigen (^{177}Lu-PSMA) is being explored for the treatment of prostate cancer [53]. For these treatments high specific activity ^{177}Lu is needed. ^{177}Lu is currently mostly produced by neutron

activation of enriched ^{176}Lu targets [54]. However, during neutron activation co-currently meta stable lutetium-177 (^{177m}Lu) is produced. ^{177m}Lu has a half-life of 160.4 days [51], resulting in a potential waste problem for its users, due to this long lived contamination. It is impossible to separate ^{177m}Lu from ^{177}Lu using conventional separation methods as ^{177}Lu and ^{177m}Lu are physically and chemically alike. Furthermore, hospitals prefer an on-demand supply and therefore would like to have a radionuclide generator. In 2012 DeVries and Wolterbeek [55] proposed a method in which ^{177m}Lu is used to produce ^{177}Lu. Bhardwaj et al. [22] showed in their work that separation of ^{177}Lu from ^{177m}Lu using chelators and hot atom chemical principles is possible. It is important to note that the quality of the produced ^{177}Lu strongly depends on the stability of the Lu bond with the chelator or carrier material on which it is immobilised. Furthermore, the hot atom chemical principles are only effective over a short range. As ALD can apply thin, covalently bonded layers to the carrier material, it is an ideal technique to make Lu-containing particles for radionuclide production purposes.

Theoretical approach and stability

For a radionuclide generator to be able to provide one patient dose of ^{177}Lu a day (7.4 GBq [56]), 32 w% of Lu should be deposited on the carrier material using ALD. It is assumed that natural Lu is used for the coating, the elution efficiency of the radionuclide generator is 80%, the radionuclide contains 2 g of column material and that the particles are activated with a thermal neutron flux of $1*10^{18}$ n/m²s for 30 days. If now the assumption is made that the Lu-layer deposited is insoluble the specific activity produced will be the theoretical maximum SA, namely 4100 GBq/mg. However, a completely insoluble layer is unlikely due to molecular interactions, but for the radionuclide generator to compete with the current nuclear reactor produced benchmark (500 GBq/mg [57]) a Lu loss of maximum 0.002% can be tolerated.

To determine whether these theoretical expectations can be met, we deposited lutetium oxide on TiO_2 particles using $Lu(TMHD)_3$ as precursor and ozone as co-reactant [58]. The obtained particles are shown in Figure 7. The stability of the Lu particles is crucial for the final product quality. Hence, the stability of Lu_2O_3 on TiO_2 particles prepared by ALD is determined by suspending the particles in different solvents and measuring the Lu concentration in the solvent by ICP-OES. The Lu concentration in the solvent is a measure for the stability of the particles and can be used to calculate the percentage of Lu loss from the particles. Lu losses up to 3.1 % are observed for

solvent contact times up to half an hour (data not published). Unfortunately, this low stability makes Lu_2O_3 on TiO_2 particles unfit to be used in radionuclide generators. However, particles suited with an insoluble layer, like for instance LuN, still hold a promise.

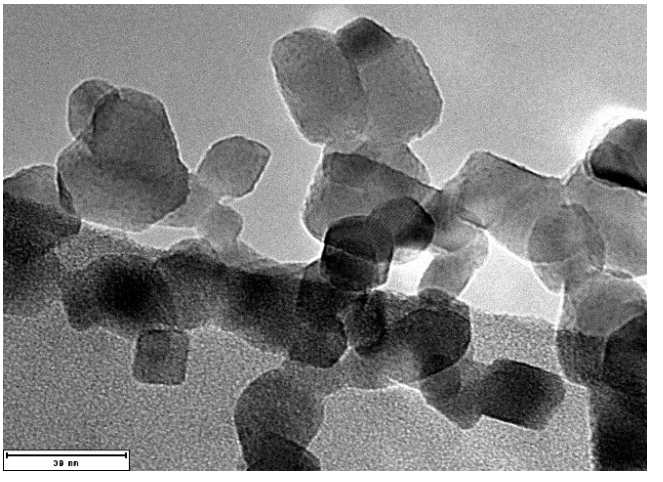

Figure 7: TEM image of P25 coated with lutetium oxide. 13 w% of lutetium was deposited on the particles.

Szilard-Chalmers enrichment using Lu_2O_3 on TiO_2 particles

The particles can theoretically also be used for Szilard-Chalmers enrichment of ^{177}Lu. The bond energy of a Lu-O bond is 7.2 eV. Using Equation 3 it is calculated that a prompt gamma of 1407 keV is needed to break this bond. The $^{176}Lu(n,\gamma)^{177}Lu$ reaction has 5% of its emitted prompt gammas with an energy higher than 1407 keV. To this extent Lu_2O_3 on TiO_2 particles prepared by ALD were irradiated with neutrons at the Hoger Onderwijs Reactor (HOR) TU Delft. The activated particles were then washed with water to remove the recoiled ^{177}Lu and to determine the yield and the enrichment factor. Unfortunately, the theoretical maximum yield was never reached. The maximum yield was 2.5% with an enrichment factor of 300 when water was used as solvent. When higher yields were observed, the Lu loss was significantly higher, indicating that the Lu coating had dissolved, and no enrichment was observed. All in all, this indicates that the use of these particles is only feasible when an insoluble layer is provided, as mentioned in the other examples. This will be the topic of future research.

Case study: Molybdenum

^{99}Mo is the parent isotope of ^{99m}Tc, the most commonly used medical isotope [59]. Historically, the most common method of production of ^{99}Mo is by the fission of high enriched uranium [60]. However, due to proliferation more and more low enriched uranium targets have to be used. This increases the amount of waste produced [61]. Furthermore, only a few nuclear research reactors worldwide have the neutron flux to produce the quantity and quality needed [1]. Therefore, alternative production routes are being developed [61] (Figure 8).

Alternative ^{99}Mo production routes include neutron activation of ^{98}Mo targets ($^{98}Mo(n,\gamma)^{99}Mo$) [62], irradiation of ^{100}Mo targets with bremsstrahlung ($^{100}Mo(\gamma,n)^{99}Mo$) [63] and irradiation of Mo targets with protons ($^{nat}Mo(p,x)^{99}Mo$) [64]. The advantage of these production methods is that ^{99}Mo can be produced in more facilities around the world. However, the specific activity produced is much lower compared to fission-produced ^{99}Mo. The specific activity can be increased by utilising hot atom chemical effects induced by the irradiation of the targets. To optimally benefit from these effects, thin Mo containing layers are beneficial. These thin layers can be deposited using atomic layer deposition.

For the deposition of Mo-containing thin conformal layers the use of $MoCl_5$ [65], $Mo(CO)_6$ [66] and MoF_6 [67] have been reported. These precursors have in common that they are solids at room temperature. This means that they have to be heated up, to be able to be transported to the reactor chamber in the gas phase. The reported deposition temperature for $Mo(CO)_6$ is 146-165°C, while the reported reactor temperature for $MoCl_5$ 400-500°C.

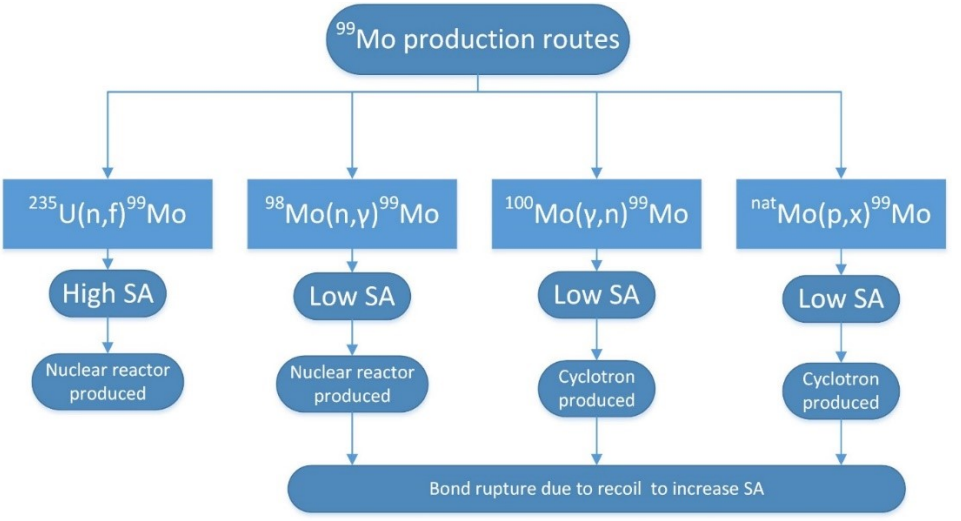

Figure 8: Schematic overview of the several ^{99}Mo production routes.

^{99}Mo by Szilard-Chalmers enrichment (neutron activation)

In order to produce neutron activated ^{99}Mo with a higher specific activity compared to standard neutron activated ^{99}Mo, a Szilard-Chalmers enrichment can be utilised. This means that Mo has to be immobilised using a compound that allows for easy separation of ^{99}Mo from the non-activated Mo target. Examples are $Mo(CO)_6$ [62], Mo oxinate compounds [68] and Mo oxide nano-particles [69]. However, in their work-up procedure either dichloromethane [62, 68] or strong acids [69] need to be applied. If a water solution can be used to separate the ^{99}Mo from the rest of the bulk, the obtained ^{99}Mo can be directly applied for loading radionuclide generators. Furthermore, organic compounds are easily damaged by the gammas present in the reactor pool during irradiation. Inorganic targets are much more stable. Therefore, using ALD-prepared Mo-targets are beneficial. Also, in such targets only the outer layer will contain Mo. This allows for removal of the produced ^{99}Mo without the need to completely dissolve the target.

During the neutron irradiation of the Mo-targets, a surplus of energy is emitted in the form of prompt gammas. A Mo-Mo bond has an energy of 4.6 eV, while a Mo-O bond has an energy of 5.3 eV [70, 71]. Using Equation 3 the needed prompt gamma energy can be calculated showing that prompt gamma energy of 920 or 989 keV is needed to break these chemical bonds, respectively. 14.0 - 15.7 % of the emitted prompt gammas have high enough energy [49]. This means that the expected yield is 14.0-15.7 %. In order to

reach a non-carrier added specific activity no Mo should dissociate from the deposited layer. To that extent the deposited layer must be stable during neutron irradiation and the layer must be insoluble in the solvents used during the work up. Possible Mo compounds are metallic Mo, $MoSi_2$, MoO_2 and MoI_2 [44] when considering water to be the most optimal solvent.

^{99}Mo by cyclotron production

^{99}Mo can be produced by irradiating ^{100}Mo targets with protons using cyclotrons, according to the $^{100}Mo(p,pn)^{99}Mo$ reaction. When irradiating ^{100}Mo targets also ^{99m}Tc is produced directly: $^{100}Mo(p,2n)^{99m}Tc$. The cross sections for these reactions are 153 ± 7 mbarn and 195 ± 8 mbarn, respectively, using 20 MeV protons [72]. For the direct production of ^{99m}Tc it is advisable to use as an enriched ^{100}Mo target as possible to avoid contamination of other Tc isotopes [13, 72]. For ^{99}Mo production this is less important as Mo and Tc isotopes can be chemically separated [73].

Cyclotron targets for ^{99}Mo production are wafers. The limiting factor in production of ^{99}Mo production using protons is the ability of the targets to dissipate generated heat during irradiation. [13] Atomic layer deposition can be used to apply a thin layer of (metallic) Mo on the substrate material that has excellent heat transfer properties, like porous materials [74]. Furthermore, if the Mo-precursor dosing time is chosen in such a way that the substrate is underexposed, no significant amount of expensive enriched ^{100}Mo will be lost during the preparation of the targets. To be able to produce 2 Ci ^{99}Mo, the common activity for radionuclide generators for the European market, targets with 31 w% Mo (80% enriched) need to be prepared using ALD, assuming a 66h irradiation at a proton flux of $4*10^{18}$ p/sm² and a 2.5g target.

$^{(99)}$Mo particles for radionuclide generator use

Current ^{99}Mo/^{99m}Tc radionuclide generators are based on the electrostatic interactions between the Mo ions and the surface of the sorbent material used in the radionuclide generators. The commonly used sorbent material for these radionuclide generators is acid activated alumina. [59] This material has a limited adsorption capacity for Mo and therefore, high specific activity Mo is needed. The change from high specific activity fission produced ^{99}Mo to low specific activity neutron activation produced ^{99}Mo requires a 10-fold increase in adsorption capacity of the sorbent materials [75]. Instead of increasing the

adsorption capacity of the sorbent material it is also possible to apply a Mo layer to the support material. The Mo-particles can then be irradiated with neutrons to produce ^{99}Mo[Mo]-particles which will serve to generate ^{99m}Tc directly.

Upon β^- decay of ^{99}Mo to ^{99m}Tc a beta minus with a maximum energy of 1214.5 keV (82.4% prevalence) is emitted [51]. This results in a maximum recoil energy of 14.7 eV. With bond energies of maximal 6 eV [71] the recoil energy is large enough to break the chemical bond and in principle 82.4% can be eluted. It has to be considered that Tc is chemically different from Mo. As only the atoms undergoing decay will recoil, in theory, only ^{99m}Tc will be present in the eluate. However, this is only possible when no dissolution of the Mo layer is taking place. The solvent used to elute the current radionuclide generators is a 0.9 w% NaCl solution [59]. Therefore, the Mo-layer should be insoluble in saline solution. Possible candidates are metallic Mo, $MoSi_2$, MoI_2 and MoO_2 [44]. These compounds have the potential to reduce the Mo breakthrough in the eluate and to omit the use of alumina and so the Al breakthrough in the eluate, as the layer can, in principle, be deposited on any support material. The support material should be chosen wisely to avoid unnecessary activation of the support.

Taking the European market into account and assuming that a ^{99}Mo/^{99m}Tc radionuclide generator has the ability to hold 2.5 g of column material, the minimum amount of Mo to be deposited can be calculated. It is assumed that the particles are irradiated with a thermal neutron flux of $4*10^{18}$ n/sm² for 66h. If natural occurring Mo is used for the coating 120w% would be needed. This is not feasible. However, using enriched ^{98}Mo (90% enrichment) a coating of 33w% is needed. When this amount of Mo is deposited on, for example, P25 (TiO_2 nanoparticles, a common ALD substrate), the layer is equivalent to approximately 0.7 nm. The deposition of this amount of Mo is feasible, but the cost of enriched ^{98}Mo would require recycling of the target.

Concluding remarks

Atomic layer deposition can find several applications in the production of medical relevant radionuclides. Advantages of using ALD are its versatility, covalent bonding of the coating to the carrier material, the nanoscale structures that are formed, and its scale-up potential. Combining these advantages of ALD with the use of hot atom chemistry principles, such as the Szilard-Chalmers effect, medical relevant radionuclides can be produced in

more nuclear facilities around the world while maintaining the quantity and quality required. This will allow for a more reliable supply of medical radionuclides. However, the case studies showed that the non-solubility of the applied coatings is crucial for the application of the obtained materials in the production of the medical relevant radionuclides, and that future research should be targeted to this aspect.

References

[1] W.N. Association, Radioisotopes in medicine, http://www.world-nuclear.org/info/non-power-nuclear-applications/radioisotopes/radioisotopes-in-medicine/, Accessed on 24 february 2015

[2] P.J. Blower, A nuclear chocolate box: the periodic table of nuclear medicine, Dalton Transactions 44 (2015) 4819-4844.

[3] S. Carlson, A Glance At The History Of Nuclear Medicine, Acta Oncologica 34 (2009) 1095-1102.

[4] L.P. Roobol, A.v.d. Reijden, I.R. de Waard - Schaik, H. Bijwaard, Productie en gebruik van medische radio-isotopen in Nederland. Huidige situatie en toekomstverkenning, RIVM Rapport 2017-0063

[5] V.J. Molinski, A review of ^{99m}Tc generator technology, The International Journal of Applied Radiation and Isotopes 33 (1982) 811-819.

[6] V.S. Le, Z.P.H. Do, M.K. Le, V. Le, N.N.T. Le, Methods of increasing the performance of radionuclide generators used in nuclear medicine: Daughter nuclide build-up optimisation, elution-purification- concentration integration, and effective control of radionuclidic purity, Molecules 19 (2014) 7714-7756.

[7] S.M. Qaim, Nuclear data for production and medical application of radionuclides: Present status and future needs, Nuclear Medical Biology 44 (2017) 31-49.

[8] D. Handkiewicz-Junak, T.D. Poeppel, L. Bodei, C. Aktolun, S. Ezziddin, F. Giammarile, R.C. Delgado-Bolton, M. Gabriel, EANM guidelines for radionuclide therapy of bone metastases with beta-emitting radionuclides, European journal of nuclear medicine and molecular imaging 45 (2018) 846-859.

[9] E.M. Agency, EPAR summary for the public: Luthetra, EMA/524726/2017

[10] K. Hashimoto, Y. Nagai, 8.14 - Radionuclide Production, in: A. Brahme (Ed.) Comprehensive Biomedical Physics, Elsevier, Oxford, 2014, pp. 219-227.

[11] A.C. Perkins, Ethical, Green And Sustainable Nuclear Medicine, European Journal of Nuclear Medical Molecular Imaging 40 (2013) 979–981.

[12] M. Fišer, K. Kopička, P. Hradilek, P. Hanč, O. Lebeda, J. Pánek, M. Vognar, Cyclotron targets and production technologies used for radiopharmaceuticals in NPI, Czechoslovak Journal of Physics 53 (2003) A737-A743.

[13] A. Boschi, P. Martini, M. Pasquali, L. Uccelli, Recent achievements in Tc-99m radiopharmaceutical direct production by medical cyclotrons, Drug Dev Ind Pharm 43 (2017) 1402-1412.

[14] F. Rösch, F.F. Knapp, Radionuclide Generators, Handbook of Nuclear Chemistry 2011, pp. 1935-1976.

[15] H.K. Yoshihara, T. Sekine, Hot Atom Chemistry, Handbook of nuclear chemistry 2011, pp. 1333-1378.

[16] G. Choppin, J.-O. Liljenzin, J. Rydberg, C. Ekberg, Chapter 17 - Production of Radionuclides, in: G. Choppin, J.-O. Liljenzin, J. Rydberg, C. Ekberg (Eds.) Radiochemistry and Nuclear Chemistry (Fourth Edition), Academic Press, Oxford, 2013, pp. 513-544.

[17] Types of Radioactive Decay, Radioactivity Radionuclides Radiation, Springer Berlin Heidelberg 2005, pp. 59-87.
[18] Y.-R. Luo, Bond Dissociation energies, CRC handbook of Chemistry and Physics 2009, pp. 9-65 to 69-98.
[19] P.V. Demekhin, S. Scheit, L.S. Cederbaum, Recoil by Auger electrons: theory and application, Journal of chemical physics 131 (2009).
[20] E.P. Cooper, On the separation of nuclear isomers, Physical Review 61 (1942) 1-5.
[21] S. Wexler, G.R. Anderson, Dissociation of methyl bromide by neuclar isomeric transition of 4.4hr Br80m, Journal of chemical physics 33 (1960) 850.
[22] R. Bhardwaj, A. van der Meer, S.K. Das, M. de Bruin, J. Gascon, H.T. Wolterbeek, A.G. Denkova, P. Serra-Crespo, Separation of nuclear isomers for cancer therapeutic radionuclides based on nuclear decay after-effects, Scientific reports 7 (2017) 44242.
[23] L. Szilard, T.A. Chalmers, Chemical separation of the radioactive element from its bombarded isotope in the Fermi effect, Nature 134 (1934) 462.
[24] K. Song, D. Le, Chemical Bond Energies, https://chem.libretexts.org/Core/Physical_and_Theoretical_Chemistry/Chemical_Bonding/Fundamentals_of_Chemical_Bonding/Bond_Energies, Accessed on 2018
[25] E.L. Hetherington, P.J. Sorby, J. Camakaris, The preparation of high specific activity Copper-64 for medical diagnosis, Applied Radiation and Isotopes 37 (1986) 1242-1243.
[26] S.K. Zeisler, K. Weber, Szilard-Chalmers effect in Holmium complexes, J Radioanal Nucl Chem 227 (1998) 105-109.
[27] L.V.C. Rees, Z. Tao, Szilard- Chalmers recoil of rare-earth cations in zeolite Y, Zeolites 6 (1985) 234.
[28] B.J. O'Neill, D.H. Jackson, J. Lee, C. Canlas, P.C. Stair, C.L. Marshall, J.W. Elam, T.F. Kuech, J.A. Dumesic, G.W. Huber, Catalyst design with atomic layer deposition, ACS Catalysis 5 (2015) 1804-1825.
[29] D. Zhang, D. La Zara, M.J. Quayle, G. Petersson, J.R. van Ommen, S. Folestad, Nanoengineering of Crystal and Amorphous Surfaces of Pharmaceutical Particles for Biomedical Applications, ACS Applied Bio Materials 2 (2019) 1518-1530.
[30] V. Miikkulainen, M. Leskelä, M. Ritala, R.L. Puurunen, Crystallinity of inorganic films grown by atomic layer deposition: overview and general trends, Applied Physics Reviews 113 (2013).
[31] D. Valdesueiro, G. Meesters, M. Kreutzer, J.R. van Ommen, Gas-Phase Deposition of Ultrathin Aluminium Oxide Films on Nanoparticles at Ambient Conditions, Materials 8 (2015) 1249-1263.
[32] A.W. Weimer, Fluidized Bed Reactor Processes, in: A.W. Weimer (Ed.) Carbide, Nitride and Boride Materials Synthesis and Processing, Springer Netherlands, Dordrecht, 1997, pp. 169-180.
[33] D. Kunii, O. Levenspiel, Fluidization engineering, Elsevier2013.
[34] H. Van Bui, F. Grillo, J.R. Van Ommen, Atomic and molecular layer deposition: Of the beaten track, Chemical Communications 53 (2017) 45-71.
[35] J.R. van Ommen, A. Goulas, Atomic layer deposition on particulate materials, Materials Today Chemistry 14 (2019) 100183.
[36] R.L. Puurunen, Growth per cycle in atomic layer deposition: A theoretical Model, Chemical Vapor Deposition 9 (2003) 249-258.
[37] R.W. Johnson, A. Hultqvist, S.F. Bent, A brief review of atomic layer deposition: from fundamentals to applications, Materials Today 17 (2014) 236-246.
[38] J.E. Crowell, Chemical methods of thin film deposition: Chemical vapor deposition, atomic layer deposition, and related technologies, Journal of Vacuum Science & Technology A 21 (2003) S88-S95.

[39] F. Grillo, J.A. Moulijn, M.T. Kreutzer, J.R. Ommen, Nanoparticle sintering in Atomic layer deposition of supported catalysts: Kinietic modeling of the size distribution, Catalysis Today (2018).
[40] S. Mirzadeh, L.F. Mausner, M.A. Garland, Reactor-Produced Medical Radionuclides, Handbook of nuclear chemistry 2011, pp. 1857-1902.
[41] E. Kessels, Overview of all materials prepared by atomic layer deposition (ALD) - an up-to-date and colourfull periodic table, https://www.atomiclimits.com/2019/01/28/overview-of-all-materials-prepared-by-atomic-layer-deposition-ald-an-up-to-date-and-colorful-periodic-table-to-download/, Accessed on 7 October 2019
[42] R. Formento Cavaier, Very high specific activity Er-169 production at MEDICS from xternal ILL target, CERN Experiments, CERN, 2018.
[43] K.V. Vimalnath, A. Rajeswari, S. Chakraborty, A. Dash, Large scale production of ^{51}Cr for medical application in a medium flux research reactor: a comparative investigation of Szilard-Chalmers process and direct (n,gamma) route, Applied Radiation and Isotopes 91 (2014) 104-108.
[44] Physical constants of Inorganic compounds, in: J.R. Rumble (Ed.) CRC handbook of Chemistry and Physics, CRC press, Ohio.
[45] G. Brewer, Copper in medicine, Current Opinion in Chemical Biology 7 (2003) 207-212.
[46] K.I. Kim, S.J. Jang, J.H. Park, Y.J. Lee, T.S. Lee, K.S. Woo, H. Park, J.G. Choe, G.I. An, J.H. Kang, Detection of increased ^{64}Cu uptake by human copper transporter 1 gene overexpression using PET with $^{64}CuCl_2$ in human breast cancer xenograft model, Journal of Nuclear Medicine 55 (2014) 1692-1698.
[47] R. Chakravarty, S. Chakraborty, A. Dash, $^{(64)}Cu^{(2+)}$ Ions as PET Probe: An Emerging Paradigm in Molecular Imaging of Cancer, Molecular pharmaceutics 13 (2016) 3601-3612.
[48] D.W. McCarthy, R.E. Shefer, R.E. Klinkowstein, L.A. Bass, W.H. Margeneau, C.S. Culter, C.J. Anderson, M.J. Welch, Efficient production of high specific activity ^{64}Cu using a biomedical cycloton, Nuclear Medical Biology 24 (1997) 35-43.
[49] J.K. Tuli, Thermal neutron capture gamma-rays, https://www.orau.org/ptp/PTP%20Library/library/DOE/bnl/tnc/ngtblcontentbyn.shtml.htm, Accessed on 2018
[50] Z. Li, R.G. Gordon, Thin, Continuous, and Conformal Copper Films by Reduction of Atomic Layer Deposited Copper Nitride, Chemical Vapor Deposition 12 (2006) 435-441.
[51] B.N. Laboratory, Exploring the table of isotopes, http://ie.lbl.gov/education/isotopes.htm, Accessed on 2014
[52] W.A.P. Breeman, M. de Jong, D.J. Kwekkeboom, R. Valkema, W.H. Bakker, P.P. Kooij, T.J. Visser, E.P. Krenning, Somatostatin receptor-mediated imaging and therapy: basic science, current knowledge, limitations and future perspectives, European Journal of Nuclear Medicine 28 (2001) 1421-1429.
[53] L. Emmett, K. Willowson, J. Violet, J. Shin, A. Blanksby, J. Lee, Lutetium (177) PSMA radionuclide therapy for men with prostate cancer: a review of the current literature and discussion of practical aspects of therapy, Journal of Medical Radiation and Science 64 (2017) 52-60.
[54] M.R.A. Pillai, S. Chakraborty, T. Das, M. Venkatesh, N. Ramamoorthy, Production logistics of ^{177}Lu for radionuclide therapy, Applied Radiation and Isotopes 59 (2003) 109-118.
[55] D.J. De Vries, H.T. Wolterbeek, The production of medicinal ^{177}Lu and the story of ^{177m}Lu: Detrimental by-product of future friend?, Tijdschrift voor Nucleaire Geneeskunde 34 (2012) 899-904.
[56] E.M. Agency, Lutathera, INN-lutetium(177Lu)oxodetreotide - Annex I, EPAR, 2018.
[57] I.-H. bv, Lutetium 177 - LuMark(R) Lu-177 chloride, http://www.idb-holland.com/our-products/lutetium-177-lumark/, Accessed on 14 October 2019

[58] J.L.T.M. Moret, M.B.E. Griffiths, J.E.B.M. Frijns, B.E. Terpstra, H.T. Wolterbeek, S.T. Barry, A.G. Denkova, J.R. Ommen, Lutetium coating of nanoparticles by atomic layer deposition, Journal of Vacuum Science & Technology A 38 (2020).
[59] IAEA, Human health campus - Design of the ^{99}Mo -> ^{99m}Tc generator, http://nucleus.iaea.org/HHW/Radiopharmacy/VirRad/Eluting_the_Generator/Generator_Module/Design_principles/index.html, Accessed on 2015
[60] P. Richards, W.D. Tucker, S.C. Srivastava, Technetium-99m: An historical perspective, The International Journal of Applied Radiation and Isotopes 33 (1982) 793-799.
[61] IAEA, Non-HEU production technologies for molybdenum-99 and technetium-99m, IAEA, Vienna, Austria, 2013.
[62] J.W.J. van Dorp, D.S. Mahes, P. Bode, H.T. Wolterbeek, A.G. Denkova, P. Serra-Crespo, Towards the production of carrier-free $^{(99)}$Mo by neutron activation of $^{(98)}$Mo in molybdenum hexacarbonyl -Szilard-Chalmers enrichment, Applied Radiation and Isotopes 140 (2018) 138-145.
[63] A. Tsechanski, A.F. Bielajew, J.P. Archambault, E. Mainegra-Hing, Electron accelerator-based production of molybdenum-99: Bremsstrahlung and photoneutron generation from molybdenum vs . tungsten, Nuclear Instruments and Methods in Physics Research Section B: Beam Interactions with Materials and Atoms 366 (2016) 124-139.
[64] G. Almeida, On the production of molybdenum-99 and technetium-99m by cyclotron, Radiochemical and Radioanalytical Letters 28 (1977) 205-214.
[65] M. Juppo, M. Vehkamäki, M. Ritala, M. Leskelä, Deposition of molybdenum thin films by an alternate supply of $MoCl_5$ and Zn, Journal of Vacuum Science and Technology A: Vacuum, Surfaces and Films 16 (1998) 2845-2850.
[66] D.K. Nandi, S.K. Sarkar, Atomic Layer Deposition of Molybdenum Oxide for Solar Cell Application, Applied Mechanics and Materials 492 (2014) 375-379.
[67] K. Bernal Ramos, M.J. Saly, Y.J. Chabal, Precursor design and reaction mechanisms for the atomic layer deposition of metal films, Coordination Chemistry Reviews 257 (2013) 3271-3281.
[68] B.S. Tomar, O.M. Steinebach, B.E. Terpstra, P. Bode, H.T. Wolterbeek, Studies on production of high specific activity ^{99}Mo and ^{90}Y by Szilard Chalmers reaction, Radiochimica Acta 98 (2010) 499-506.
[69] N.P. Dikiy, A.N. Dovbnya, N.V. Krasnoselsky, Y.V. Lyashko, E.P. Medvedeva, D.V. Medvedev, V.L. Uvarov, I.D. Fedorets, The use of molybdenum oxide nanoparticles for production of free isotope Mo-99, Problems of Atomic Science and Technology 100 (2015) 154-156.
[70] M.B. Hall, Bond Energy and Conformation of the Molybdenum-to-Molybdenum Triple Bond, Journal of the American Chemical Society 102 (1980) 2104-2106.
[71] B.B. Mandal, S.C. Kundu, Calcium alginate beads embedded in silk fibroin as 3D dual drug releasing scaffolds, Biomaterials 30 (2009) 5170-5177.
[72] S. Manenti, U. Holzwarth, M. Loriggiola, L. Gini, J. Esposito, F. Groppi, F. Simonelli, The excitation functions of $^{(100)}$Mo(p,x)$^{(99)}$Mo and $^{(100)}$Mo(p,2n)$^{(99m)}$Tc, Applied Radiation and Isotopes 94 (2014) 344-348.
[73] J. Esposito, G. Vecchi, G. Pupillo, A. Taibi, L. Uccelli, A. Boschi, M. Gambaccini, Evaluation of Mo99 and Tc99m Productions Based on a High-Performance Cyclotron, Science and Technology of Nuclear Installations 2013 (2013) 1-14.
[74] M. Aghajani Delavar, Azimi, Using porous material for heat transfer enhancement in heat exchanger: Review, International Journal of Heat and Technology 31 (2012).
[75] J.L.T.M. Moret, J. Alkemade, T.U. Upcraft, E. Oehlke, H.T. Wolterbeek, J.R. Ommen, A.G. Denkova, Sorbent production using atomic layer deposition of ^{99}Mo/^{99m}Tc radionuclide generators, Applied radiation and isotopes : including data, instrumentation and methods for use in agriculture, industry and medicine Under review (2020).

3. Sorbent production using Atomic Layer Deposition for $^{99}Mo/^{99m}Tc$ radionuclide generators[2]

Abstract

New production routes for ^{99}Mo are steadily gaining importance. However, the obtained specific activity is much lower than currently produced by the fission of U-235. To be able to supply hospitals with $^{99}Mo/^{99m}Tc$ generators with the desired activity, the adsorption capacity of the column material should be increased. In this paper we have investigated whether the gas phase coating technique Atomic Layer Deposition (ALD), which can deposit ultra-thin layers on high surface area materials, can be used to attain materials with high adsorption capacity for ^{99}Mo. For this purpose, ALD was applied on a silica-core sorbent material to coat it with a thin layer of alumina. This sorbent material shows to have a maximum adsorption capacity of 120 mg/g and has a ^{99m}Tc elution efficiency of 55 ± 2% based on 3 executive elutions.

Keywords: sorbent materials, $^{99}Mo/^{99m}Tc$

[2] This chapter is currently under review by Applied Radiation and Isotopes. Authors J.L.T.M. Moret, J. Alkemade, T.M. Upcraft, E. Oehlke, H.T. Wolterbeek, J.R. van Ommen, A.G. Denkova

Introduction

^{99m}Tc is the most commonly used medical radionuclide accounting for around 40 million annual procedures worldwide [1]. This large demand is due to its favourable decay characteristics, i.e. emission of a low energetic gamma that can accurately be detected outside the body and a half-life of 6 h allowing for reasonable handling without exposing the patient to high radiation dose. In addition, its versatile chemistry allows Tc to be incorporated in diverse radiopharmaceuticals to study a variety of dysfunctions [1-3]. Nevertheless, ^{99m}Tc would not have become such a widely used medical radionuclide if it was not for the development of a ^{99}Mo/^{99m}Tc radionuclide generator [2]. This radionuclide generator allows hospitals on demand supply of ^{99m}Tc. In the ^{99}Mo/^{99m}Tc radionuclide generator the parent isotope ^{99}Mo ($t_{1/2}$ = 66h) is immobilised on an alumina sorbent column, where it decays to ^{99m}Tc. The immobilisation of Mo occurs due to electrostatic interactions between the alumina sorbent and the molybdate ions. The produced ^{99m}Tc is eluted from the column using a saline solution whenever required [4].

Currently, the majority of ^{99}Mo is produced via the fission of enriched uranium targets in nuclear research reactors, resulting in ^{99}Mo with a specific activity of ~10^4 Ci/g. The major drawbacks of uranium targets are that they produce large volumes of high activity (liquid) waste and that the production of ^{99}Mo depends on only six nuclear research reactors worldwide [1, 5, 6]. In 2008 unexpected shutdowns and maintenance led to worldwide shortages of ^{99}Mo [5, 7]. To overcome these major shortcomings, several alternative routes have been proposed and are currently being implemented. The most promising alternative routes at the moment are the following two reactions: the photon reaction with ^{100}Mo(γ,n)^{99}Mo and the neutron activation of ^{98}Mo, ^{98}Mo(n,γ)^{99}Mo [1, 5]. However, these alternative routes produce low specific activity ^{99}Mo ranging roughly from 10 to 100 Ci/g [4, 5]. Simply increasing the sorbent mass of the generator is not an option, as this will require more shielding making transportation difficult and expensive, and will lead to larger elution volumes resulting in too low concentrations of ^{99m}Tc for medical applications [5]. Therefore, a more appropriate option is to develop sorbent materials having much higher adsorption capacity.

In previous research it was observed that when the surface area of the alumina sorbent material was increased the adsorption capacity for Mo increased [8]. However, there are no suitable alumina sorbents with very high surface areas available (i.e. surface area above 300 m²/g). Therefore, our

strategy is to take a different substrate with a very high surface area (e.g. silica), and to provide this surface with an ultrathin film of alumina via atomic layer deposition (ALD) allowing to alter the iso-electric point of the substrate and facilitate the adsorption of molybdenum ions. ALD is a versatile gas phase coating technique commonly used in the semi-conductor industry: many different substrates can be coated with a large number of different (functional) coatings [9, 10]. One ALD cycle consists of a precursor pulse and a co-reactant pulse separated by purge pulses. In ALD these reactions are self-limiting, meaning when the surface is saturated the reaction stops [9, 11]. This cyclic approach allows for nano-control of the material deposited. Furthermore, if ALD is carried out in a fluidised bed reactor (i.e. particles suspended in an upward gas flow) the process can be scaled up [12-14].

In this article we focus on the development of sorbent materials with increased adsorption capacity. We use ALD to introduce a thin layer of alumina on the surface of mesoporous silica, to alter its surface chemistry. After application of the alumina layer the adsorption capacity for Mo was determined and its potential to be used as sorbent material for a $^{99}Mo/^{99m}Tc$ radionuclide generator was assessed.

Materials and method

Chemicals

The SBA-15 substrate (highly structured SiO_2) was purchased from ACS materials (USA) and had a surface area of 570 m^2/g, a pore diameter of 7.5 nm and a particle size distribution of 1-4 µm. The substrate was dried overnight at 120°C before use. Trimethylaluminum (TMA) was obtained from Akzo Nobel (Amersfoort, Netherlands) in a stainless steel bubbler. Purified water was obtained from an in-house Millipore System. The nitrogen was grade 5.0, supplied by a central gas line. MoO_3 99.9% was purchased from J.K. Baker. Radioactive Mo was obtained by irradiation MoO_3 for 1h at a thermal neutron flux of $4.72*10^{16}$ n/m^2s, an epithermal neutron flux of $8.0*10^{14}$ n/m^2 and a fast neutron flux of $3.48*10^{15}$ at the Reactor Institute Delft. NaOH, NaCl, HCl 30% and acid activated alumina (AA) were obtained from Sigma Aldrich and used without further purification.

Preparation of the sorbents

Set up

Atomic layer deposition (ALD) was performed in a custom-made fluidised bed reactor. The fluidised bed reactor consisted of a glass column with a diameter of 25 mm and a length of 500 mm mounted on a stainless steel wind box with a stainless steel porous plate. On top of the column also a porous plate and a metal vessel were connected. In this column the powdered substrate was suspended in an upward gas flow, allowing it to fluidize (i.e., it seems to behave like a liquid). The precursors were fed alternatingly into the reactor chamber using nitrogen as a carrier gas from the bottom of the reactor. The carrier gas flow was 0.5 l/min ($1.52 * 10^{-2}$ m/s). The fluidised bed was heated using an infra-red lamp. The whole system was controlled using a PC with a custom made Lab view program. The off gasses were washed with a series of wash bottles containing kydol oil and then a HEPA filter. The system was operated at atmospheric pressure at a temperature of 170° C [15].

Coating

The SBA-15 substrate was coated with alumina during 3 to 5 ALD cycles, each cycle consisting of 16 min - 20 min – 13 min - 20 min TMA – purge – water – purge, respectively.

Adsorption experiments

The adsorption capacity of the sorbents was determined by soaking the sorbents in Mo containing solutions of starting concentrations ranging between 0.5 and 20 mg/ml for time periods of 1 min to 120 min. The Mo solutions were prepared by dissolving MoO_3 in 1 M NaOH at a concentration of 25 Mo mg/ml. At the day of experiments, the stock solution was brought to pH 4 using 1M HCl and then diluted to the desired concentration. For tracer experiments a small amount of ^{99}Mo (4MBq) was added to the dilutions. Before analysis the eluates were filtered using a 0.45 µm Whatman syringe filters to remove sorbent fines.

^{99m}Tc elution efficiency

The ^{99m}Tc elution efficiency was determined by soaking the sorbents in a Mo solution containing ^{99}Mo. Therefore, MoO_3 was irradiated with neutrons at the Hoger Onderwijs Reactor (HOR) at TU Delft for 1 h at a thermal neutron flux of $4.72*10^{16}$ n/m²s, epithermal thermal neutron flux of $4.5*10^{14}$ n/m²s and a fast neutron flux of $3.5*10^{15}$ n/m²s. After irradiation the Mo solution

was prepared in the same way as the adsorption experiments. After soaking for 1.5 hours the sorbent materials were washed three times with a physiological salt solution until pH of the liquid was 7. After washing the sorbent materials were set aside in a physiological salt solution to establish equilibrium between ^{99}Mo and ^{99m}Tc. After the ingrowth period the liquid was removed from the solid and filtered over a 0.45 µm filter before analysis.

Analysis

Elemental analysis of the sorbents was done by ICP-OES (Optima 4300, Perkin and Elmer). For this purpose, 50 mg of the sorbent material was dissolved in 6 ml Aqua Regia and 0.4 ml HF 40% under microwave assistance and then diluted to 50 ml with milliQ water in a volume flask. Furthermore, the coating was visualised by TEM and the change in surface area was determined by nitrogen adsorption BET theory (Tri-Star). The elemental content of the initial solution and of the eluents of adsorption were either determined by ICP-OES (non-radioactive samples and radioactive samples) or gamma spectroscopy (radioactive samples) (NaI crystal, Wallac² gamma counter, Perkin and Elmer). The adsorbed amount of Mo was determined by $q = \frac{m_{Mo,initial} - m_{Mo,eluate}}{m_{sorbent}}$.

Results and discussion

Characterisation of the sorbent material

The SBA-15 substrate material is coated with an alumina layer via ALD in a fluidised bed reactor using TMA and water. Samples are prepared applying 3 and 5 ALD cycles. The layer thickness of the deposited Al_2O_3 layer (d_{Al2O3}) is calculated according to Valdesueiro et al. [13] based on the amount of Al deposited on the particles as determined by ICP-OES. Using this data, the growth per cycle (GPC) is derived (Table 1). The GPC is 0.32 ± 0.09 nm/cycle for deposition at 170°C, which is rather high compared to literature values of 0.14 nm/cycle [13] or 0.1 nm/cycle [16]. However, comparable GPC (0.2 nm/cycle) has been reported by Beetstra et al. [17] under similar conditions. The dosing times calculated for coating the SBA-15 substrate are conservative, meaning that the substrate will be overexposed to TMA and water to make sure that the surface is saturated. Therefore, it is well possible that the high GPC is caused by overexposure of precursor in combination with a relatively short purging time. The atmospheric pressure in de reactor and the porous substrate can make it difficult to purge the system completely, which could contribute to the rather high GPC.

Table 1: Comparison of the physical characteristics of the currently used acid activated alumina (AA), the bare silica substrate (SBA-15) and the coated with Al_2O_3 silica sorbent (denoted as silica core xC, with x number of cycles). The film thickness (d_{Al2O3}) is calculated based on the ICP-OES results for the Al deposition on the particles.

Material	Al [w%]	d_{Al2O3} [nm]	GPC [nm/cycle]	Surface area [m²/g]	Pore diameter [nm]	Iso-electric point
AA (current sorbent standard)	54.9	N.A.	N.A.	170 ± 10	-	~6
SBA-15 (bare substrate)	-	-	-	592 ± 62	7.5	~2
Silica core 3C	12.9 ± 3.52	1.09 ± 0.36	0.37 ± 0.12	286 ± 36	6	n.d.
Silica core 5C	17.57 ± 0.04	1.64 ± 0.44	0.32 ± 0.09	247 ± 25	5.5	n.d.

The surface area of the sorbent material decreases when applying the aluminium oxide coating (Table 1). This can be explained by the high porosity of SBA-15, which includes micro- and meso-pores (Figure S2) that can get blocked when applying the aluminium oxide coating either due to their size or to the incomplete diffusion of TMA molecules all the way to the end of the pore. The initial pore size is around 6 nm while TMA molecule has a diameter of approximately 0.6 nm [18]. It can therefore be expected that as the coating proceeds diffusion will become more difficult, and finally pore blockage will occur, leading to reduction of the surface area of the material. The micro-pores are expected to be almost entirely blocked when applying the coating, assuming a full layer is deposited. However, the surface area of the coated material is still 1.5 times higher than the acid activated alumina (AA) reference material.

Transmission electron microscopy (TEM) is used to visualise the coating. SBA-15 is described as a highly structured material with a honeycomb like structure [19]. This structure can be seen in Figure 1 A. The Al_2O_3 layer as deposited is amorphous, which allows distinguishing between the substrate and the coating. Based on the TEM images a layer thickness of 2 nm is estimated for silica core 5C. This is in agreement with the calculated value using ICP-OES data and the estimated layer thickness based on the change in

pore diameter. The layer thickness and the surface area for silica core 3C show large variation between batches. The differences probably originate from the fact that the first few cycles do not completely cover the surface of the support, due to for instance steric hindrance, creating a partial coating of Al_2O_3.[11]. Additional cycles cover also the initially uncoated parts, resulting in a full layer of Al_2O_3. During the coating experiments it is observed that interactions between the glass column and the powder seems to change around the 4th cycle (i.e. less powder is sticking to the column wall) indicating a coating has been formed.

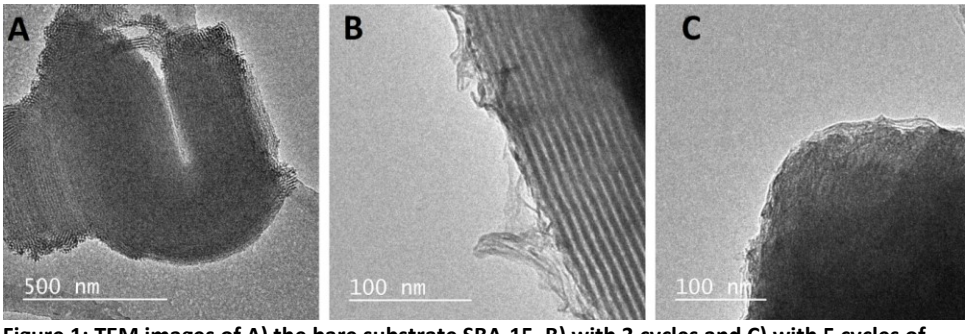

Figure 1: TEM images of A) the bare substrate SBA-15, B) with 3 cycles and C) with 5 cycles of Al_2O_3.

Stability assessment of the sorbent material

An important criterion for the sorbents is their stability during their use in a radionuclide generator and their behaviour during loading with ^{99}Mo. Therefore, a stability assessment of the SBA-15 core sorbent has been performed. In Figure 2 the results of the stability assessment are shown. Almost the entire applied Al-layer has disappeared from the sorbent material at pH 1. This is expected considering the solubility of aluminium oxide at pH 1. Increasing the pH of the solution decreases the loss of Al from the sorbent material. At pH 3 only 0.19 ± 0.08 % of the Al deposited is lost, while at pH 4 and above no detectable amount of Al is present in the eluents. The detection limit for Al on ICP-OES is 0.02 mg/l [20]. Therefore, adsorption experiments of ^{99}Mo have been carried out at pH 4 or higher.

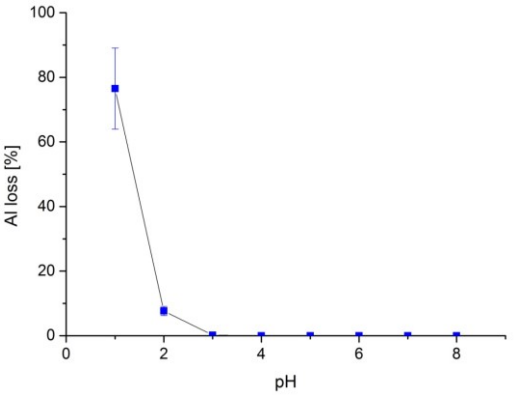

Figure 2: Loss of Al from the sorbent material (silica core 5C) as function of pH. For each pH value a solution was prepared either with HCl or NaOH. The loss of Al is given as a percentage of the Al deposited on the substrate. Sorbent material with 5 cycles of ALD was used. The error bars correspond to the experimental uncertainty determined by n=3. Above pH 4 and higher no Al could be measured in solution. The detection limit for ICP-OES is 0.02 mg/l.

pH influence on Mo adsorption

It is known that the pH of the solution has an influence on the adsorption capacity of the sorbent material due to the formation of different Mo species and their interaction with the sorbent [8]. Therefore, to determine the optimal pH for Mo adsorption Mo solutions of different pH vales have been prepared. The Mo adsorption of the silica core sorbent materials compared to the non-coated material at different pH values is shown in Figure 3.

Clearly visible is that Mo adsorption decreases at higher pH values. The decrease in adsorption capacity can be explained by difference in speciation of Mo. At pH 4 and 5 there is a relatively large amount of Mo species present that are highly negatively charged (e.g. $HMo_7O_{24}^{5-}$ and $Mo_7O_{24}^{6-}$), allowing for strong interaction with the positively charged surface. Increasing the pH causes the speciation to shift to less negatively charges species (Figure 4). However, this speciation data is just an estimation of the speciation during adsorption which does not consider influences induced by the sorbent material (e.g. loss of Al from the sorbent material). Even though the used software to calculate the speciation, i.e. CHEAQs [21] (Chemical Equilibria in Aquatic solutions), has an extensive database, other species might exist. In addition, the iso-electric point of Al_2O_3 is 9 and as the pH increases, the sorbent material will become less positively charged weakening the interaction with negatively charged species. However, the coated material having 5 cycles shows a significant increase in Mo adsorption capacity compared to bare SBA-15 and the sorbent material made with 3 cycles of ALD.

This trend can be explained by the amount of Al present on the sorbent material. Bare SBA-15 (No Al) has an iso-electric point of 2, meaning that at the pH tested the material is negatively charged, limiting its interaction with the negatively charged Mo species. The material coated with 3 ALD cycles has an incomplete coating, as explained above, and so will have spots where reduced adsorption is occurring due to bare SBA-15 being exposed. Because of the decrease in Mo adsorption at higher pH values, further experiments have been carried out at pH 4, which is in agreement with the loading conditions currently used in $^{99}Mo/^{99m}Tc$ generators. [4].

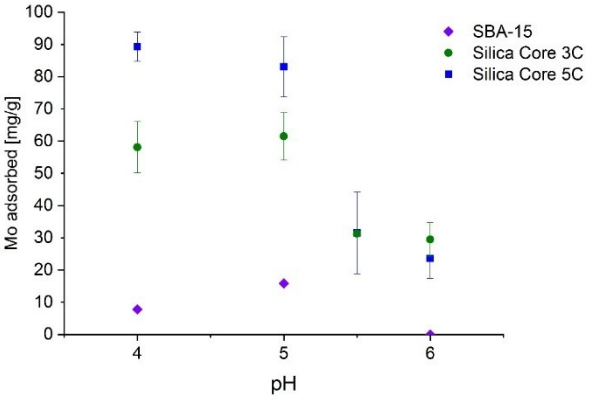

Figure 3: **Mo adsorption capacity of the sorbent material as function of pH compared to bare SBA-15 (590m²/g) with a Mo concentration of 6 mg/ml and a sorbent concentration of 17 ± 3 mg/ml. A decrease in adsorption capacity is observed with increasing pH. Error bars are based on experimental uncertainties of n=3. Purple diamonds are bare SBA-15, blue squares are the silica core 5C sorbent and the green rounds are the silica core 3C sorbent.**

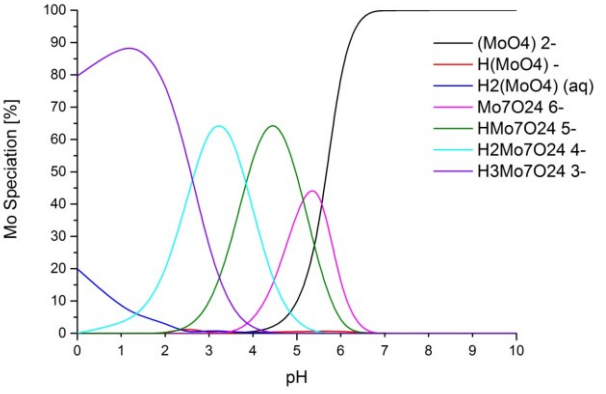

Figure 4: The Mo speciation in solution at equilibrium for different pH values. The speciation is calculated using CHEAQS for a fixed concentration (6mg/ml Mo) at 20°C and without any sorbent material. Black line: $(MoO_4)^{2-}$, red line: $H(MoO_4)^-$, blue line: $H_2(MoO_4)_{(aq)}$, pink line: $Mo_7O_{24}^{6-}$, green line: $HMo_7O_{24}^{5-}$, cyan line: $H_2Mo_7O_{24}^{4-}$ and purple line: $H_3Mo_7O_{24}^{3-}$

Kinetic behaviour of the sorbent material

The adsorption kinetics of the ALD prepared sorbent materials is determined by submersing the sorbent materials in a Mo solution for different time periods. After filtration the Mo and Al concentration in the eluate is determined. The amount of Mo adsorbed is calculated from the difference in Mo concentrations before and after contact with the sorbent material. Acid activated alumina (AA) is always used as control sorbent. The adsorption results are given in Figure 5.

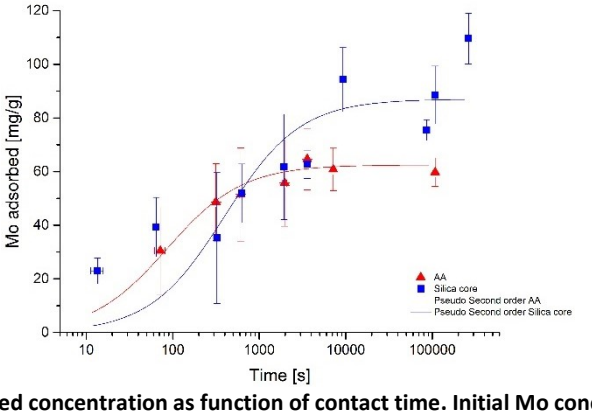

Figure 5: Mo adsorbed concentration as function of contact time. Initial Mo concentration is 9.1 ± 0.7 mg/ml, initial pH 4, sorbent concentration is 17 ± 3 mg/ml and temperature is 20°C. Blue squares represent silica core 5C and red triangles denote AA. The lines represent the pseudo second order fit of the data. Error bars are based on experimental uncertainties of n=4.

Table 2: Pseudo second order parameters obtained for the adsorption of Mo on the silica core 5C sorbent compared to AA using a starting concentration of 9 mg/ml of Mo at pH 4 and T = 20°C, with a sorbent concentration of 17 ± 3 mg/ml. The data is nonlinearly fitted according to equation 1.

Sorbent	k_2 [g/mg s]	q_e [mg/g]	R^2
AA	$(1.85\pm0.53)*10^{-4}$	62.53 ± 2.82	0.60
Silica core 5C	$(2.86\pm0.96)*10^{-5}$	87.04 ± 5.59	0.50

The experimental data is analysed using a kinetic model: a pseudo – second order fit (Equation 1). In this model q_t is the adsorption capacity at time t, q_e is the adsorption capacity at equilibrium and k_2 is the pseudo second order rate constant. The pseudo – second order model is generally used to describe molybdenum adsorption and is therefore used to be able to compare our results to other sorbent materials reported in literature. The obtained fit parameters are given in Table 2.

$$q_t = \frac{k_2 q_e^2 * t}{1 + k_2 q_e * t} \qquad [1]$$

As already can be seen in Figure 5 the data points are rather scattered, especially for the silica core sorbent material. This scattered data is reflected in the low values for the correlation coefficient (R^2) (Table 2) of the fit. During the production of the silica core sorbent material agglomerates are formed. Where the particles permanently attached to each other within these agglomerates no coating will take place at these touching points. This causes the individual particles to be heterogeneously coated. When suspending the silica core sorbent material in solution, it is possible that the agglomerates break, exposing uncoated sorbent material. Also there could be a slight difference in speciation of the molybdate ions between experiments, due to batch differences. Unfortunately, due to the low correlation coefficients the obtained values cannot be compared to the literature. However, it is clear that the Mo adsorption is very fast and equilibrium for both the AA and the silica core sorbent are reached within 2 hours. Furthermore, the adsorption rate constant for the silica core sorbent is an order of magnitude smaller compared to the AA sorbent. Considering the high porosity of this material it is possible that there are diffusion limitations which lowers the adsorption rate, as to

fully utilise all available surface area the molybdate ions have to diffuse into the 6 ± 0.5 nm pores of the silica core sorbent material.

Stability of the coating during loading

The Al concentration measured in the eluate is a measure for the stability of the sorbent material during loading of Mo. Using this concentration, the Al loss percentage was determined. The Al loss of AA is negligible, while for the silica core sorbent this Al loss percentage is 4.27 ± 3.07 % of the amount of Al originally present on the sorbent material. It is assumed that this Al loss is caused by the interaction of the molybdate ions with the amorphous alumina surface. Crystalline alumina is more stable than amorphous alumina [9]. Therefore, part of the silica core sorbent material was annealed at 800-1100°C, to transform the amorphous alumina layer to a more crystalline structure. XRD indicates that a crystalline structure was formed at 900°C (see supplemental information S3). However, annealing of the silica core sorbent caused the pore structure of SBA-15 to collapse, reducing the surface area significantly (Table 3). That in return reduces the adsorption capacity enormously (Figure 6). At 800 °C the surface area appeared unaffected but nevertheless the adsorption capacity decreased indicating that other processes play a role. It is possible that due to annealing the hydroxyl groups on the surface of the Al_2O_3 coating got removed or replaced by hydrogen groups, reducing the amount of active adsorption sites. The deposited Al_2O_3 coating is –OH terminated, because of the water pulse in the ALD process.

The instability of the alumina coating can also be attributed to the Cl^- concentration of the solution. When preparing the Mo solutions prior to use, the pH of part of the stock solution is lowered by adding HCl. As different Mo concentrations were prepared, also different HCl concentrations were needed. In order to determine the influence of the Cl^- ions Mo solutions of same concentration (5 mg/ml and 24 mg/ml at pH 5) are prepared with a different Cl^- concentration. Either the desired Mo concentration was prepared in 1 M NaOH and then brought to pH 5 with HCl or first a stock solution was made, of which a part was brought to pH 5 and then diluted to the desired Mo concentration. Mo adsorption results and Al loss are given in Table 4. The results actually indicate that a higher Cl^- concentration seems to stabilise the Al_2O_3 coating. However, this also decreases the adsorption capacity of the silica core sorbent material. This is observed for both Mo concentrations. It is assumed that the Cl^- is occupying active sites where otherwise molybdenum species would adsorb.

Table 3: Surface area of the silica core sorbent after annealing at several temperatures in air.

Annealing temperature [°C]	Surface area [m²/g]
As deposited	276
800	265
900	175
1000	5.2*
1100	4.9*
800 (argon atmosphere)	266

*Some care must be taken with these numbers, as they are around the detection limit of the machine.

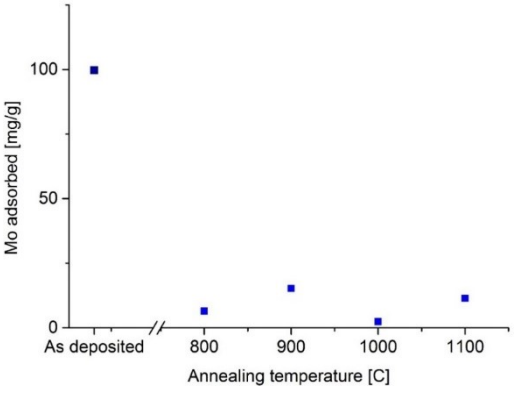

Figure 6: Mo adsorption capacity as function of the annealing temperature for the silica core sorbent material. The temperature of the reaction chamber at which the Al_2O_3 layer was deposited was 230°C. Mo concentration was 6 mg/ml and the sorbent concentration was 17 mg/ml.

Table 4: The effect of the Cl^- concentration on the Al loss of the silica core sorbent material and its Mo adsorption capacity for both a Mo start concentration of 5 mg/ml and 24 mg/ml. The initial pH of the solutions was pH 5. Direct preparation means that the desired Mo concentration was prepared in 1 M NaOH and then brought to pH 5 with HCl, diluted preparation means first a stock solution was made, of which a part was brought to pH 5 and then diluted to the desired Mo concentration.

	Mo start concentration 5 mg/ml		Mo start concentration 24 mg/ml	
	Direct preparation	Diluted preparation	Direct preparation	Diluted preparation
HCl concentration [M]	1.06	0.189	2.08	0.667
Al loss [mg/g sorbent]	3.6	10.5	10.6	146
Mo adsorption [mg Mo/g sorbent]	70.5	90.5	121	171

Isotherm behaviour of the sorbent material – Standard method

To determine the maximum adsorption capacity of the sorbent materials, an adsorption isotherm is made. To this extent the sorbent materials is contacted with Mo solutions of different concentrations for 60 min to reach different equilibrium concentrations (Figure 7). The experimental data is then analysed using three isotherm models: the Langmuir model (Equation 2), the extended Langmuir model (Equation 3) and the Freundlich model (Equation 4), to describe the adsorption process. In these models q_e is the adsorption capacity at equilibrium, $q_{e,max}$ the maximum adsorption capacity, C_e the concentration of Mo at equilibrium, K_L, K_{eL} and K_F are the Langmuir constant, the extended Langmuir constant and the Freundlich constant, respectively. n_F and n_{eL} are model parameters. The Langmuir model is used to describe the adsorption of monolayers on the sorbent surface. It assumes that after adsorption the molecules stay at their adsorption site. The extended Langmuir model takes multilayer adsorption into account. The Freundlich model is an empiric model that can describe the adsorption on a heterogeneous surface for both monolayer and multilayer systems. The fitted results are given in Table 5.

$$q_e = \frac{q_{e,max} K_L C_e}{1 + K_L C_e} \qquad [2]$$

$$q_e = \frac{q_{e,max} K_{eL} C_e}{1 + K_{eL} C_e} \exp\left(\frac{n_{eL} C_e}{C_{max}}\right) \qquad [3]$$

$$q_e = K_F C_e^{\frac{1}{n_F}} \qquad [4]$$

Table 5: Adsorption parameters obtained from the isotherm fits for Mo ions at initial pH 4 for Langmuir, and Freundlich model.

	Langmuir			Freundlich		
Sorbent	K_L [ml/mg]	$q_{m,L}$ [mg/g]	R^2	K_F [ml/g]	$1/n_F$ [-]	R^2
AA	7.52 ± 1.54	62.55 ± 1.67	0.812	46.81 ± 1.8	0.16 ± 0.02	0.634
Silica core 5C	2.18 ± 0.61	88.09 ± 6.66	0.582	51.87 ± 3.65	0.26 ± 0.04	0.472

From the fitted models, the Langmuir model fit the data best (R^2 = 0.81 and R^2 = 0.58 for AA and Silica core sorbent, respectively). Even though, the extended Langmuir model has comparable correlation coefficients (S4), using a more complex model has no added value when it does not give a significant improvement. However, the Langmuir model does have its shortcomings. It assumes no interaction between the adsorbent and the sorbent material and no movement of adsorbent over the surface [22]. Judging by the Al loss from the silica core sorbent material during loading, there is some kind of interaction between the adsorbent and the sorbent. The stability of the formed Mo-sorbent complex is given by the Langmuir constant. This indicates that the adsorption on the silica core sorbent is slightly less stable compared to that of AA (by a factor 3.4, Table 5). However, the obtained Langmuir constant of AA is an order of magnitude lower then reported by Denkova et al. [8]. Partially, the difference can be attributed to the different adsorption pH values used in this paper. Furthermore, temperature and additional elements like Na^+ and Cl^- in solution can influence the Mo-sorbent complex stability. The obtained from the fit maximum adsorption capacities are in accordance with the plotted data.

Even though the Freundlich model does not fit the data as well as the Langmuir models, it still gives some information about the adsorption process. An n_F >1 indicates a strong affinity between the adsorbent and the sorbent, which is in agreement with the rapid adsorption process.

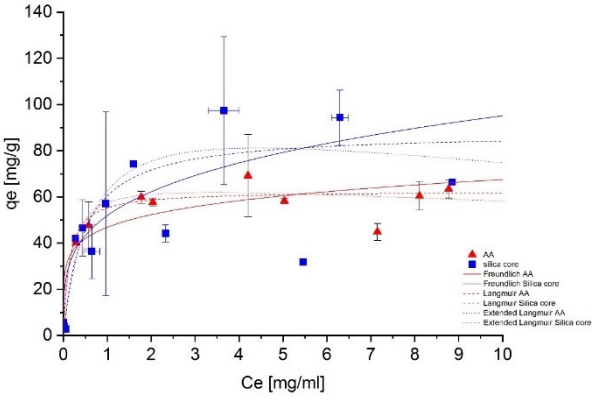

Figure 7: Mo adsorption capacity as function of Mo equilibrium concentration. Red triangle is AA and blue square is Silica core. Dotted line corresponds to the extended Langmuir model, dashed line to the Langmuir model and full line to the Freundlich model. Sorbent concentration is 17 mg/ml, initial pH is 4 and T is 20°C. Error bars are based on the experimental uncertainty of n = 3.

Isotherm behaviour of the sorbent material – Compartment method

The ionic strength of the Mo solutions partly depends on the Mo concentration of the different concentrations used to determine the isotherm. Therefore, to take this effect into account, the Mo starting concentration was kept constant and the ratio between the solid sorbent and the Mo-liquid was varied. By doing so the adsorption of Mo to the sorbent material can be represented by a two-compartment closed system. Assuming that the interaction of Mo with the container can be neglected due to inert container material, a simple model as shown in Figure 8 can be derived.

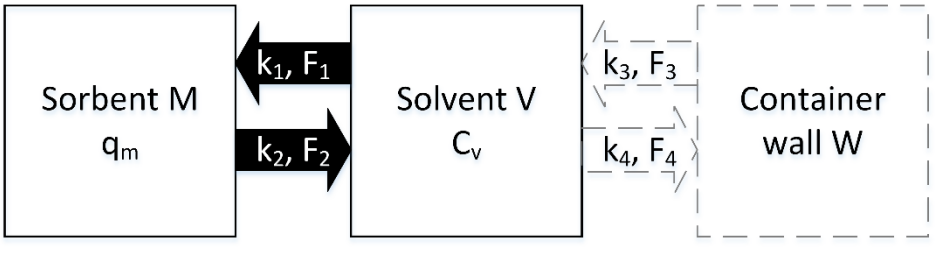

Figure 8: Schematic representation of the compartments in the sorbent-solvent system during adsorption. The container wall is assumed not to participate in the adsorption of Mo. *k1* and k_2 are the rate constants for adsorption and desorption respectively and F_1 and F_2 are the corresponding mass flow rates.

The Mo concentration in the solvent can be described by equation 5 and the adsorbed Mo onto the sorbent material by equation 6. For derivation of these equations see supporting information S1. These equations assume a linear correlation between the adsorbed Mo amount and the sorbent to solvent ratio. However, as see in Figure 9 the data shows somewhat exponential correlation and would be more appropriate using a model such as shown by equation 7. The determined q_m for AA is 81 mg/g and for silica core 5c is 127 mg/g.

$$C_V = \frac{C_0 + \frac{M}{V} q_0}{k_1 + k_2} k_2 + \left(\frac{C_0 + \frac{M}{V} q_0}{k_1 + k_2} k_1 - \frac{M}{V} q_0 \right) e^{-(k_1 + k_2)t} \quad [5]$$

$$q_m = \frac{\frac{V}{M} C_0 + q_0}{k_1 + k_2} k_1 - \left(\frac{\frac{V}{M} C_0 + q_0}{k_1 + k_2} k_1 - q_0 \right) e^{-(k_1 + k_2)t} \quad [6]$$

$$q_e = \frac{q_m * \frac{V}{M}}{K + \frac{V}{M}} \quad [7]$$

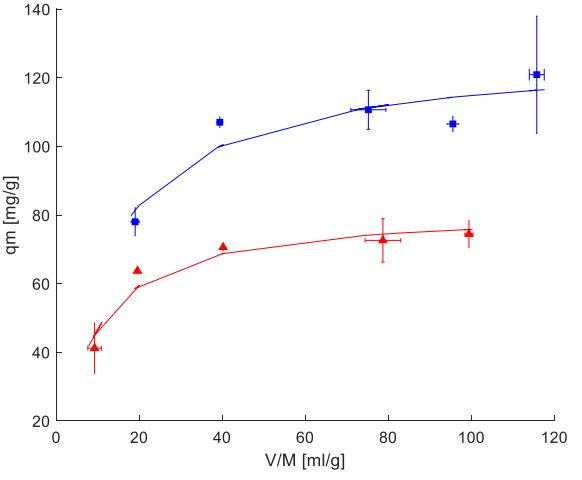

Figure 9: Adsorption isotherm of Mo ions, using the compartment method, at pH 4. Blue squares represent the silica core 5c sorbent and the red triangles represent AA. The lines represent the fit using equation 6. Error bars are based on n=3.

When the system is at equilibrium the mass flow rates will be equal in magnitude: $F_1 \stackrel{\text{def}}{=} F_2$. From this equilibrium definition the equation describing the adsorbed amount as function of the solvent over sorbent ratio can be derived. Logic dictates that when *V/M* goes to infinity, q_m reaches its maximum and C_V assumes C_0. At large *V/M* ratios the mass of the sorbent becomes insignificant compared to the amount of solvent in the system and therefore the amount of adsorbed Mo will have no impact on the concentration in solution. The sorbent has reached it maximum adsorption capacity. This effect is already visible in the data presented in Figure 9.

During analysis of the eluents it is noted that the concentrations in the eluents after adsorption still differ, meaning that the ionic strength of the solutions is still different. Therefore, for the attempt to keep the ionic strength of the solution constant, the compartment method has no added value over the standard method. Also, the adsorption capacities determined using this method do not significantly differ from the adsorption capacities determined using the standard method. However, the use of the compartment method seems to be a more reliable method due to smaller deviations in the results. This could be because at the start of the experiment the speciation for all the samples is the same, as the same Mo-solution is used. Using the standard method, the starting concentrations of Mo in solution differs and hence its speciation.

Pilot generator

For the sorbents to be a viable alternative for the currently used sorbent not only the adsorption capacity for Mo should be high enough, also ^{99m}Tc should be efficiently eluted from the radionuclide generator. Therefore, the sorbents are loaded with neutron activated ^{99}Mo and then eluted with a physiological salt solution. After loading the sorbents are washed with a physiological salt solution until pH was 7. Then the sorbents are left to reach equilibrium. The ingrowth period until elution 1 and 2 is 1 day, and the ingrowth period until elution 3 is 3 days.

Table 6: Batch extraction properties of the different sorbents. The sorbent and Mo concentration during loading were 19 ± 3 mg/ml and 6.7 mg /ml respectively. The AA sorbent and the silica core 5C sorbent were loaded with *43.8 ± 20 mg Mo/g sorbent and 19.8 ± 4.2 mg Mo/g/ sorbent respectively. Extraction* properties are based on the experimental average of n=3. Loading capacity is based on n=2. Extraction 1 and 2 are after 1 day of ingrowth. Between extraction 2 and 3 there is a period of 3 days ingrowth.

	Extraction 1			*Extraction 2*			*Extraction 3*		
Sorbent	***^{99m}Tc [%]***	***^{99}Mo/ ^{99m}Tc [%]***	***Al [ppm]***	***^{99m}Tc [%]***	***^{99}Mo/ ^{99m}Tc [%]***	***Al [ppm]***	***^{99m}Tc [%]***	***^{99}Mo/ ^{99m}Tc [%]***	***Al [ppm]***
AA	*66.4 ± 1.9*	*2.08 ± 0.02*	*28.3 ± 0.9*	*56.8 ± 1.7*	*0.36 ± 0.01*	*4.63 ± 0.16*	*68.2 ± 4.3*	*0.18 ± 0.0*	*2.91 ± 0.11*
Silica core 5C	*54.9 ± 0.9*	*1.01 ± 0.09*	*1.32 ± 0.36*	*50.7 ± 0.5*	*0.34 ± 0.01*	*0.60 ± 0.01*	*59.5 ± 1.9*	*0.31 ± 0.02*	*0.54 ± 0.03*

With a loading capacity of 43.8 ± 20 mg/g, the loading of the AA sorbent material is as expected and comparable to previous results. On the other hand, the loading capacity of the silica core sorbent material is only 19.8 ± 4.2 mg/g, which is rather low and different from previously obtained results. Due to circumstances, between the production of the silica core 5C sorbent material and the use of this material as a sorbent at least a year has passed. Silica is known to be hygroscopic, which could affect the loading capacity. To minimise this effect the silica core sorbent material is stored under vacuum until use. Before these pilot generator experiments the silica core 5C sorbent material has been dried overnight, but it is possible that still water was present. In comparison, the undried silica core sorbent material has an adsorption capacity of 10.2 ± 1.6 mg/g.

It has to be noted that the extraction experiments were carried out in batch mode, while radionuclide generators are operated in column mode. Unfortunately, batch mode makes it more difficult to remove residual Mo from the sorbent material, indicated by the reduction of Mo loss with each consecutive extraction. In batch mode the sorbent material is fully loaded, while in column mode this is usually not the case. Therefore, in column mode any desorbed Mo can re-adsorb somewhere further on the column, while this is impossible in batch mode.

The set limits for Mo-breakthrough and Al concentration in the eluate are 5.55 kBq Mo per 37 MBq ^{99m}Tc (0.15%) and 10 ppm Al [23, 24]. This means that for both the AA sorbent and the silica core sorbent the Mo-concentrations in the

eluate exceed the set limits. The relative high Mo breakthrough could be due to the high loading of the sorbent material. If a Mo-atom desorbs it is difficult to reabsorb when the sorbent material is close to its maximum loading capacity. Secondly, these experiments are carried out in batch mode. Together, this could cause the elevated breakthrough.

The Al breakthrough for the silica sorbent material is structurally lower compared to the AA sorbent material. This is surprising, as during loading of the sorbent materials the silica core sorbent material had a higher loss of Al. It is possible that the Cl^- ions in the salt solution stabilises the alumina layer on the silica core sorbent material. The Al concentration of the first elution of the AA sorbent material is comparable to the concentrations reported by Denkova et al. [8].

The extraction efficiency of the silica core sorbent material (~55%) is structurally lower compared to the AA sorbent material (~65%). During the experiments it proved to be more difficult to separate the liquid phase from the solid phase for the silica core sorbent compared to the AA sorbent due to the fine structure of the silica sorbent material.

Overall Discussion

The aim of this paper was to investigate novel sorbent materials for a $^{99}Mo/^{99m}Tc$ radionuclide generator. A simple and straight forward calculation shows that an adsorption capacity of at least 166 mg Mo/g sorbent is required when a specific activity of 222 GBq/g is used for a 2 g column, taking into account that the European market wants to be supplied with 74 GBq ^{99}Mo generators. This calculation is based on 100 % loading which will not be applied due to high Mo breakthrough. Loadings of 30% are more realistic to reduce the chance of Mo breakthrough, and therefore an adsorption capacity of at least 555 mg Mo/g sorbent would be required. This adsorption capacity means that a 27 fold increase compared to the currently used aluminium oxide sorbent material needs to be achieved [3]. Attempts have been made to find sorbents with a higher adsorption capacity [25-27], only none has succeeded in reaching the desired capacity of 555 mg Mo/g sorbent, however values up to 200 mg Mo/g sorbent were reported [26]. The adsorption capacity of 555 mg Mo/g sorbent can also not be reached using the silica core sorbent. The most likely cause for this is the reduction in surface area due to the applied coating. However, compared to the bare material, the adsorption capacity is significantly increased (by a factor 9), showing that the iso-electric

point of the material can be properly changed. Also, the adsorption capacity of the silica core material is two-fold increase compared to the currently used AA.

Conclusions

ALD is a versatile coating technique that can be used to modify the surface properties of high-surface-area materials. The silica core sorbent material obtained using ALD can be used to adsorb Mo. The adsorption capacity obtained for this material is twice higher than that of the currently used AA. However, the adsorption capacity should be further increased to make it deployable in radionuclide generators using low specific activity ^{99}Mo. As the speciation of molybdenum seems to interfere with the adsorption capacity, using a compartment method over the standard method to determine isotherms increases the reliability of the obtained results. ^{99m}Tc can be eluted from the particles with an efficiency of 59.5 ± 1.9 %, which should increase. Furthermore, the Mo breakthrough should be reduced.

References

[1] W.N. Association, Radioisotopes in medicine, http://www.world-nuclear.org/info/non-power-nuclear-applications/radioisotopes/radioisotopes-in-medicine/, Accessed on 24 february 2015

[2] P. Richards, W.D. Tucker, S.C. Srivastava, Technetium-99m: An historical perspective, The International Journal of Applied Radiation and Isotopes 33 (1982) 793-799.

[3] V.J. Molinski, A review of ^{99m}Tc generator technology, The International Journal of Applied Radiation and Isotopes 33 (1982) 811-819.

[4] IAEA, Human health campus - Design of the ^{99}Mo -> ^{99m}Tc generator, http://nucleus.iaea.org/HHW/Radiopharmacy/VirRad/Eluting_the_Generator/Generator_Module/Design_principles/index.html, Accessed on 2015

[5] IAEA, Non-HEU production technologies for molybdenum-99 and technetium-99m, IAEA, Vienna, Austria, 2013.

[6] M.R. Pillai, A. Dash, F.F. Knapp, Jr., Sustained availability of ^{99m}Tc: possible paths forward, Journal of nuclear medicine : official publication, Society of Nuclear Medicine 54 (2013) 313-323.

[7] L.P. Roobol, A.v.d. Reijden, I.R. de Waard - Schaik, H. Bijwaard, Productie en gebruik van medische radio-isotopen in Nederland. Huidige situatie en toekomstverkenning, RIVM Rapport 2017-0063

[8] A.G. Denkova, B.E. Terpstra, O.M. Steinbach, J.t. Dam, H.T. Wolterbeek, Adsorption of Molybdenum on Mesoporous Aluminum Oxides for Potential Application in Nuclear Medicine, Separation Science and Technology 48 (2013) 1331-1338.

[9] V. Miikkulainen, M. Leskelä, M. Ritala, R.L. Puurunen, Crystallinity of inorganic films grown by atomic layer deposition: overview and general trends, Applied Physics Reviews 113 (2013).

[10] R.L. Puurunen, Surface chemistry of atomic layer deposition: A case study for the trimethylaluminum/water process, Journal of Applied Physics 97 (2005) 121301.

[11] R.L. Puurunen, Growth per cycle in atomic layer deposition: A theoretical Model, Chemical Vapor Deposition 9 (2003) 249-258.

[12] D.M. King, J.A. Spencer Ii, X. Liang, L.F. Hakim, A.W. Weimer, Atomic layer deposition on particles using a fluidized bed reactor with in situ mass spectrometry, Surface and Coatings Technology 201 (2007) 9163-9171.
[13] D. Valdesueiro, G. Meesters, M. Kreutzer, J.R. van Ommen, Gas-Phase Deposition of Ultrathin Aluminium Oxide Films on Nanoparticles at Ambient Conditions, Materials 8 (2015) 1249-1263.
[14] D. Kunii, O. Levenspiel, Fluidization engineering, Elsevier2013.
[15] J.R. van Ommen, A. Goulas, Atomic layer deposition on particulate materials., Materials Today Chemistry 14 (2019).
[16] C.C. Kei, Y.S. Yu, J. Racek, D. Vokoun, P. Šittner, Atomic Layer-Deposited Al2O3 Coatings on NiTi Alloy, Journal of Materials Engineering and Performance (2014).
[17] R. Beetstra, U. Lafont, J. Nijenhuis, E.M. Kelder, J.R. Van Ommen, Atmospheric pressure process for coating particles using atomic layer deposition, Chemical Vapor Deposition 15 (2009) 227-233.
[18] E. Wiberg, N. Wiberg, A.F. Holleman, Inorganic chemistry, Academic Press ; De Gruyter, San Diego; Berlin; New York, 2001.
[19] A.G. Denkova, Synthesis of SBA-15, applying the knowledge, Fundamentals of tri-block copolymer self-assambly into solutions, and its realtion to nano-templating 2009.
[20] E.A. Group, ICP-OES and ICP-MS detection limit guidance, (2007).
[21] W. Verweij, CHEAQS Next, 2014-2017, pp. Calculating CHemical Equilibria in AQuatic Systems.
[22] M. Toor, B. Jin, Adsorption characteristics, isotherm, kinetics, and diffusion of modified natural bentonite for removing diazo dye, Chemical Engineering Journal 187 (2012) 79-88.
[23] P. Tkac, A. Paulenova, Speciation of molybdenum (VI) in aqueous and organic phases of selected extraction systems, Separ. Sci. Technol 43 (2008) 2641–2657.
[24] U.S.P. Convention, Official monograph USP 28, Sodium Pertechnetate 99mTc injection,
[25] M.A. Aulmann, G.J. Siri, M.N. Blanco, C.V. Caceres, H.J. Thomas, Molybdenum adsorption isotherms on y-alumina, Applied Catalysis 7 (1983) 139-149.
[26] R. Chakravarty, R. Ram, A. Dash, M.R. Pillai, Preparation of clinical-scale ^{99}Mo/^{99m}Tc column generator using neutron activated low specific activity ^{99}Mo and nanocrystalline gamma-Al_2O_3 as column matrix, Nuclear medicine and biology 39 (2012) 916-922.
[27] M.A. El-Absy, M.A. El-Amir, T.W. Fasih, H.E. Ramadan, M.F. El-Shahat, Preparation of ^{99}Mo/^{99m}Tc generator based on alumina ^{99}Mo-molybdate (VI) gel, J Radioanal Nucl Chem 299 (2014) 1859-1864.

Supplemental information

S1: Compartment method - derivation of the equation

In this compartment model the adsorption rate constant is given by k_1 and the desorption rate constant is given by k_2. The total mass of Mo in the solvent fraction can be described by $m_V = C_V V$ and total mass of Mo in the sorbent fraction by $m_M = q_M M$. Therefore, the adsorption and desorption can be described by: $\frac{dm_V}{dt} = -k_1 m_V + k_2 m_M$ and $\frac{dm_M}{dt} = k_1 m_V - k_2 m_M$, which can also be given by the matrix form: $\frac{d}{dt}\begin{bmatrix} m_V \\ m_M \end{bmatrix} = \begin{bmatrix} -k_1 & k_2 \\ k_1 & -k_2 \end{bmatrix}\begin{bmatrix} m_V \\ m_M \end{bmatrix}$. The system was solved by integrating, using the boundary conditions $\boldsymbol{m}(0) = \begin{bmatrix} m_{V,0} \\ m_{M,0} \end{bmatrix}$, resulting in : $\boldsymbol{m} = \frac{m_{V,0}+m_{M,0}}{k_1+k_2}\begin{bmatrix} k_2 \\ k_1 \end{bmatrix} + \left(\frac{(m_{V,0}+m_{M,0})k_1}{k_1+k_2} - m_{M,0}\right)\begin{bmatrix} 1 \\ -1 \end{bmatrix} e^{-(k_1+k_2)t}$.

S2: Nitrogen adsorption

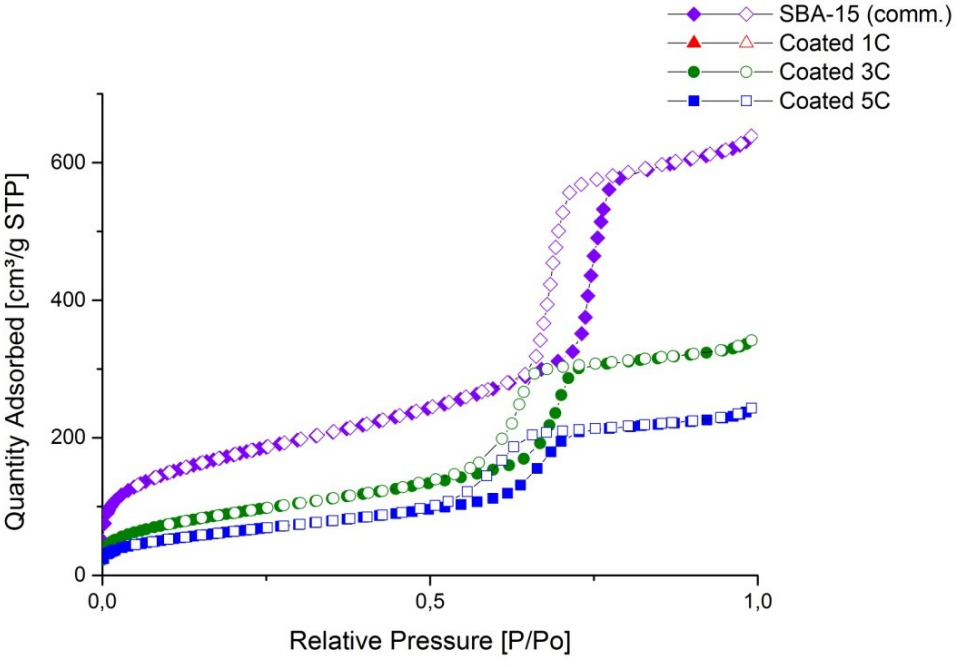

Figure S 1: Nitrogen adsorption and desorption plot of the different silica core sorbent materials. Both the adsorption (closed symbols) and desorption (open symbols) are given.

S3: X-ray diffraction patterns of the annealed silica sorbent material

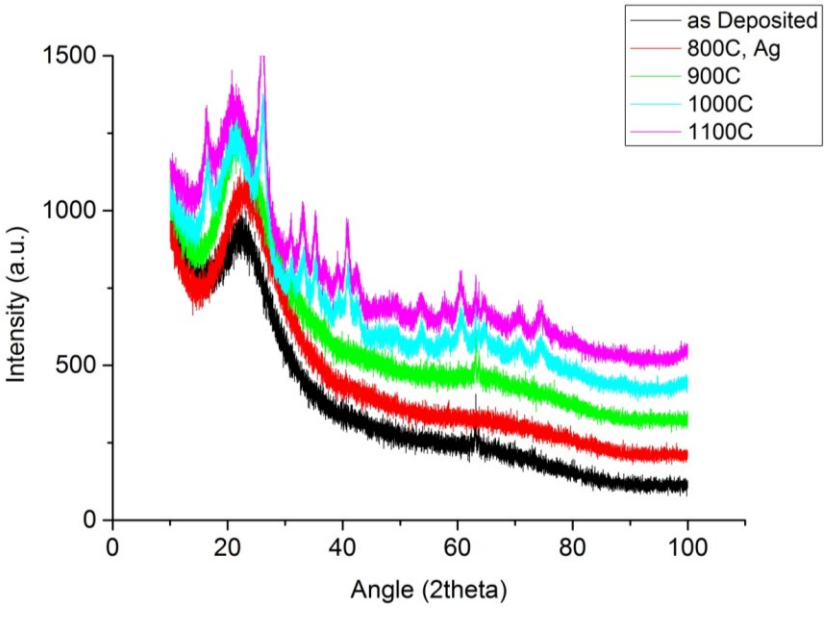

Figure S 2: XRD patterns of several annealed silica core sorbent materials compared to the as deposited layer (black line).

S4: Parameters for the extended Langmuir model

Table S 1: Calculated parameters of the extended Langmuir model for both the AA and silica core sorbent material.

	Extended Langmuir			
Sorbent	K_{eL} [ml/mg]	n_{eL}/C_{max} [ml/mg]	$q_{m,eL}$ [mg/g]	R^2
AA	5.67 ± 1.37	-0.015 ± 0.008	68.44 ± 3.94	0.819
Silica core	1.59 ± 0.6	-0.027 ± 0.024	104.6 ± 17.8	0.587

S5: pH change

During the kinetic experiments it was observed that the pH of the Mo - solution significantly changes when added to the sorbent material, up to one pH point for the silica core sorbent and 0.1 pH point for the AA sorbent. This increase in pH is quite rapidly and then levels off (figure x). This pH increase is extremely replicable and seems irrespective of the Mo starting concentration (Table S 2). This pH change is assumed to be caused by electrostatic interactions with the surface.

Table S 2 Final pH of the adsorption experiments for different starting concentrations of Mo and starting pH.

Sorbent	pH 5			pH 2
	10 mg/ml	5 mg/ml	1 mg/ml	5 mg/ml
AA	5.11	5.14	5.43	N/A
Silica core	6.01	6.05	6.10	4.46

4. Lutetium coating of nanoparticles by Atomic Layer Deposition[3]

Abstract

Atomic layer deposition (ALD) is a versatile gas phase coating technique that allows coating of complex structured materials, as well as high-surface area materials such as nanoparticles. In this work ALD is used to deposit a lutetium oxide layer on TiO_2 nano-particles (P25) in a fluidised bed reactor, to produce particles for nuclear medical applications. Two precursors were tested: the commercially available $Lu(TMHD)_3$ and the custom-made $Lu(HMDS)_3$. Using $Lu(TMHD)_3$ a lutetium loading up to 15 w% could be obtained, while $Lu(HMDS)_3$ only 0.16 w% Lu could be deposited due to decomposition of the precursor. Furthermore, it was observed that vibration-assisted fluidisation allows for better fluidisation of the nanoparticles and hence a higher degree of coating.

Keywords: Atomic layer deposition, Fluidised bed reactor, lutetium, lutetium acetylacetonate, lutetium tetra methyl heptadione, lutetium tris[bis(trimethylsilyl)amido)], titania p25, nuclear medical application

[3] A version of this chapter is published as J.L.T.M. Moret, M.B.E. Griffiths, J.E.B.M. Frijns, B.E. Terpstra, H.T. Wolterbeek, S.T. Barry, A.G. Denkova, J.R. van Ommen; Journal of Vacuum Technology A **38**, 022414 (2020); https://doi.org/10.1116/1.513444

Introduction

Lutetium has various applications. For instance, lutetium oxide is used in semiconductor devices due to its favourable high dielectric constant [1, 2], as well as in catalysis because of its ability to reduce band gap energy and hence increase the catalytic effect [3]. In the field of nuclear medicine, lutetium – specifically the radioactive isotope ^{177}Lu – is one of the most promising therapeutic radionuclides due to its favourable decay characteristics [4, 5]. Upon radioactive decay, ^{177}Lu emits both a β^- particle and a gamma ray. The energy of the β^- particle (498 keV) is ideal for the treatment of (metastasised) tumours, while the gamma energy is suitable for imaging purposes, making ^{177}Lu a so-called theranostic (therapeutic *and* diagnostic) radionuclide. To ensure weekly patient treatment of various cancer types, hospitals are currently relying on weekly supplies of ^{177}Lu. However, hospitals prefer an 'on demand' supply to ensure patient treatment that is independent of suppliers. Radionuclide generators are ideal for this purpose, providing not only 'on demand' supply but usually also high specific activity (i.e. activity per unit mass), which is important to realise optimal therapeutic outcome [6]. A radionuclide generator typically consists of a material packed in a column holding the parent radioisotope. Upon radioactive decay of this parent radioisotope, a daughter radioisotope is formed. When eluting the radionuclide generator, the desired daughter radioisotope can be obtained, while the parent radioisotope remains on the column. In view of the extended use of ^{177}Lu, a radionuclide generator for this isotope is very much desired. However, the parent radionuclide ^{177m}Lu is chemically and physically identical to the daughter, so conventional separation techniques cannot be used. However, radiochemical properties can be exploited [5, 7]. In order to make use of these radiochemical properties, the parent radionuclide should be strongly immobilised, so that upon decay only the ^{177}Lu is released and can be extracted. This process has been previously demonstrated by Bhardwaj et al [7], indicating that the yield depends on the stability of the parent-substrate complex. Furthermore, this process is most efficient when the released ^{177}Lu can escape from its environment, therefore, thin lutetium nanostructures are beneficial.

If we were to build such a radionuclide generator, aiming at one patient dose (7.4 GBq [8]) per day, a coating of at least 32 w% Lu is required

(Supplementary information S4) when considering an column elution efficiency of 80% and using 2 g of column material coated with natural occurring lutetium. To obtain this coating, atomic layer deposition (ALD) can be used. The advantage of using ALD is that a thin coating across the whole substrate can easily be fabricated due to the self-limiting behaviour of the process. Additionally, the amount of lutetium deposited can be tuned based on the application, as the lutetium content will depend on the number of cycles applied. In their 2012 review, Miikkulainen et al [9] reported three different Lu containing precursors used for ALD of lutetium-containing materials; namely $[Lu((Me_3Si)C_5H_4)_2Cl]_2$ [10], $Lu(^iPrO)_3$ [11], and $Lu[N(SiMe_3)_2]_3$ [12]. However, these precursors are not commercially available, which would be detrimental to practical implementation at a later stage. A fourth Lu-containing precursor, $Lu(TMHD)_3$, was reported by Roeckerath et al. [13]. This precursor is commercially available and was used in combination with a La containing compound to deposit the mixed-metal oxide $LaLuO_3$. The process is carried out in vacuum and, like with the other Lu precursors reported, Si-wafers were used as the substrate. Wafers have a small specific surface area in comparison to nanoparticles, which limits the amount that can be deposited. For the preparation of a radionuclide generator, nanoparticles having large surface area are necessary in order to achieve the desired Lu loading while still preserving the thin layer morphology.

The goal of this study is to deposit insoluble lutetium nanostructures on larger TiO_2 nanoparticle supports using a fluidised bed reactor (FBR). In an FBR, the substrate nanoparticles are suspended in a gas flow from below the reactor chamber, allowing the particles to behave as if they are a liquid. FBRs allow for scale-up of the coating process and permit good solid-gas mixing [14] and good heat transfer [15]. The applicability of lutetium tris(2,2,6,6-tetramethyl-3,5-heptanedionato) ($Lu(TMHD)_3$), lutetium tris hexamethyldisilazane ($Lu(HMDS)_3$), and lutetium tris acetylacetonate ($Lu(acac)_3$) in combination with the co-reactants O_3 and NH_3 is investigated in this paper.

Materials and methods

Chemicals

Lutetium tris(2,2,6,6-tetramethyl-3,5-heptanedionato) ($Lu(TMHD)_3$) was purchased from Strem chemicals (France). Lutetium trisacetylacetonate ($Lu(acac)_3$) was purchased from ABC Chemicals (Germany). Both substrates used in this study, silica (Aerosil 130) and titania (P25), were obtained from Evonik industries and dried overnight at 120°C before use. The carrier gas was 5.0 grade nitrogen. Ozone was produced with an ozone generator (Sanders C200) and synthetic air. NH_3 was obtained as mixture gas of 15w% NH_3 in N_2 from Linde gas. All precursors were transferred into custom-made stainless steel bubblers under inert conditions (nitrogen atmosphere). $LuCl_3$ was purchased from Strem Chemicals USA and used as received. Lithium bis(trimethylsilylamide) was purchased from Sigma-Aldrich chemical company and was used as received.

Preparation of $Lu(HMDS)_3$

$Lu(HMDS)_3$ was prepared according to Bradley et al. [16] Under inert conditions lithium bis(trimethylsilylamide) was dissolved in tetrahydrofuran and cooled. To this mixture $LuCl_3$ was added and after 24 h stirring at room temperature all solvent was removed under vacuum. The compound was then extracted to n-pentane and recrystalised three times before being purified by sublimation.

Thermogravimetric analysis

TGA measurements were performed using a Mettler Toledo TGA apparatus. A temperature sweep from 20 °C to 800 °C was undertaken with a heating rate of 10 °C/min in a nitrogen flow of 0.1 l/min.

Additional TGA measurements were performed using a National instruments TGA instrument, under inert loading conditions. The temperature sweep was from 20 °C to 600 °C with a heating rate of 10 °C/min in a nitrogen flow of 0.06 l/min.

Coating

Atomic layer deposition (ALD) was performed in a custom-made fluidised bed reactor (Figure 1). The fluidised bed reactor consisted of a glass column with

an internal diameter of 25 mm and a length of 500 mm mounted on a stainless steel windbox with a stainless-steel distributer plate. On top of the column a distributer plate and a metal chamber were also connected. The required dosing time for $Lu(TMHD)_3$ was calculated to be 23 minutes and $Lu(HMDS)_3$ to be 10 minutes. For the co-reactants O_3 and NH_3 the dosing times were calculated to be 1.62 minutes and 2 minutes, respectively. The precursor and co-reactant were alternatively fed into the reactor chamber from the bottom of the reactor using nitrogen as a carrier gas, separated by 10 minute purge pulses. The carrier gas flow was 0.5 l/min ($1.52 * 10^{-2}$ m/s). During the purge an additional nitrogen flow of 0.1 l/min ($0.30 * 10^{-2}$ m/s) was added. The lutetium precursor was kept in a custom-made stainless-steel bubbler heated with heating tape and was transported to the reaction chamber through heated stainless-steel tubing. The fluidised bed was heated using an infra-red lamp. The whole system was controlled using a PC with a custom made Labview program. The off gasses were washed with a series of wash bottles containing acidic water and kaydol oil and then an active carbon/HEPA filter.

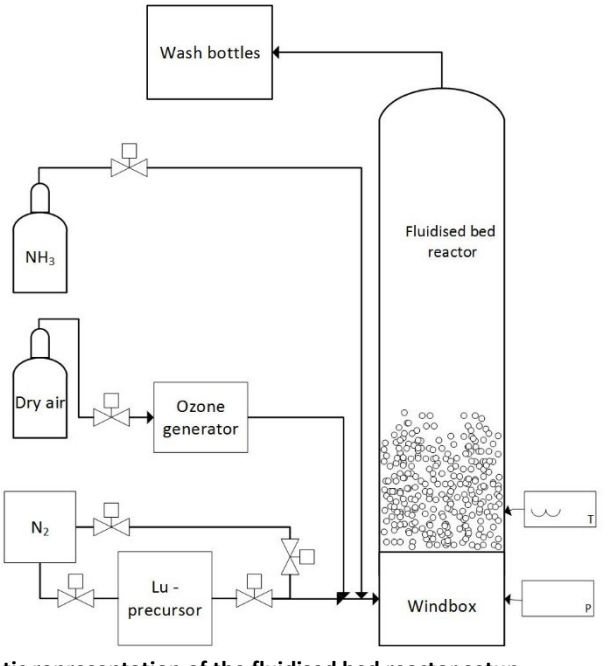

Figure 1: Schematic representation of the fluidised bed reactor setup.

Particle Analysis

The lutetium content of the obtained particles was determined using instrumental neutron activation analysis (INAA) at the Reactor institute Delft. For this purpose, the particles were irradiated with a thermal neutron flux of $5*10^{16}$ n /s m^2, epithermal neutral flux of 9 $*10^{14}$ n/s m², and a fast neutron flux of 3.6 $*10^{15}$ n/s m² for 5 minutes. Using the obtained lutetium mass fraction, the layer thickness can be determined according to Valdesueiro et al. [17]:

$$\delta = \frac{\sqrt[3]{\frac{6}{\pi} \cdot V_{Lu_2O_3}^{1p} + d_{3,2}^3} - d_{3,2}}{2}$$

with

$$V_{Lu_2O_3}^{1p} = \frac{x_{Lu}}{1 - \frac{M_{Lu_2O_3}}{2M_{Lu}} \cdot x_{Lu}} \cdot \frac{M_{Lu_2O_3}}{2M_{Lu}} \cdot \frac{\rho_{TiO_2}}{\rho_{Lu_2O_3}} \cdot \frac{\pi}{6} \cdot d_{3,2}^3$$

using a particle diameter of $d_{3,2}$ = 32.7 nm and density of 4200 kg/m³ [18]. The density of Lu_2O_3 as deposited was assumed to be 9420 kg/m³ [19]. Dividing the layer thickness by the number of cycles gives the growth per cycle (GPC). Transmission electron microscopy (TEM) and scanning electron microscopy-electron dispersive spectroscopy (SEM-EDS, Jeol) were used to image the coating. The chemical environment of the deposited lutetium was characterised using X-ray photoelectron spectroscopy (XPS).

Results and discussion

Precursor and co-reactant selection

The three potential precursors, $Lu(acac)_3$, $Lu(TMHD)_3$ and $Lu(HMDS)_3$, were first characterized using thermogravimetric analysis (TGA) to determine their applicability as ALD precursors. These TGA measurements were also used to calculate the vapour pressure of the compounds [20]. Considering the sensitivity of the precursors to air and moisture, measurements were carried in air as well as under a nitrogen atmosphere. Figure 2 shows indeed that air has a strong influence on the stability of the precursors. $Lu(HMDS)_3$ loaded under inert conditions shows a smooth mass loss curve during the analysis,

while the same measurement in air resulted in low mass loss and a high residual mass.

A suitable precursor should have one single mass loss over the temperature range tested with virtually no remaining mass [21]. Therefore, based on these criteria, $Lu(THMD)_3$ is the most suitable precursor from the candidates tested, with a single mass loss starting at 190°C and virtually no mass remaining. However, even though $Lu(HMDS)_3$ has about 20% residual mass, it shows potential if kept under inert conditions, because of its single mass loss starting at 110°C. The advantage of using $Lu(HMDS)_3$ over $Lu(THMD)_3$ is that $Lu(HMDS)_3$ can be used to deposit lutetium at lower temperatures. $Lu(acac)_3$, on the other hand, showed a stepwise mass loss, the first mass loss is between 280 °C and 400°C with the most significant mass loss at 310°C. The second mass loss is between 800°C and 850°C with around 80% of the initial mass remaining, indicating that the compound decomposes when heated. Therefore, $Lu(acac)_3$ was determined to be unsuitable to use as an ALD precursor (Figure 2).

Selection of a co-reagent for deposition of a lutetium containing film requires the ability to oxidise the precursor on the surface of the substrate. Initially, ozone was considered as a co-reagent because it is known for its strong oxidising potential. However, when an in water insoluble Lu layer is required a different co-reactant is needed. Lutetium is able to form several insoluble compounds like LuF and LuN [22]. Although HF is reported by Miikkulainen et al. [9] to make fluorides, it is strongly corrosive to the experimental setup and requires extra care when handled in the lab. Therefore, deposition of the nitride was preferred over the fluoride. The first experiments were carried out with ozone as co-reactant, as ozone was readily available.

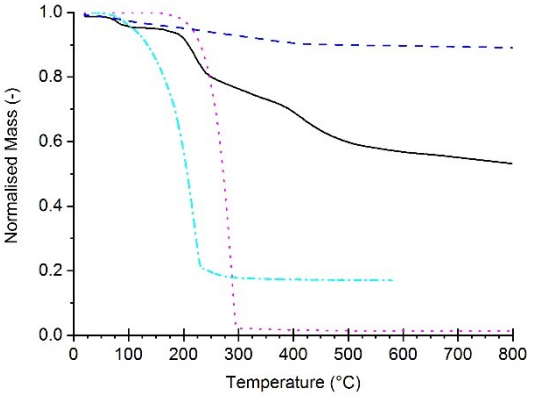

Figure 2: Thermogravimetric analysis using nitrogen as carrier gas of $Lu(acac)_3$ [——], $Lu(TMHD)_3$ [·····], $Lu(HMDS)_3$ [- - -] exposed to air during loading and $Lu(HMDS)_3$ [- · - · -] loaded under inert conditions.

Lutetium deposition

$Lu(TMHD)_3$ with O_3

The dosing time for $Lu(TMHD)_3$ was determined by calculating the dosing time for a single cycle based on the vapour pressure of $Lu(TMHD)_3$ at 210°C (P_{vap}=42.7 Pa). (See section S1 in the supplementary information for vapour pressure calculation and section S2 for dose time calculation.) These calculated dosing times were taken as the base case: 23 minutes of $Lu(THMD)_3$ and 0.81 min O_3 for 1.3 g titania P25 as the substrate. Titania P25 was chosen as substrate for its strong metal-substrate interactions [23]. The expected Lu deposition for one cycle is 1.5w%. The precursor pulses were separated by 10-minute purge pulses. Then several experiments with dosing times deviating from these times were conducted in order to determine if there is self-limiting behaviour. The lutetium loading on the particles was determined using INAA. The measurement uncertainty in the INAA measurements range from 2 to 4 % (Figure 3).

The first observation during the experiments is, due to the low mass of the nano-particle agglomerates, some of the substrate material was sticking to the top of the column and reducing the bed volume, which might have led to earlier saturation. Tapping the column caused this cake to break down and fall back into the fluidised bed. Alternatively, the cake could be broken down by a small back pulse of nitrogen after every cycle. This caking could have an

influence on the coating applied. As the cake was not fluidising, a limited surface area was then exposed to the gas flow and could be coated. The influence on the lutetium loading of the particles in the bed was minimal, as we found that the cake had a comparable Lu loading to the particles in the bed.

Secondly, the coating process is delicate. Because of the relatively high precursor temperature, heat sinks could easily occur in the setup, even with extensive insulation. These heat sinks caused condensation of the precursor compound, leading to blockage of the system, which in turn reduced the nitrogen carrier gas flow and therefore the amount of Lu deposited. Also, large heat sinks in the wind box were sometimes observed. This resulted in large deposition of precursor in the windbox (Fig. S3). On the other hand, hot spots in the bubbler caused by inhomogeneous heating of the bubbler could give unexpectedly high Lu loading on the particles. During the experiments a temperature difference up to 40 °C between the front and back of the bubbler was observed. Furthermore, during the experiments it became clear that the state of the $Lu(TMHD)_3$ was influenced by its residence time in the heated bubbler. Upon refilling of the bubbler, it was observed that the remaining precursor had changed colour (from white to pale yellow), indicating some amount of decomposition. During the initial TGA this was not noticed because the decomposition is a rather slow process compared to evaporation. An additional TGA of the $Lu(TMHD)_3$ precursor that was heated up and cooled down showed that its temperature response had changed and some mass remained (Fig. S2), indicating decomposition.

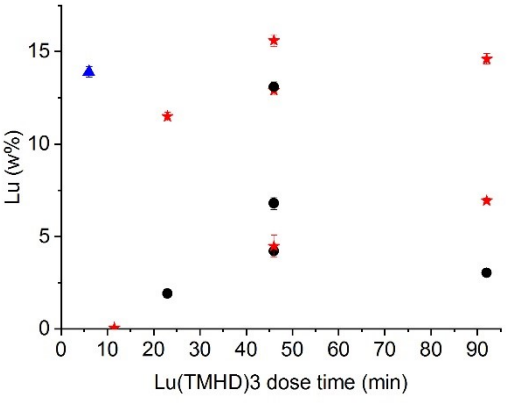

Figure 3: Lu weight fraction versus the dosing time of $Lu(TMHD)_3$. Precursor temperature was 210°C, reactor temperature was 230°C and 4 cycles were applied using O_3 as co-reactant. Red stars are obtained with vibration assisted fluidisation while black rounds refer to non-vibration assisted fluidisation. The blue triangle is an experiment were 25 cycles were applied. Error bars represent the measurement uncertainty of INAA. Because of the spread in results, it was chosen to report the individual experiments rather than the average.

Figure 3 shows the deposition of lutetium as function of the exposure time to $Lu(TMHD)_3$. It seems that for the experiments of 46 min and longer, self-limiting behaviour occurs, as the amount of lutetium deposited goes to an asymptotic value. Typically, vibration assistance led to higher Lu loading. Vibration assistance allows for more efficient fluidisation compared to non-vibration assisted fluidisation as it leads to effective breaking of inter particle forces [24]. This means that more bare surface area of the particles is exposed to the precursor, explaining the difference in Lu loading in both regimes. The corresponding growth per cycle (GPC) ranges from about 0.03 nm to about 0.11 nm. Compared to other lutetium ALD processes this GPC is relatively low [12]. Nevertheless, it should be noted that those processes were operated under vacuum and using a different precursor, therefore they are not directly comparable to the process described here. However, GPCs reported for other lanthanide $(TMHD)_3$ ALD processes [25] are comparable or are much lower [26]. The large deviation in the data can also be caused by the low vapour pressure of the precursor in combination with the gas flow rate. Possibly the vapour above the precursor in the bubbler cannot saturate the headspace quickly enough during a pulse cycle, resulting in a decrease in precursor concentration over the duration of the Lu pulse. Keeping this in mind, the Lu

precursor pulse was reduced to 6 minutes, while the number of cycles was increased (Blue triangle in Figure 3). The accumulated $Lu(TMHD)_3$ dose then was comparable to 3 cycles of 46 minutes. The deposited amount of Lu for the 25 cycles at 6 minutes per cycle was similar to the deposition for the 4 cycles at 46 minutes per cycle. Even though the accumulated $Lu(TMHD)_3$ pulse was shorter, the lutetium deposited was higher, which suggests that more and shorter pulses is indeed more effective for this low vapour pressure precursor. Furthermore, the GPC (Figure 6) seemed to decrease when the number of cycles was increased. We attributed this mainly to the TiO_2 having more active surface sites for chemisorption than the overlayers of Lu_2O_3. The first reaction deposits more Lu when $Lu(TMHD)_3$ reacts with TiO_2 surfaces than subsequent reactions where $Lu(TMHD)_3$ reacts with Lu_2O_3 surfaces [27-29]. This might also be due to decomposition of the precursor during use, since increasing the number of cycles resulted in exposing the precursor to high temperature over a prolonged period of time.

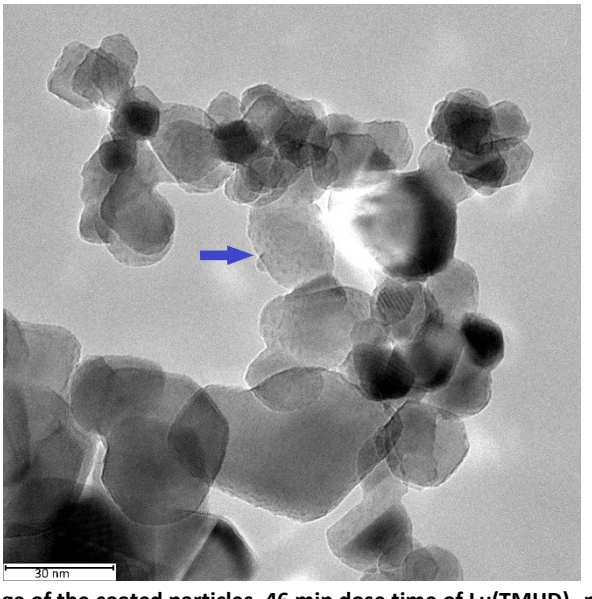

Figure 4: TEM image of the coated particles. 46 min dose time of $Lu(TMHD)_3$ per cycle and 4 cycles, loading 13 w% Lu. Arrow indicates possible island formation.

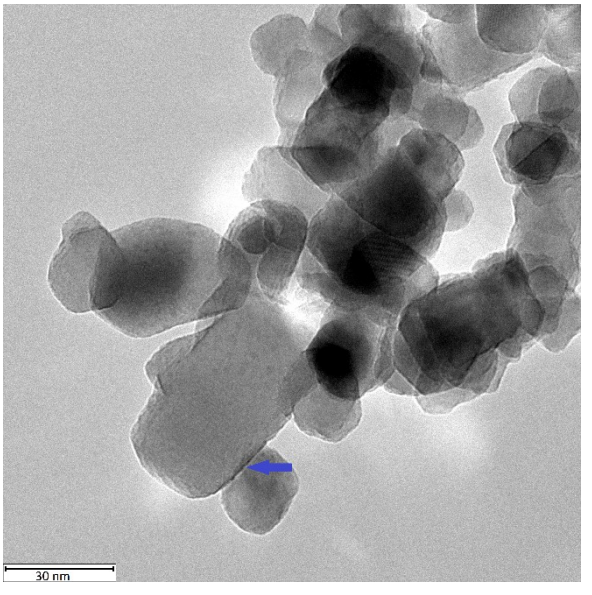

Figure 5: TEM images of coated particles. 6 min dose time of $Lu(TMHD)_3$ per cycle and 25 cycles, loading 14 w% Lu. The arrow indicates the deposited film.

The lutetium coating can be visualised using transmission electron microscopy (TEM), however it is very difficult to get an accurate visualisation of the coating within the 2 nm resolution. Because lutetium is a heavy element, it should appear darker in the image compared to the titania substrate. Using TEM, the layer thickness was estimated to be 0.75 nm and is therefore not comparable to the calculated layer thickness based on the INAA measurements (0.12 nm). However, the calculations are based on the assumption that a uniform layer is achieved. Due to agglomeration, it is possible that at some places a thicker coat resulted, while at other places no film was formed. As well, the dose time seems to have an influence on the layer growth. While 4 cycles at 46 min per cycle resulted in mainly island growth (see arrow Figure 4), 25 cycles at 6 min per cycle resulted in mainly film growth (see arrow Figure 5). This may be due to the preferential chemisorption or decomposition of the precursor at newly-nucleated Lu sites: in a long pulse, decomposition carried on with precursor being continually supplied, where with short pulses, once the oxide formed, decomposition of the precursor was less likely.

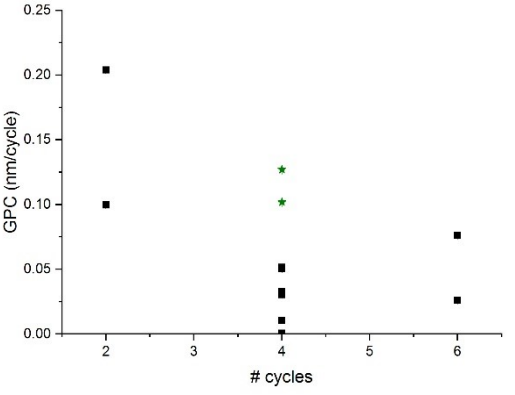

Figure 6: Growth per cycle for precursor pulses $Lu(TMHD)_3$ and O_3 46min and 1.6 min, respectively. The layer thickness is derived from the amount of lutetium deposited determined by INAA. The squares are non-vibration assisted, while the stars are vibration assisted. Because of the wide spread in results, it was chosen to report the individual experiments rather than the average.

$Lu(TMHD)_3$ and NH_3

For the application of the Lu-support particles in a radionuclide generator, an insoluble lutetium containing layer is needed. LuN is reported to be insoluble in water [22]. Using NH_3 as a co-reactant it is possible to deposit such a coating [9]. Therefore, coating experiments using $Lu(TMHD)_3$ and NH_3 were conducted. The Lu coating results are given in Figure 7. The Lu deposition is comparable to the coating results using ozone as co-reactant and again there was a large spread in the amount of lutetium that is deposited, which is again due to the varying fluidization conditions.

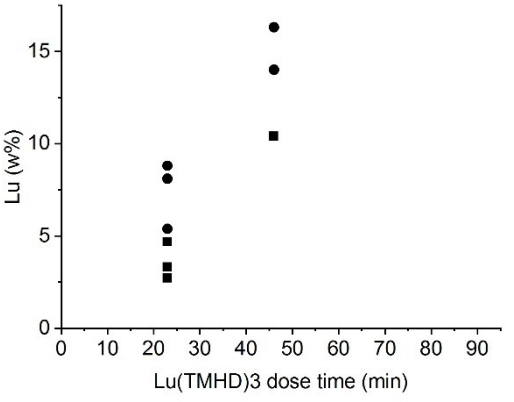

Figure 7: Lu loading as function of precursor dosing time using $Lu(TMHD)_3$ and NH_3. The circles represent a NH_3 pulse of 10 min while the squares represent a NH_3 pulse of 1 min. Precursor temperature was 210°C, deposition temperature was 230°C, and 4 cycles were applied. The Lu loading was determined by INAA. Because of the wide spread in results, it was chosen to report the individual experiments rather than the average.

In order to determine the deposition of N on the particles, X-ray photoelectron spectroscopy (XPS) measurements were performed on the coated particles. Unfortunately, no N was detected on the particles. Firstly, it was assumed that the amount of N on the particles was too small to be detected, indicating that the amount of NH_3 supplied to the reaction chamber was too low. However, a tenfold increase in the NH_3 pulse still resulted in no N present on the coated particles. This could indicate that the concentration of NH_3 in the co-reactant feed it too low (i.e. a conservative concentration was chosen for safety reasons) or that undesired reactions are taking place (i.e. decomposition of NH_3). M. Guarino et al [30] reported that TiO_2 is used to reduce NH_3 concentrations in gas flows. This could mean that NH_3 is decomposed at the substrates surface instead of oxidising the precursor molecules. Future research in our group will be aimed at investigating whether further increasing the NH_3 concentration does clearly lead to LuN deposition.

$Lu(HMDS)_3$ and O_3

The second precursor that showed potential in the TGA characterization was $Lu(HMDS)_3$. The advantage of using $Lu(HMDS)_3$ over $Lu(TMHD)_3$ is that the coating process can be undertaken at a lower bubbler temperature (130°C

instead of 210°C). However, $Lu(HMDS)_3$ is more sensitive to oxygen and moisture. Based on the calculated vapour pressure of $Lu(HMDS)_3$ (P_{vap}=130 Pa, For calculation see section S1 in the Supplementary Information) and the same assumptions made for the coating as with $Lu(THMD)_3$ the dosing times for a full monolayer are a 10 minute pulse of $Lu(HMDS)_3$ and a 0.81 minute pulse of O_3 separated by 10 minute purge pulses. These dosing times were taken as the base case. Again, experiments with other pulse times were conducted to prove self-limiting behaviour. The Lu deposition was determined via neutron activation analysis (INAA). For these measurements the measurement uncertainty was 2 to 7%.

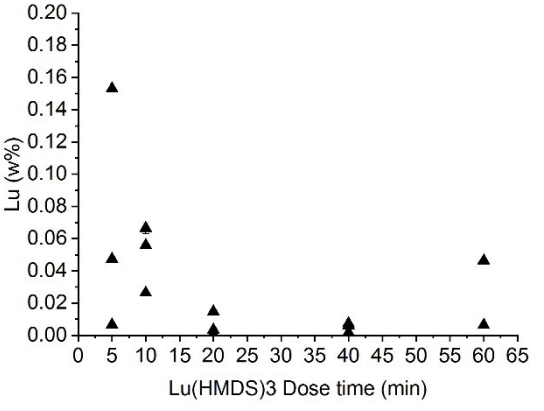

Figure 8: Lu deposition as function of the precursor dosing time for $Lu(HMDS)_3$ as precursor and ozone co-reactant. Precursor temperature was kept at 130°C while the reactor temperature was at 200°C. 4 cycles were applied. Lu deposition was determined by INAA. Because of the wide spread in results, it was chosen to report the individual experiments rather than the average.

Figure 8 shows that the Lu deposition using $Lu(HMDS)_3$ is much lower compared to $Lu(TMHD)_3$. The most likely explanation for these results is that the precursor decomposed during operation. This possibility was supported by visual inspection of the bubbler showing that the $Lu(HMDS)_3$ precursor had changed colour from white to a pale yellow. In addition, the experiment conducted with a freshly filled bubbler showed the higher Lu deposition compared to experiments conducted thereafter.

In previous research by G. Scarel et al. [12] using $Lu(HMDS)_3$ as precursor growth rates up to 0.5 nm/cycle were obtained. The growth rate of our

experiments was at least three orders of magnitude lower. It must be noted that Scarel's experiments were conducted on wafers while our experiments were performed on particles. The order of magnitude change in surface area can have an influence on the deposition rate.

Furthermore, as the TGA already indicated, $Lu(HMDS)_3$ decomposes when in contact with air and moisture as well as when heated up to elevated temperatures. Even though the bubbler was operated at relatively low temperature, prolonged exposure to elevated temperature led to decomposition of the precursor. All in all, $Lu(HMDS)_3$ seems less attractive to be used as ALD precursor than $Lu(THMD)_3$.

Conclusions

We have shown that atomic layer deposition of lutetium is possible at atmospheric pressure using a fluidised bed reactor. The amount of lutetium strongly depends on the precursor chosen. Even though TGA measurements indicated two potential precursors ($Lu(HMDS)_3$ and $Lu(TMHD)_3$), only the latter gave a significant amount of lutetium deposition. Furthermore, proper fluidisation of the bed has a strong influence on the amount of Lu deposited on the particles. Also, reproducibility of the system is low. Future research will aim at increased and more constant deposition of Lutetium on particles for use in a radionuclide generator.

References

[1] P. Darmawan, M.Y. Chan, T. Zhang, Y. Setiawan, H.L. Seng, T.K. Chan, T. Osipowicz, P.S. Lee, Lu_2O/Al_2O_3 gate dielectrics for germanium metal-oxide-semiconductor devices, Applied Physics Letters 93 (2008) 062901.
[2] P. Darmawan, P.S. Lee, Y. Setiawan, J. Ma, T. Osipowicz, Effect of low fluence laser annealing on ultrathin Lu_2O_3 high-k dielectric, Applied Physics Letters 91 (2007) 092903.
[3] D. Wu, C. Li, Q. Kong, Z. Shi, D. Zhang, L. Wang, L. Han, X. Zhang, Q. Lin, Photocatalytic activity of Lu 3+ /TiO 2 prepared by ball milling method, Journal of Rare Earths 36 (2018) 819-825.
[4] M.R.A. Pillai, S. Chakraborty, T. Das, M. Venkatesh, N. Ramamoorthy, Production logistics of ^{177}Lu for radionuclide therapy, Applied Radiation and Isotopes 59 (2003) 109-118.
[5] D.J. De Vries, H.T. Wolterbeek, The production of medicinal ^{177}Lu and the story of ^{177m}Lu: Detrimental by-product of future friend?, Tijdschrift voor Nucleaire Geneeskunde 34 (2012) 899-904.
[6] W.N. Association, Radioisotopes in medicine, http://www.world-nuclear.org/info/non-power-nuclear-applications/radioisotopes/radioisotopes-in-medicine/, Accessed on 24 february 2015
[7] R. Bhardwaj, A. van der Meer, S.K. Das, M. de Bruin, J. Gascon, H.T. Wolterbeek, A.G. Denkova, P. Serra-Crespo, Separation of nuclear isomers for cancer therapeutic radionuclides based on nuclear decay after-effects, Scientific reports 7 (2017) 44242.

[8] E.M. Agency, Lutathera, INN-lutetium(177Lu)oxodetreotide - Annex I, EPAR, 2018.
[9] V. Miikkulainen, M. Leskelä, M. Ritala, R.L. Puurunen, Crystallinity of inorganic films grown by atomic layer deposition: overview and general trends, Applied Physics Reviews 113 (2013).
[10] G. Scarel, E. Bonera, C. Wiemer, G. Tallarida, S. Spiga, M. Fanciulli, I.L. Fedushkin, H. Schumann, Y. Lebedinskii, A. Zenkevich, Atomic-layer deposition of Lu_2O_3, Applied Physics Letters 85 (2004) 630.
[11] H.L. Lu, G. Scarel, L. Lamagna, M. Fanciulli, S.-J. Ding, D.W. Zhang, Effect of rapid thermal annealing on optical and interfacial properties of atomic-layer-deposited Lu_2O_3 films on Si (100), Applied Physics Letters 93 (2008) 152906.
[12] G. Scarel, C. Wiemer, G. Tallarida, S. Spiga, G. Seguini, E. Bonera, M. Fanciulli, Y. Lebedinskii, A. Zenkevich, G. Pavia, I.L. Fedushkin, G.K. Fukin, G.A. Domrachev, Atomic Layer Deposition of Lu Silicate Films Using $[(Me_3Si)_2N]_3Lu$, Journal of The Electrochemical Society 153 (2006) F271.
[13] M. Roeckerath, T. Heeg, J.M.J. Lopes, J. Schubert, S. Mantl, A. Besmehn, P. Myllymäki, L. Niinistö, Characterization of lanthanum lutetium oxide thin films grown by atomic layer deposition as an alternative gate dielectric, Thin Solid Films 517 (2008) 201-203.
[14] D. Kunii, O. Levenspiel, Fluidization engineering, Elsevier2013.
[15] A.W. Weimer, Fluidized Bed Reactor Processes, in: A.W. Weimer (Ed.) Carbide, Nitride and Boride Materials Synthesis and Processing, Springer Netherlands, Dordrecht, 1997, pp. 169-180.
[16] D.C. Bradley, J.S. Ghotra, F.A. Hart, Low co-ordination numbers in lanthanide and actinide compounds. Part I. The preparation and characterization of tris{bis(trimethylsilyl)-amido}lanthanides, Journal of the Chemical Society, Dalton Transactions (1973) 1021-1023.
[17] D. Valdesueiro, G. Meesters, M. Kreutzer, J.R. van Ommen, Gas-Phase Deposition of Ultrathin Aluminium Oxide Films on Nanoparticles at Ambient Conditions, Materials 8 (2015) 1249-1263.
[18] E. Industries, Basic characteristics of AEROSIL fumed silica.
[19] C. Solutions, SciFinder - Substance Identifier, www.scifinder.cas.org, Accessed on 15 March 2016
[20] D.M. Price, Vapor pressure determination by thermogravimetry, Thermochimica Acta 367-368 (2000) 253.
[21] S. Barry, ALD precursor design and synthesis, ALD 2016Dublin, Ireland, 2016.
[22] Physical constants of Inorganic compounds, in: J.R. Rumble (Ed.) CRC handbook of Chemistry and Physics, CRC press, Ohio.
[23] J.S. Tauster, S.C. Fung, R.L. Garten, Strong metal-support interactions. Group 8 noble metals supported on TiO_2, Journal of the american chemical society 100 (1978) 170.
[24] S.W. Park, J. Woo Kim, H. Jong Choi, J. Hyung Shim, Vibration atomic layer deposition for conformal nanoparticle coating, Journal of Vacuum Science & Technology A: Vacuum, Surfaces, and Films 32 (2014) 01A115.
[25] J. Päiväsaari, M. Putkonen, L. Niinistö, A comparative study on lanthanide oxide thin films grown by atomic layer deposition, Thin Solid Films 472 (2005) 275-281.
[26] T. Boekhoudt, Coating Methodologies for Tracer Particles for Radioactive Particle Tracking in a Fluidised Bed, Chemical Engineering, Technische Universiteit Delft, Delft, 2016, pp. 65.
[27] R.L. Puurunen, Growth per cycle in atomic layer deposition: A theoretical Model, Chemical Vapor Deposition 9 (2003) 249-258.
[28] R.L. Puurunen, Surface chemistry of atomic layer deposition: A case study for the trimethylaluminum/water process, Journal of Applied Physics 97 (2005) 121301.
[29] R.L. Puurunen, W. Vandervorst, Island growth as a growth mode in atomic layer deposition: A phenomenological model, Journal of Applied Physics 96 (2004) 7686-7695.
[30] M. Guarino, A. Costa, M. Porro, Photocatalytic TiO2 coating-to reduce ammonia and greenhouse gases concentration and emission from animal husbandries, Bioresource technology 99 (2008) 2650-2658.

[31] S.F. Wright, D. Dollimore, J.G. Dunn, K. Alexander, Determination of the vapor pressure curves of adipic acid and triethanolamine using termogravimatric analysis, Thermochimica Acta 421 (2004) 25-30.

Supplementary information

S1. Vapour pressure calculation

Using the thermographimetric data vapour pressures can be calculated using the Langmuir equation [31]: $\left(\frac{1}{a}\right)\frac{dm}{dt} = p\alpha\sqrt{\frac{M}{2\pi RT}}$, with *a* the area of the pan [m²], *dm/dt* mass loss rate [kg/sm²], *M* molar mass [kg/mol], *R* the gas constant and *T* absolute temperature [K], *p* vapour pressure [Pa] and α vaporisation coefficient. Rewriting gives $p = k\upsilon$, with $k = \sqrt{2\pi R}/\alpha$ and $\upsilon = \left(\frac{1}{a}\right)\frac{dm}{dt}\sqrt{\frac{T}{M}}$. The *k* value is system depended. Hence, the system was calibrated using pentanediol, resulting in a *k* value of 130861. Next to this, the enthalpy of evaporation can be determined using the Clausius-Clapeyron equation [31]: $\ln p = A - \frac{\Delta H}{RT}$. The slope of the plot *ln v* against *1/T* gives $\Delta H/R$. So, the Enthalpy of evaporation is 84 kJ/mol for $Lu(TMHD)_3$ and 2.8 kJ/mol for $Lu(HMDS)_3$. (Figure S1). The difference in the enthalpies makes sense, as $Lu(TMHD)_3$ evaporates at a higher temperature than $Lu(HMDS)_3$.

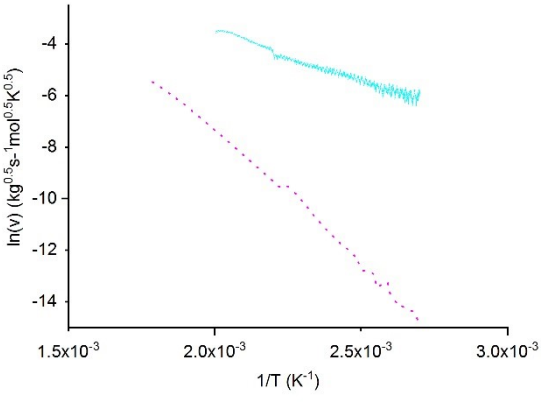

Figure S 1: Clausius-Clapeyron plot for $Lu(TMHD)_3$ [·····] from 97°C to 287°C and for $Lu(HMDS)_3$ [- - -] from 97°Cto 226°C

S2. Dose time calculation

P25 has a surface area of 52.4 m²/g. The carrier gas velocity (U_{ALD}) is 0.5 l/min. Vapour pressure of Lu(TMHD)3 was calculated at 38 Pa at 210°C and of Lu(HMDS)3 70 Pa at 120°C. It is assumed that $1.0*10^{18}$ molecules /m² can be

deposited assuming the projected size of Lu(TMHD)3 is 1nm². The ozone generator produces 200 mg/h and the NH3 supply had a concentration of 15 ppm.

The amount of moles that can be deposited was calculated by $M_{Lu} = \frac{O_{p25} * m * O_{mol}}{N_a}$ with O_{p25} the surface area of P25, m the mass of P25 used, O_{mol} the projected area of a precursor molecule and N_a Avogadro's constant.

Using the ideal gas law the concentration of Lu-precursor (C_{Lu}) in the gas phase can be calculated. The dosing time can then be calculated using $t_{Lu-prec} = \frac{M_{Lu}}{U_{ALD} * C_{Lu}}$.

Assuming Lu_2O_3 formation, per Lu atom ½ molecule of O_3 is needed. This results in a dosing time of $t_{O3} = \frac{M_{Lu} * 1/2}{C_{O3}}$. Assuming LuN formation, per Lu atom 1 molecule of NH_3 is needed. This results in a dosing time of $t_{NH3} = \frac{M_{Lu}}{C_{NH3}}$.

The expected weight fraction of Lu deposited per cycle is calculated $w\%Lu = \frac{M_{Lu} * 174.9}{M_{Lu} * 174.9 + m} * 100\%$

S3. Additional TGA: TGA of heated and cooled down precursor

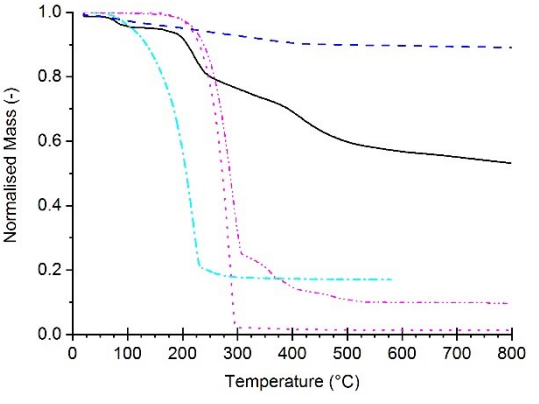

Figure S2: TGA of used Lu(TMHD)3 [┈┈] with the potential precursors as comparison. (Lu(acac)₃ [——], Lu(TMHD)₃ [┈┈], Lu(HMDS)₃ [- - -] exposed to air during loading and Lu(HMDS)₃ [—·—] loaded under inert conditions.)

S4. Wind box residue

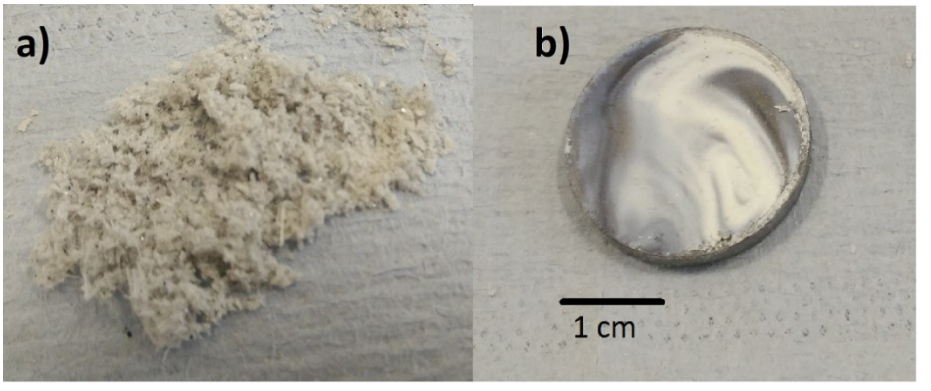

Figure S 3: Residue found in the wind box (a) and on the distributor plate (b) after some of the experiments. Lu content of the residue is determined at 5.45 w%.

S5. Calculations and assumptions to determine desired deposited amount of Lu on the substrate particles

A single patient dose (*PD*) requires 7.4 GBq of ^{177}Lu. Assumed is 1 day (*dt*) between executive elutions with 80% elution efficiency (*EF*) of a column that contains 2 g of coated column material (m_c). For the neutron activation of the particles is assumed that the irradiation takes 30 days (*t*) with a neutron flux (φ) of 10^{18} neutrons/cm²/s. It is also assumed that neutral occurring lutetium (*f*=2.59%) is used to coat the particles.

The parent activity needed for such a patient dose can be calculated using:

$$A_{0,^{177m}Lu} = \frac{\frac{PD}{EF}}{\left(e^{-\lambda_{177m_{Lu}} * dt} - e^{-\lambda_{177_{Lu}} * dt}\right) * -\frac{\lambda_{177_{Lu}}}{\lambda_{177_{Lu}} - \lambda_{177m_{Lu}}}} \quad [S1]$$

The needed activity can be converted into number of atoms by:

$$N_{177m_{Lu}} = \frac{A_{0,^{177m}Lu}}{\lambda_{177m_{Lu}}} \quad [S2]$$

Then the required Lu atoms for that activity can be calculated using equation S3:

$$N_{0,^{176}Lu} = \frac{N_{177m_{Lu}} - N_{0,177m_{Lu}} * e^{-\lambda_{177m_{Lu}} * t}}{\frac{b}{\lambda_{177m_{Lu}} - \varphi * x} * \left(e^{-\varphi * x * t} - e^{-\lambda_{177m_{Lu}} * t * x}\right) * \frac{1-f}{f} + \sigma_{176m_{Lu}} * \frac{\varphi}{\lambda_{177m_{Lu}} - \varphi * y} * e^{(-\varphi * y * t)} + b * \frac{1-f}{f} - \sigma_{176m_{Lu}} * \frac{\varphi}{\lambda_{177m_{Lu}} - \varphi * y} * e^{-\lambda_{177m_{Lu}} * t}} \quad [S3]$$

With

$$x = \sigma_{^{175}Lu} + \sigma_{^{175m}Lu} \quad [S4]$$

$$y = \sigma_{^{176}Lu} + \sigma_{^{176m}Lu} \quad [S5]$$

$$b = \sigma_{^{176m}Lu} * \varphi * \frac{\sigma_{^{175}Lu}}{y - x} \quad [S6]$$

The mass of the required amount of Lu can be calculated as follows:

$$w = \frac{\frac{m_{^{176}Lu}}{f}}{m_c} * 100\% \quad [S7]$$

With

$$m_{^{176}Lu} = \frac{N_{0,^{176}Lu}}{N_a} * M_w \quad [S8]$$

The physical constants belonging to lutetium are given below:

$\lambda_{^{177}Lu} = \frac{log(2)}{6.7}$ [d^-1]

$\lambda_{^{177m}Lu} = \frac{log(2)}{160.7}$ [d^-1]

$\sigma_{^{175}Lu} = 8e-28$; %cross section to produce 176Lu, [m²]

$\sigma_{^{175m}Lu} = 16e-28$; %cross section to produce 176mLu, [m²]

$\sigma_{^{176}Lu} = 2100e-28$; %cross section to produce 177Lu, [m²]

$\sigma_{^{176m}Lu} = 2e-28$; %cross section to produce 177mLu, [m²]

S6: Lutetium deposition with $Lu(acac)_3$ and O_3

Table S 1 Coating results for $Lu(acac)_3$ and O_3 on Aerosil130, using a dosing time of 33.55 min and 2.6 min, respectively. Error is based on n=3.

#cycles	Lu [w%]	GPC [nm/cycle]
2	0.0015 ± 0.002	$1.06 * 10^{-5}$
4	0.0034 ± 0.004	$1.23 * 10^{-5}$
8	0.0060 ± 0.006	$1.10 * 10^{-5}$
16	0.0080 ± 0.006	$7.29 * 10^{-6}$
32	0.0156 ± 0.013	$7.12 * 10^{-6}$

The amount of lutetium deposited using $Lu(acac)_3$ on the Aerosil substrate is very small. However, with an increased number of cycles an increased amount of Lu was deposited. Also, the amount of Lu deposited varied significantly between experiments, hence the large uncertainties reported. Larger amounts of Lu were deposited when the bubbler was just filled with fresh $Lu(acac)_3$. Referring back to the TGA measurements of $Lu(acac)_3$ (fig.1.) the low Lu deposition can be explained by decomposition of the precursor. Upon opening of the bubbler to check the precursor black flakes were discovered, confirming that $Lu(acac)_3$ decomposed.

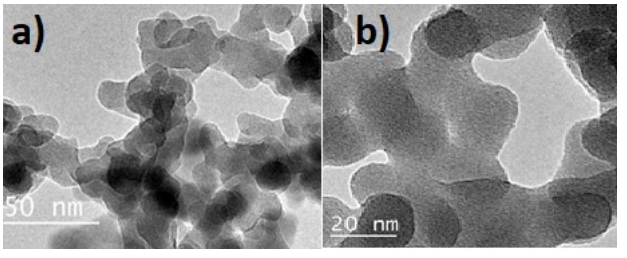

Figure S 4: TEM images of Lu coating on Aerosil 130 using Lu(acac)3 as precursor. The dark spots on the edge of the particles are assumed to be the Lu containing islands (a). These islands are even difficult to spot in the zoom in (b).

Calculating the layer thickness using previously mentioned equation, the lutetium oxide coat is only a hundredth of an Ångstrom. Therefore, only islands of Lu_2O_3 can be present. And, based on the growth per cycle calculations, these islands will be very small. This means that the islands are difficult to visualise using TEM. The darker spots on the edge of the particles are thought to be the Lu islands formed. The low deposition of Lu and the decomposition of the precursor resulted in finding better precursors for Lu-ALD.

5. ^{64}Cu enrichment using the Szilard-Chalmers effect – the influence of γ-dose[4]

Abstract

Cu is an important trace metal which plays a role in many biological processes. The radioisotope ^{64}Cu is often used to study such processes. Furthermore, ^{64}Cu finds applications in cancer diagnostics as well as therapy. For all of these applications ^{64}Cu having high specific activity is needed. ^{64}Cu can be produced in cyclotrons or in nuclear reactors. In this paper we study the effect of gamma dose on the production of ^{64}Cu according to the Szilard-Chalmers reaction using Cu(II)-phthalocyanine as a target. For this purpose, irradiations were performed in in the nuclear reactor of the Delft University of Technology using a novel irradiation facility helping to limit the dose produced by gammas present in the reactor pool. The obtained ^{64}Cu activity yield was in general above 60 % in accordance to the theoretical expected value. An increase in gamma dose has no significant influence on the obtained activity yield but increases the loss of Cu from Cu(II)-phthalocyanine up to 0.9% and hence decreases the specific activity that can be obtained. However, without optimisation, when reducing the gamma dose specific activities in the order of 30 TBq/g can be achieved.

Keywords: ^{64}Cu, Szilard-Chalmers reaction, Cu-phthalocyanine, gamma dose influence, high specific activity

[4] A version of this chapter is published as J.L.T.M. Moret, T.A. Hardens, O. van Batenburg, H.T. Wolterbeek, J.R. van Ommen, A.G. Denkova; Applied Radiation and Isotopes **160**; 109135 (2020); https://doi.org/10.1016/j.apradiso.2020.109135

Introduction

Cu is a trace element important in numerous biological processes like neurotransmitter synthesis and iron metabolism [1], but it is also involved in tumour angiogenesis and neurodegenerative diseases [2]. ^{64}Cu is an radioactive isotope of Cu with a half-life of 12.7h, decaying either by electron capture (44%) and β^+ (17.5%) to stable ^{64}Ni or by β^- (38.5%) to stable ^{64}Zn [3]. Because of these decay characteristics ^{64}Cu can be used in imaging i.e. in positron emission tomography (PET) and/or in radionuclide therapy [2, 4]. For these applications a specific activity of at least 1 TBq/g is needed [1].

^{64}Cu can either be produced by proton activation in a cyclotron or by neutron activation in a nuclear reactor. In proton activation nickel targets are bombarded with a beam of 15.5 MeV protons [5], allowing for the ^{64}Ni(p,n)^{64}Cu reaction to take place. After irradiation ^{64}Cu has to be separated from the Ni target. The advantage of this method is that non-carrier added ^{64}Cu is produced. However, special targets and cooling are needed [6]. In neutron activation either Zn or Cu targets can be used. The ^{64}Zn(n,p)^{64}Cu reaction needs fast neutrons to take place, which are available in irradiation facilities situated in the core of nuclear reactors [5]. In those facilities often only small volumes can be irradiated, making this production less likely to meet regular clinical demands [4]. Furthermore, long lived ^{65}Zn is co-produced as waste. For the ^{63}Cu(n,γ)^{64}Cu reaction thermal neutrons are needed. Although many reactors exist where this production route can be implemented, the specific activity of the produced ^{64}Cu is low. Using enriched targets and high flux reactors leads to higher specific activity, but increases costs. Moreover, as natural Cu contains 69.18% ^{63}Cu [3], using enriched targets only allows for a factor of maximum 1.5 increase in SA.

The problem of low specific activity ^{64}Cu can be overcome by utilising the recoil effect that occurs during (n,γ) reactions. In 1934 L. Szilard and T.A. Chalmers [7, 8] already showed that enriched ^{125}I can be produced using natural targets and chemical effects due to nuclear transformations. During neutron activation the energy of the excited state is distributed between the emitted prompt gamma and the newly formed product nucleus. (Figure 1). The recoil energy of the product nucleus can be calculated using the following equation: $E_r = 537 \frac{\bar{E}_\gamma^2}{M_r}$, in which E_r is the recoil energy of the product nucleus in eV, $\bar{E}_\gamma$ the average energy of the prompt gamma in MeV and M_r the mass of the recoiling atom in u. If the recoil energy is higher than the energy of

chemical bonds (typically in the order of eV [9]) the product nucleus will be released from its chemical environment [10]. Provided that the recoiling atoms and the target are in different chemical form, the enriched isotope can easily be collected.

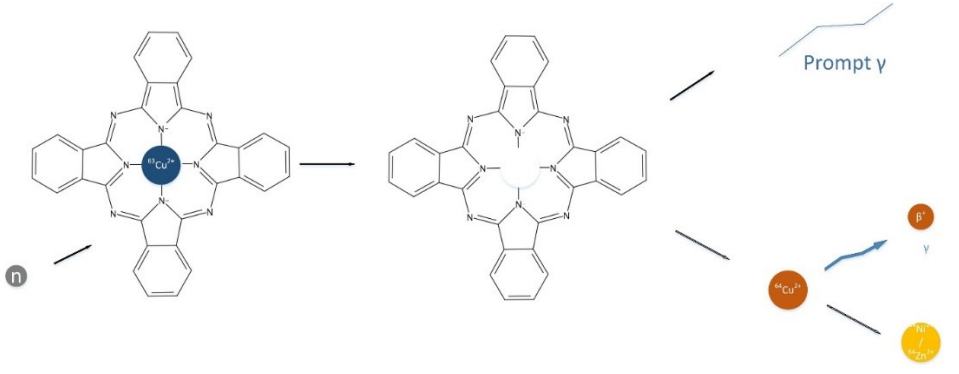

Figure 1: Schematic representation of the recoil effect induced by neutron activation of Cu-phthalocyanine. Upon neutron activation a nucleus in exited state is formed, which lowers its energy by directly emitting a prompt gamma. When this prompt gamma is energetic enough the daughter will recoil from the complex. This recoil effect can be used to produce enriched radionuclides. The formed ^{64}Cu will decay by electron capture, beta plus or beta minus decay.

In 1986 E.L. Hetherington et al. [11] reported that they could achieve specific activities up to 40 TBq/g Cu using 250 mg Cu(II)-phthalocyanine targets utilising the Szilard-Chalmers effect for an irradiation of 12 hours with a neutron flux of $5*10^{17}$ n/m²s. Longer irradiations resulted in lower specific activities. These irradiations were performed in the high flux Australian Reactor (HIFAR), a heavy water nuclear reactor. They concluded that using the Szilard-Chalmers method is an effective way to produce ^{64}Cu in nuclear reactors with a moderate thermal neutron flux, however no explanation was given for the decrease in specific activity. This decrease can possibly be attributed to the destruction of the target due to gamma radiation present in the reactor pool, leading to non-active Cu being released. However, the effect of the gamma dose on the specific activity of Cu-64 using this target or similar has not been researched so far.

The objective of the present paper is to investigate the influence of the gamma dose on the specific activity of ^{64}Cu using Cu(II)-phthalocyanine as a target and a special irradiation facility allowing for decreasing the gamma dose with little loss of neutron flux. Cu(II)-phthalocyanine is chosen because of its known chemical stability [12].

Method

The applied method was based on the procedure described by Hetherington et al. [11]. Samples of 1, 5, 10, 20 and 100 mg of Cu(II)-phthalocyanine (dye content 9, Sigma Aldrich, 11w% Cu) were irradiated in different facilities having different characteristics at the Hoger Onderwijs Reactor at the Delft University of Technology which we simply numbered as 1 and 2. We also used a special lead shielded facility allowing to change the gamma dose. This facility was denoted with FB3, 6 and 9, where 3, 6 and 9 refer to the cm of lead used. The neutron fluxes and the gamma dose of all facilities are given in Table 1. After irradiation the samples were opened and dissolved in 2 ml 97% H_2SO_4 (J.K. Baker). This solution was slowly transferred into 20 ml MilliQ water (in house Millipore MilliQ system). 12 ml of 20% NH_4OH (J.K. Baker) was added to the Cu(II)-phthalocyanine solution to neutralise the pH. The neutralised solution was transferred onto a 1 g acetic acid buffer conditioned Chelex 100 (100-200 mesh, sodium form, Sigma- Aldrich). A 1 M pH 5 acetic acid buffer was used to condition the Chelex. After all Cu(II)-phthalocyanine solution was passed over the column, the column was rinsed with 8 ml of MilliQ water. Then 16 ml of 1M HCl (stock solution was made by diluting 30% HCl (Sigma Aldrich)) was passed over the column to remove the trapped Cu-ions. Again, the column was rinsed with 8 ml of MilliQ water. All fractions were collected in separate PE counting vials (Wheatman). Also, the Chelex was transferred to a counting vial. All fractions were measured by gamma spectroscopy (Wallac² gamma counter, Perkin Elmer). The Cu concentration of all liquid fractions was determined by elemental analysis using ICP-OES (Optima 4300, Perkin Elmer). Using this data the yield of the reaction was determined according to: $yield = \frac{CPM_{HCl\ fraction(s)}}{\sum_1^i CPM_{i\ fractions}}$, with $CPM_{HCl\ fraction(s)}$ the activity measured in the HCl fractions that contain the freed ^{64}Cu and $\sum_1^i CPM_{i\ fractions}$ the sum of the activity of all the fractions. The enrichment factor of the Szilard-Chalmers method over normal neutron activation was calculated using: $EF = \frac{SA_{SC}}{SA_n}$, with $SA_{SC} = \frac{A_{HCl\ fraction}}{C_{Cu,ICP} * V_{HCl\ fraction}}$ and $SA_n = A_{produced}/m_{Cu}$.

Table 1: The neutron fluxes for the different irradiation facilities of the Hoger Onderwijs Reactor Delft that were used in this work with their corresponding gamma dose rates. The gamma dose was actually a combination of neutron and gamma dose since the two cannot be measured independently. To be able to compare the different facilities and the impact of the gammas, the gamma dose was normalised relative to the thermal neutron flux.

Name of Irradiation facility	Thermal neutron flux [n/m²s]	Epithermal neutron flux [n/m²s]	Fast neutron flux [n/m²s]	Gamma dose rate [Gy/s]	γ Dose per thermal neutron [fGy/n]
FB3	$6.22*10^{16}$	$1.44*10^{15}$	$4.39*10^{15}$	29.33	0.469
FB6	$5.64*10^{16}$	$1.04*10^{15}$	$3.28*10^{15}$	19.47	0.359
FB9	$3.88*10^{16}$	$6.00*10^{14}$	$1.94*10^{15}$	11.61	0.299
1 (a pneumatic facility)	$3.11*10^{16}$	$7.20*10^{14}$	$2.60*10^{15}$	62.65	2.01
2	$2.30*10^{17}$	$1.74*10^{16}$	$7.91*10^{16}$	485.8	2.11
^{60}Co source	-	-	-	0.210	-

Results and discussion

Cu(II)-phthalocyanine is irradiated with neutrons at the Reactor Institute Delft in the facilities shown in table 1. Samples receiving a 0.299 fGy/n, 0.359 fGy/n or 0.472 fGy/n dose are irradiated in the lead shielded facility. Samples receiving a 2.01 fGy/n or 2.11 fGy/n dose are irradiated in non-shielded facilities. After irradiation bond ruptured ^{64}Cu is separated from the bulk to obtain enriched ^{64}Cu using a Chelex 100 column. During the separation process it is observed that the conditioning of the Chelex is very important. Improperly conditioning caused Cu to leak into the first fraction and thereby lowering the yield obtained. Furthermore, a pH of 1 for the 0.1M HCl solution is essential to be able to remove $^{(64)}$Cu from the Chelex.

Influence of the gamma dose on yield and SA

Since the samples receive simultaneously a gamma and a neutron dose irrespective of the facility, we have performed irradiations in a ^{60}Co source to determine only the effect of gamma radiation.

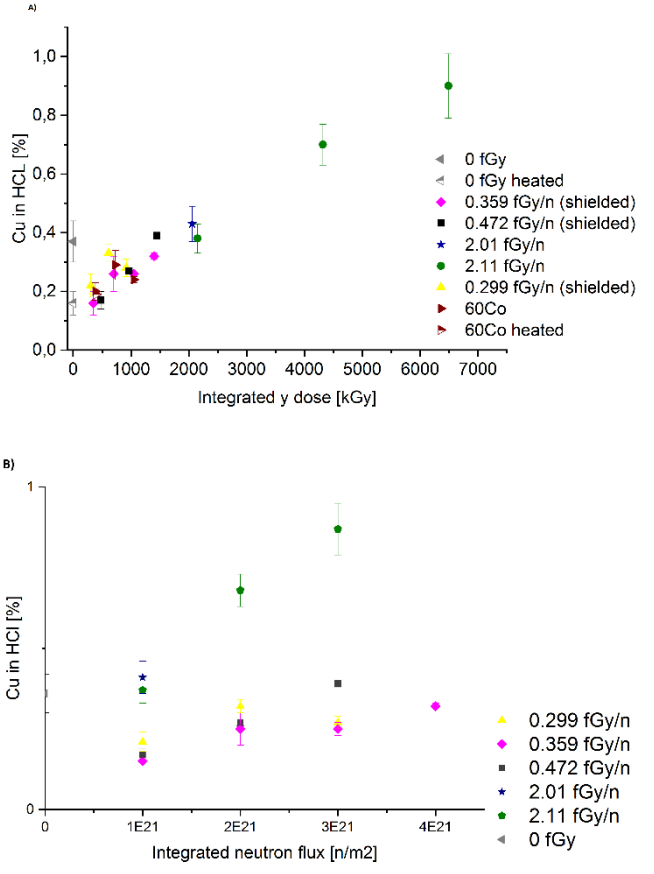

Figure 2: A) The release of Cu found in the HCl phase as function of the integrated y dose and B) the release of Cu found in the HCl phase as function of the integrated neutron flux. Cu(II)-phthalocyanine mass was 20 ± 0.2 mg. Error bars correspond to experimental uncertainties of n=3, except for the 0.359 fGy/n sample that received 700 kGy. There the error bars are based on n=8. The samples receiving 0.472 fGy/n, 0.359 fGy/n and 0.299 fGy/n were irradiated in a lead shielded facility, while the samples receiving 2.01 fGy/n and 2.11 fGy/n were non-shielded

Figure 2A shows clearly that the integrated radiation dose received by the samples influences the amount of Cu that is released from the Cu(II)-phthalocyanine complex. Although there is always a small percentage of Cu that is freed, even if irradiations do not take place, an evident increase of Cu -release is observed as the integrated radiation dose increases. The irradiations performed in the ^{60}Co source show that the gamma dose is most likely responsible for the loss of Cu since the released amount of Cu is comparable to samples that received a comparable integrated radiation dose constituted

of both a gamma dose and a neutron dose. Only the non-irradiated, non-heated sample is an outlier with its 0.37 ± 0.07 % Cu loss.

The Cu loss naturally has a direct influence on the SA produced. The effect of the integrated γ dose on the SA is given in Figure 3. According to expectations, the SA decreases when the integrated γ dose received by the samples increases. Furthermore, it can be observed that the lead shielded samples, corresponding to 0.299 fGy/n, 0.359 fGy/n and 0.472 fGy/n, have a higher SA compared to the non-shielded samples, corresponding to 2.01 fGy/n and 2.11 fGy/n, when normalised relative to the neutron flux. This indicates that the lead shielding used to reduce the gamma dose during neutron irradiation has a strong influence on the quality of ^{64}Cu that can be produced. However, the reduction in SA (i.e. factor 2 between the lowest and the highest integrated γ-dose) is not as strong as the Cu loss (i.e. factor 5.6 between the lowest and the highest integrated γ-dose) might have suggested. The SA also depends on the activity produced, which depends on the neutron flux and irradiation time. The samples with the highest integrated gamma dose received four times more neutrons compared to the samples receiving the lowest integrated gamma dose. This has a direct influence on the SA and will compensate for the Cu loss to some extent.

The gamma dose does have a small influence on the yield (Figure 4). The yield of the non-shielded irradiation samples (i.e. 2.01 fGy/n and 2.11 fGy/n) varies between 46% and 56%, while for the other samples it ranges between 58% and 64%. The theoretical yield is calculated to be 60.7%. ^{64}Cu is known to emit many energetic prompt gammas [13]. If the resulting recoil energy from these prompt gammas is high enough, chemical bonds will break [10]. The Cu bonds in Cu(II)-phthalocyanine are 6.96 eV [14, 15], so the minimal energy of the prompt gammas required to break that bond is 904 keV. 60.7% of the prompt gammas emitted during neutron irradiation of Cu are 904 keV or higher [13]. The reduction in yield can be caused by reduced solubility or crosslinking of the Cu(II)-phthalocyanine complexes limiting the amounts that can be extracted. The theoretical maximum SA (carrier free ^{64}Cu) that can be reached is $1.4*10^5$ TBq/g. However, there will always be some degree of Cu loss due to interactions within molecules, resulting in a lower SA.

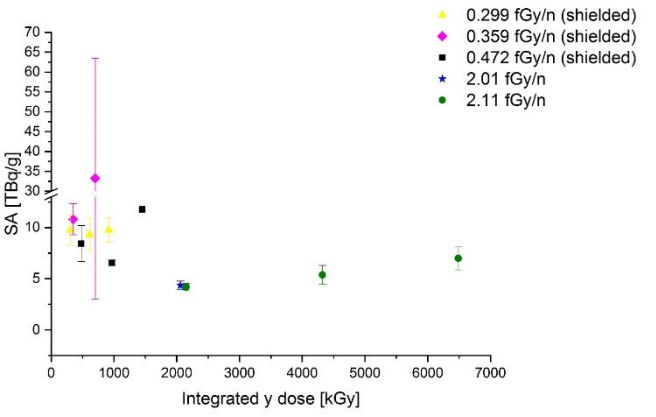

Figure 3: The specific activity (SA, calculated at the End of Bombardment) as function of the integrated γ dose. Cu(II)-phthalocyanine mass is 20 ± 0.2 mg. Error bars correspond to experimental uncertainty based on n=3, except for the 0.359 fGy/n that received 700 kGy. There the error bars are based on n=8. The samples receiving 0.472 fGy/n, 0.359 fGy/n and 0.299 fGy/n were irradiated in a lead shielded facility, while the samples receiving 2.01 fGy/n and 2.11 fGy/n had no shielding.

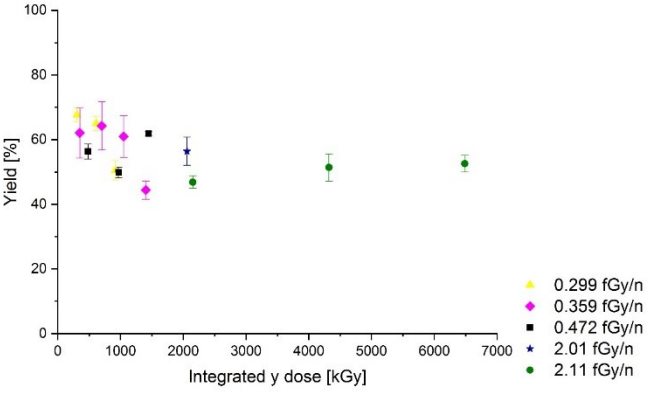

Figure 4: The ^{64}Cu yield as function of the integrate gamma dose. Cu(II)-phthalocyanine mass is 20 ± 0.2 mg. Error bars correspond to the experimental uncertainty based on n=3, except for the 0.359 fGy/n sample that received 700 kGy. There the error bars are based on n=8. The samples receiving 0.472 fGy/n, 0.359 fGy/n and 0.299 fGy/n were irradiated in a lead shielded facility, while the samples receiving 2.01 fGy/n and 2.11 fGy/n had no shielding.

Influence of the neutron dose on the yield and SA

When determining the gamma dose in the different irradiation facilities, the determined dose also contains a contribution due to the neutrons. It is impossible to determine these doses independently. Furthermore, the

different irradiation facilities have different neutron fluxes. To compensate for the different neutron fluxes the samples are irradiated for the same integrated neutron flux, producing the same amount of activity. The influence of this irradiation time difference is expected to be minimal as saturation activity is reached at much longer irradiation times. (Supplemental information S1) The ^{64}Cu yield, SA, and Cu in HCl phase is determined for four different integrated neutron fluxes (Figure 5)

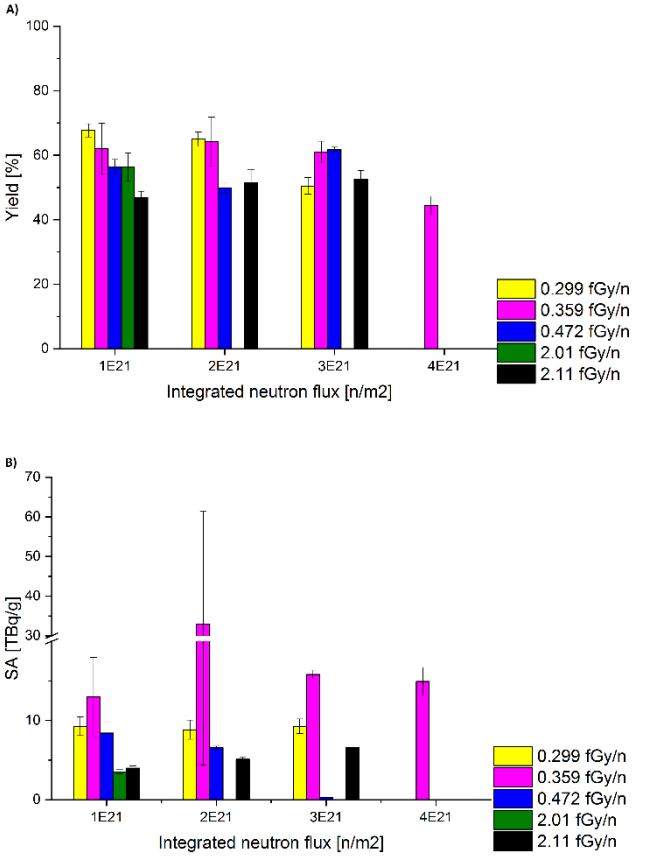

Figure 5: The influence of different y-dose to neutron ratios as function of the integrated neutron flux on the A) ^{64}Cu yield ($yield = \frac{CPM_{HCl\ fraction(s)}}{\sum_1^i CPM_{i\ fractions}}$), B) Specific activity (SA). In all cases the mass of Cu(II)-phthalocyanine was 20 ± 0.2 mg. The irradiation times are taken such that the integrated neutron flux was the same for each facility. Error bars correspond to experimental uncertainty based on n=3. The 0.473 fGy/n, 0.359 fGy/n and 0.229 fGy/n samples have lead shielding to reduce the gamma dose during irradiation.

The ^{64}Cu yield is not affected by the increase in integrated neutron flux (Figure 5 A). As the yield is defined as a fraction of the total activity, it is independent from the activity produced. On the other hand, the SA is affected by the increase in integrated neutron flux (Figure 5 B). It is expected that at some point the saturation SA is reached. With the increase in Cu loss it is more likely for the SA to decrease, unless the Cu loss and the increase in activity are at equilibrium. Furthermore, a clear difference between the shielded samples (0.473 fGy/n, 0.359 fGy/n and 0.299 fGy/n) and the non-shielded samples (2.01 fGy/n and 2.11 fGy/n) is visible. The non-shielded samples have a lower SA and a higher Cu loss compared to the shielded samples, for the same integrated neutron flux. This difference can clearly only be attributed to the gamma dose received by the samples.

Influence of irradiation time and sample mass on yield and SA

The influence of sample mass is also evaluated as function of irradiation time. The irradiations are performed in the facility having the best results of the previous experiments. The gamma dose divided by the neutron flux is in this case 0.395 fGy/n.

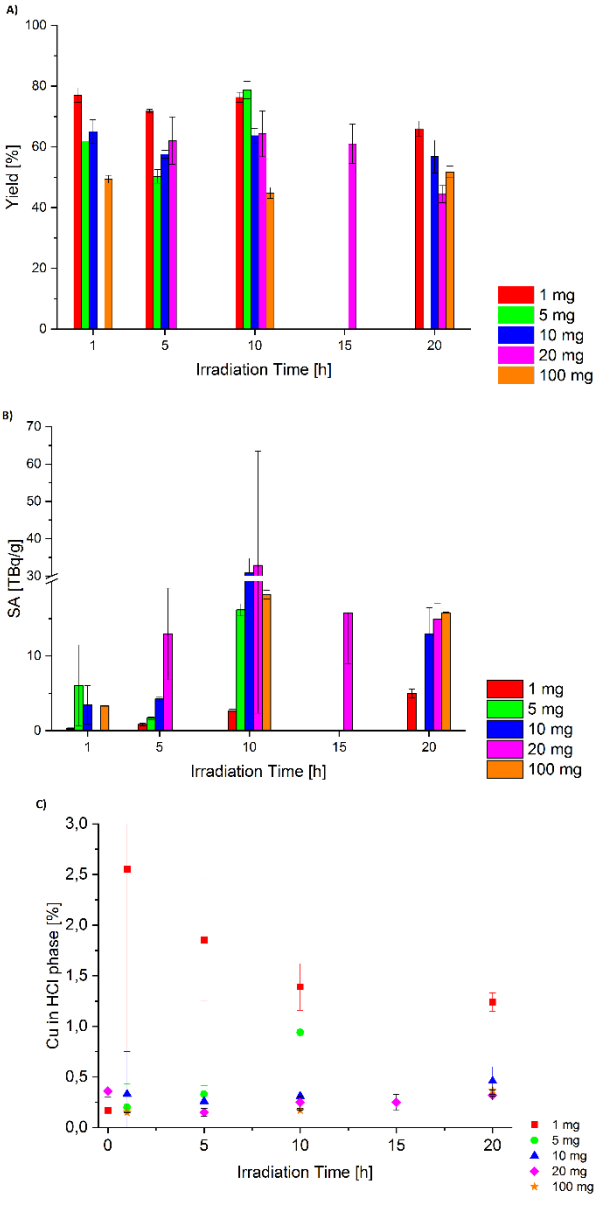

Figure 6: The influence of neutron irradiation time for different Cu(II)-phthalocyanine masses, at a constant gamma dose to neutron flux 0.395Gy/n, on the A)^{64}Cu yield ($yield = \frac{CPM_{HCl\ fraction(s)}}{\sum_1^i CPM_{i\ fractions}}$), B) Specific activity (SA) and C) Cu in HCl phase. Error bars correspond to experimental uncertainty based on n=3, except for the 10h 20 mg, 15h 20 mg and 100 mg samples. Those error bars are based on n=8, n=5 and n=1 respectively. All samples are dissolved in 2 ml H_2SO_4, except for the 20h 100 mg sample. That is dissolved in 3 ml H_2SO_4. The amount of Cu in the HCL phase is given as a fraction of the amount of Cu originally present in the sample.

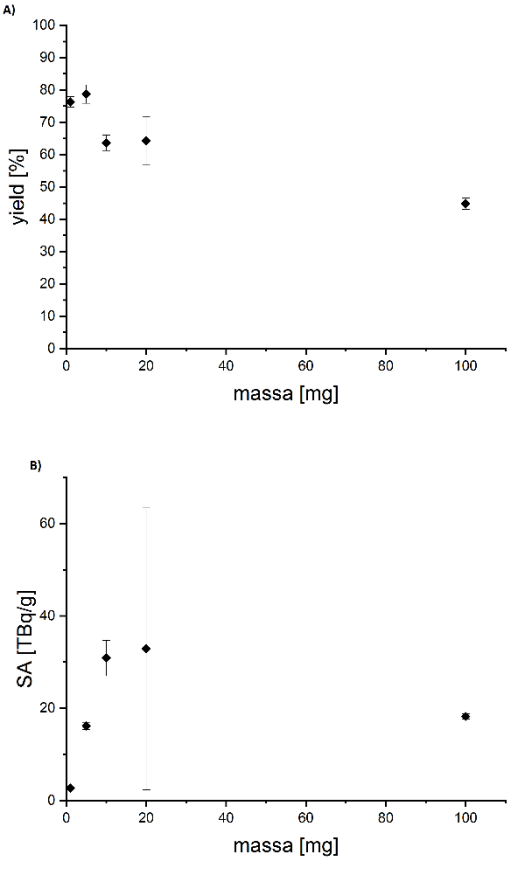

Figure 7: The influence of mass on the A) yield and B) SA of samples irradiated 10 h in the FB6 facility with a constant gamma dose to neutron flux of 0.395Gy/n. Error bars are based on the experimental uncertainty of n = 3, except for the 20 mg samples. Those are based on n = 8.

The yields of the different irradiations are above the expected value of 60.7% for most of the masses tested (Figure 7A), except for the 100 mg samples. The expected yield is an estimate based on the reported probability of the occurrence of the prompt gammas and the energy necessary to break one of the Cu(II)-phthalocyanine bonds. Deviations in either the reported probabilities or bond energies can cause higher than expected yields, as well as release of Cu from the complex. Furthermore, when increasing the Cu(II)-phthalocyanine mass the yield decreases for the same irradiation time. A possible explanation for this decrease in yield could be that the maximum solubility of Cu(II)-phthalocyanine in sulphuric acid is reached. For the samples up to 20 mg this is unlikely because the vials are shaken thoroughly before

transferring the solution into water and no relative increased amount of activity was measured in the Chelex phase. However, for the 100 mg samples this is a likely scenario, as the solution became strongly viscous and relatively more activity was found in the Chelex fraction. Increasing the volume of H_2SO_4 to dissolve the 100 mg sample, increased the yield (49.4 ± 1.3 % when using 2 ml H_2SO_4 vs 51.8 ± 1.9 % when using 3 ml H_2SO_4) Secondly, the Chelex could be saturated, but it is unlikely since it is in a 2 to 10 fold excess relative to the amount of Cu ions. Moreover, if the Chelex would be saturated an increased amount of activity would be present in the first 2 fractions collected which was not observed.

The specific activity of ^{64}Cu produced increases with the irradiation time and then stabilises for all masses (Figure 6B). This is expected as with longer irradiation times more atoms get activated and there is only a marginal increase in Cu loss when the samples are irradiated in the lead shielded facility (Figure 6C). However, these results are contradicted by what is previously reported by E.L. Hetherington et al. [11]. They reported a decrease in SA when increasing the irradiation time. It must be noted that the flux used by E.L. Hetherington et al. was approximately 10 times higher than in this research. This could explain for an important part the differences in the reached specific activity. Furthermore, the shortest irradiation time reported by E.L. Hetherington [11] was 12 h, while in this research that was 1h. It is likely that the gamma dose received by E.L. Hetherington's samples is much higher compared to the lead shielded samples in this research, resulting in the different behaviour in SA between their results and the results presented here. For the 10 mg, 20 mg and 100 mg the percentage of Cu found in the HCl phase is only slightly elevated when irradiated for 20 h, where both the neutron dose and gamma dose can have a profound influence. For the 1 mg sample it can be seen that there is a strong increase in Cu dissociation for the irradiated samples compared to the non-irradiated sample.

The enrichment factor (EF) is defined as the factor with which the specific activity is increased using the Szilard-Chalmers method compared to no separation from the target for the same irradiation conditions. An order of magnitude increase is found between the 1 mg and 10 mg samples (Figure 6B). This can be explained by the fact that for those samples there is also an order of magnitude difference between the SAs produced using the Szilard-Chalmers effect.

Influence of temperature on stability and structure

During neutron irradiation in the various facilities not only the gamma dose plays a role, but also elevated temperatures can have an effect. To determine whether the different temperatures of the irradiation facilities have an influence on the amount of Cu released from the Cu(II)-phthalocyanine complex two sets of samples are heated up to 150 °C for 5 hours, of which one set is irradiated with gammas first in the ^{60}Co source to receive a dose of 402 kGy. The results are given in Table 2.

Table 2: The Cu release from the Cu(II)-phthalocyanine complex when heated for 5 hours at 150°C compared to the release when also irradiated with gammas. The ^{60}Co irradiated samples received a gamma dose of 402 kGy. The samples contained 20 ± 0.3 mg of Cu-phthalocyanine. The experimentally determined standard deviation is based on n=3.

	Sample Treatment			
	Non-treated	**^{60}Co**	**^{60}Co and heating**	**Heating only**
Cu concentration [mg/l]	0.497 ± 0.096	0.251 ± 0.046	0.217 ± 0.005	0.233 ± 0.009
Cu in HCl phase [%]	0.371 ± 0.074	0.196 ± 0.032	0.192 ± 0.024	0.164 ± 0.038

Heating seems to have little effect on the stability of the Cu(II)-phthalocyanine complex. The total thermal energy supplied to the molecules is with $E = k_B * T = 5.84 * 10^{-21} J = 0.036\ eV$ at 150 °C not enough to break the bonds. Literatures shows that also higher temperatures show little change in the structure [16]. Hassan et al [16] shows that when heating Cu(II)-phthalocyanine crystal films to temperatures above 300 °C the Cu(II)-phthalocyanine would sublimate and leave a blue film. At temperatures of 240 °C the crystals can change from the α – to the β- form, with the only difference between the forms is a difference in the overlap with their neighbouring molecules [17]. The α – form is known to be less sensitive to irradiation while the β- form shows a higher sensitivity to irradiation [18]. Due to neutron irradiation the temperature in the irradiation facilities can reach up to 60°C.

Conclusions

Cu(II)-phthalocyanine complexes can be used in the production of high specific activity ^{64}Cu using the Szilard-Chalmers effect. Irradiations in the different facilities showed that the gamma dose in those facilities does have an influence on the Cu released from the complex and so has an influence on the SA produced. The higher the gamma dose in the facility the lower the SA. SA from 6.99 TBq/g (6488 Gy) to 33 TBq/g (700 Gy) are obtained. The decrease in SA is caused by an increase in Cu released from the phthalocyanine due to the gamma dose received. Reducing the gamma dose can be obtained by using a lead shielding during irradiation. The temperature in the facilities is not likely to have an effect on the SA produced.

References

[1] K.I. Kim, S.J. Jang, J.H. Park, Y.J. Lee, T.S. Lee, K.S. Woo, H. Park, J.G. Choe, G.I. An, J.H. Kang, Detection of increased ^{64}Cu uptake by human copper transporter 1 gene overexpression using PET with $^{64}CuCl_2$ in human breast cancer xenograft model, Journal of Nuclear Medicine 55 (2014) 1692-1698.

[2] E. Laura, L. Mansi, C. Giuseppe Lucio, New Issues for Copper-64: from Precursor to Innovative Pet Tracers in Clinical Oncology, Current Radiopharmaceuticals 6 (2013) 117-123.

[3] B.N. Laboratory, Exploring the table of isotopes, http://ie.lbl.gov/education/isotopes.htm, Accessed on 2014

[4] R. Chakravarty, S. Chakraborty, A. Dash, $^{(64)}Cu^{(2+)}$ Ions as PET Probe: An Emerging Paradigm in Molecular Imaging of Cancer, Molecular pharmaceutics 13 (2016) 3601-3612.

[5] D.W. McCarthy, R.E. Shefer, R.E. Klinkowstein, L.A. Bass, W.H. Margeneau, C.S. Culter, C.J. Anderson, M.J. Welch, Efficient production of high specific activity ^{64}Cu using a biomedical cycloton, Nuclear Medical Biology 24 (1997) 35-43.

[6] V.S. Le, J. Howse, M. Zaw, P. Pellegrini, A. Katsifis, I. Greguric, R. Weiner, Alternative method for (64)Cu radioisotope production, Applied radiation and isotopes : including data, instrumentation and methods for use in agriculture, industry and medicine 67 (2009) 1324-1331.

[7] L. Szilard, T.A. Chalmers, Detection of neutron liberated from Beryllium by gamma rays: A new technique for inducing radioactivity, Nature (1934) 494-495.

[8] L. Szilard, T.A. Chalmers, Chemical separation of the radioactive element from its bombarded isotope in the Fermi effect, Nature 134 (1934) 462.

[9] K. Song, D. Le, Chemical Bond Energies, https://chem.libretexts.org/Core/Physical_and_Theoretical_Chemistry/Chemical_Bonding/Fundamentals_of_Chemical_Bonding/Bond_Energies, Accessed on 2018

[10] H.K. Yoshihara, T. Sekine, Hot Atom Chemistry, Handbook of nuclear chemistry 2011, pp. 1333-1378.

[11] E.L. Hetherington, P.J. Sorby, J. Camakaris, The preparation of high specific activity Copper-64 for medical diagnosis, Applied Radiation and Isotopes 37 (1986) 1242-1243.

[12] G.N. Shapkin, M.A. Soroka, P.N. Moskalev, Use of sulfonated diphthalocyanines of lanthanides for enrichment of radioactive isotopes, Radiokhimiya 19 (1977) 857-859.

[13] J.K. Tuli, Thermal neutron capture gamma-rays, https://www.orau.org/ptp/PTP%20Library/library/DOE/bnl/tnc/ngtblcontentbyn.shtml.htm, Accessed on 2018

[14] Y.-R. Luo, Bond Dissociation energies, CRC handbook of Chemistry and Physics 2009, pp. 9-65 to 69-98.
[15] T.A. Sanderson, bond energies.
[16] A.K. Hassan, R.D. Gould, Structural studies of thermally evaporated thin films of cooper phthalocyanine, Physica Status Solidi (a) 132 (1992) 91-101.
[17] A. Cruickshank, C. Dotzler, S. Din, S. Heuts, M. Toney, M. Ryan, The crystalline structure of copper phthalocyanine films on zno, journal of the american chemical society 134 (2012) 14302-14305.
[18] H.K. Yoshihara, H. Ebihara, Crystal-structure effects in hot-atom chemistry copper phthalocynine, The Journal of Chemical Physics 45 (1966) 896-901.
[19] G. Choppin, J.-O. Liljenzin, J. Rydberg, C. Ekberg, Chapter 17 - Production of Radionuclides, in: G. Choppin, J.-O. Liljenzin, J. Rydberg, C. Ekberg (Eds.) Radiochemistry and Nuclear Chemistry (Fourth Edition), Academic Press, Oxford, 2013, pp. 513-544.

Supplemental information

S1: ^{64}Cu activity produced for the different thermal neutron fluxes used

To visualise where the ^{64}Cu production will saturate the activity produced is calculated for the different thermal neutron fluxes, according to equation S1.1. For the calculations 2.2 mg of natural Cu is taken. This corresponds to 20 mg of Cu-phthalocyanine. The saturation activity (i.e. the maximum activity that can be produced) can be calculated using equation S1.2. [19]

$$\frac{dN64Cu}{dt} = \sigma_{63Cu} * \varphi_{therm} * N_{63Cu} - \sigma_{64Cu} * \varphi_{therm} * N_{64Cu} - \lambda_{64Cu} * N_{64Cu} \qquad [S1.1]$$

$$N_{64Cu,s} = \frac{\sigma_{63Cu} * \varphi_{therm} * N_{63Cu,0}}{\lambda_{64Cu}} \qquad [S1.2]$$

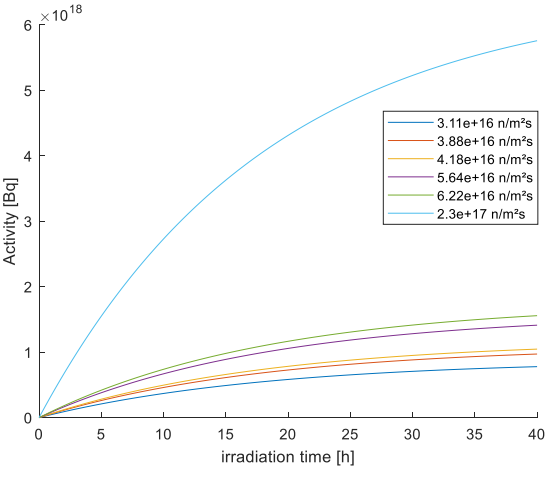

Figure S 1: ^{64}Cu activity produced as function of irradiation time for the different thermal neutron fluxes used in this work. The calculations are based on 2.2 mg of Cu, which corresponds with 20 mg of Cu-phthalocyanine.

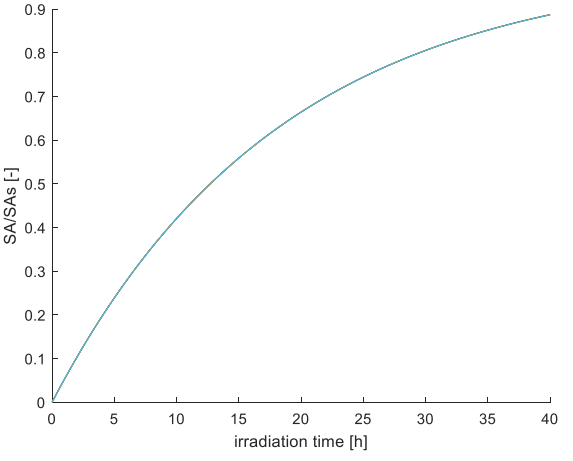

Figure S 2: ^{64}Cu activity produced normalised over the saturation activity.

S2: FTIR results of Cu-phthalocyanine

In an attempt to visualise the effect of irradiation on the structure of the Cu(II)-phthalocyanine samples are analysed using infrared spectroscopy (FTIR). However, no change is measured between the irradiated samples and control sample, as can be seen in Figure S 3. FTIR is a bulk measurement method, while irradiation effects mostly take place at molecular level. Therefore, it is concluded that compared to the bulk, the damaged molecules are severely outnumbered.

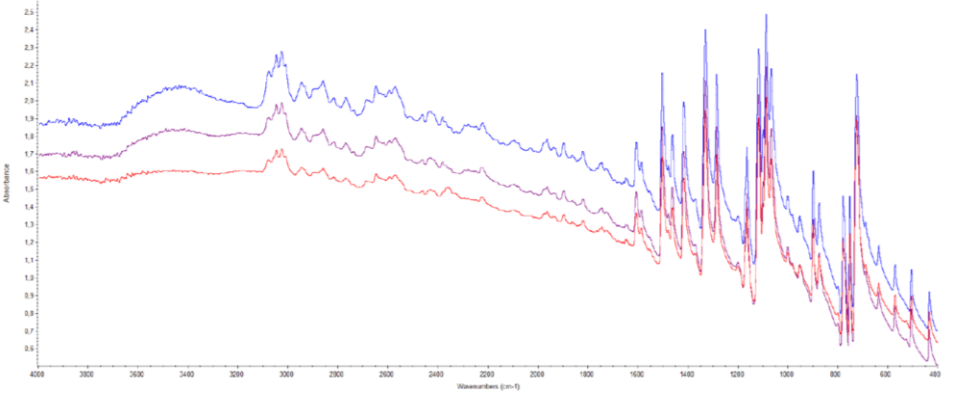

Figure S 3: Result from the FTIR measurements of Cu(II)-phthalocyanine samples receiving an integrated neutron dose of 2.9 *10^{21} n/m² and 1052 kGy (blue) or a gamma dose 386 kGy (purple) compared to a control (non – irradiated) (red).

6. Conclusions and Outlook

The overall aim of this thesis was to look into novel alternative production methods to obtain medically relevant radionuclides having high specific activity, focusing mostly, but not only, on the potential of ALD in this respect. As pointed out in more detail in Chapters 1 and 2, high specific activity of produced radionuclides is essential for application in nuclear medicine. Furthermore, hospitals prefer 'on demand' supply of medical radionuclides. In this thesis we have shown what is the potential of alternative production methods to produce radionuclides starting from the development of column material for radionuclide generators able to separate chemical identical mother and daughter pairs to evaluation of radiation conditions on the ability to produce high specific activity radionuclides.

Atomic layer deposition for medical applications

Conclusions

Due to the versatility of ALD many different materials can be coated with a broad range of precursors and co-reactants [1], resulting in atomically thin conformal coatings chemisorbed to the substrate material. For the production of medical radionuclides processes that operate at the atomic level are often required [2, 3], targets that are chemically stable and resistant to radiation, and having good heat dissipation properties, especially when applied in charged particle reactions. Considering these requirements, it is clear that ALD can contribute in the development of novel approaches for radionuclide production having the needed medical quality. In this thesis two cases have been explored as described below.

The first case is related to the development of sorbent materials for ^{99}Mo/^{99m}Tc generators. Atomic layer deposition is routinely used in the semi-conductor industry [1], but this coating technique is so versatile that it can be utilised in variety of other applications such as modification of sorbent surfaces. Due to anticipated changes in the production process of ^{99}Mo, sorbent materials with an increased adsorption capacity are needed to ensure that sufficient activity of ^{99m}Tc can be delivered to the hospitals without changing the generator size. To this extent a high surface area silica material is coated with an alumina layer using ALD to modify the isoelectric point of the

sorbent and increase it adsorption capacity for Mo. Even though the surface modification only resulted in a marginal increase in adsorption capacity compared to the current standard, it showed that there is potential in achieving much higher adsorption capacities provided that the right substrate is used and that alumina coating is crystalline. A crystalline coating would require an additional annealing step, as ALD coatings are mostly amorphous.

The second case refers to the development of a $^{177m}Lu/^{177g}Lu$ generator. Deposition of Lu using ALD is not common. In the literature only a few reports [4-6] describe the deposition of lutetium containing layers. These papers have in common that the coating takes place in vacuum, and on wafers. In this thesis we have shown that Lu-ALD is also possible at atmospheric pressure and on particles using a fluidised bed reactor, detrimental for the scale - up of the process. However, the coating process is delicate and depends on the chosen precursor, co-reactant, and temperature of bubbler and reactor chamber. Furthermore, the successful implementation of ALD coated materials in radionuclide production is strongly dependent on the ability to produce stable, insoluble coated materials. The loss of even ppb amounts will result in a decrease in specific activity that can be produced and therefore require insoluble layers. The prepared Lu_2O_3 coatings appeared to possess too high solubility to achieve the production of high specific activity of Lu-177g. Nitrides or fluorides being insoluble, would be more suitable but will require the use of NH_3 or HF as co-reactants in target production. As described in this thesis an attempt has been made to produce an insoluble LuN layer using NH_3, however no N is found in the layer, most likely due to the catalytic decomposition of the NH_3 on the TiO_2 surface.

Outlook production

The biggest challenge using ALD is to obtain thin insoluble layers, which are needed to produce radionuclides with high specific activities. The demand for radioisotopes of the lanthanide series is expected to grow due to the development of new treatments [7]. This growth in demand requires efficient production methods, as lanthanides are rare earth elements and are therefore sparse and rather expensive. Using thin insoluble layers high specific activity can be produced efficiently. However, little is known on using co-reactants required to produce such layers (such as fluorides, nitrides etc) in combination with lanthanides, requiring further research [8]. Parameters of interest in this process are the co-reactant concentration, pulse time, precursor and reactor temperature. Furthermore, the stability of the precursor needs to be

considered, to increase the reproducibility of the coating process, especially when prolonged exposures to elevated temperatures are needed.

For the production of some radionuclides the stable isotopes needed as a target have insufficient natural abundance, requiring an enrichment step (i.e. the percentage of the stable isotope has to be increased). Chemistry-wise this has no impact on the ALD coating process and the stability of the coating. However, it will have an impact on the availability and costs of the ALD-precursors. These precursors will have to be custom-made, potentially reducing the scale-up possibilities and making the whole production method expensive. The impact of the need to use precursors having enriched has to be assessed taking into account efficiency of synthesis and possible recycling of the target materials.

Gamma dose influence

Conclusions

In this work we showed that the gamma dose received during neutron activation has a strong influence on the specific activity that can be produced when utilising hot atom chemical effects using Cu-phthalocyanine as model substance. The simultaneously received neutron dose did not have an effect on the specific activity up the investigated dose. Increased gamma dose led to increased loss of Cu from the phthalocyanine complex. Irradiations in a lead shielded facility reduced the gamma dose received by the samples and resulted in much less Cu loss compared to non-shielded irradiated samples, which lead to higher specific activity produced.

Outlook effects

In the work presented in this thesis only a relatively small amount of Cu-phthalocyanine was irradiated per sample. To be able to produce clinically relevant amounts of ^{64}Cu by the Szilard-Chalmers effect the production process needs to be optimised. Increasing the activity produced can be accomplished by either irradiating the samples in an irradiation facility with at least a five-fold increase in thermal neutron flux compared to the flux used in this thesis or increase the amount of Cu-phthalocyanine irradiated from 100 mg to minimally 500 mg. The effect of longer irradiations on the achievable specific activity is not yet clear. Increasing the neutron flux reduces the amount of facilities that can be used around the world for production and

most probably increases the gamma dose the samples will receive. An optimal balance between the amount of lead shielding and neutron flux needs to be determined. Increasing the Cu-phthalocyanine mass will inevitably result in an increase in prompt gammas emitted proportional to the mass increase, which can have an effect on the dose received by the Cu(II)-phthalocyanine. However, as discussed before, this dose effect will surely be much less compared to the dose received due to the gammas of the neutron field. Furthermore, the amount of Cu(II)-phthalocyanine can have an influence on the work up procedure. However, the overall effect of this mass increase on the quality of product produced is not yet known.

The effect of the gamma dose is relevant for the production of many other radionuclides making use of hot atom chemistry principles. However, utilising the Szilard-Chalmers method requires sufficient percentage of the emitted gammas to have high energy so that reasonable yields can be obtained. It therefore remains the question, whether the decrease in loss due to gamma dose reduction by lead shielding will be sufficient in the production of enough activity of high specific activity radionuclides with few energetic prompt gammas.

References

[1] V. Miikkulainen, M. Leskelä, M. Ritala, R.L. Puurunen, Crystallinity of inorganic films grown by atomic layer deposition: overview and general trends, Applied Physics Reviews 113 (2013).
[2] G. Choppin, J.-O. Liljenzin, J. Rydberg, C. Ekberg, Chapter 17 - Production of Radionuclides, in: G. Choppin, J.-O. Liljenzin, J. Rydberg, C. Ekberg (Eds.) Radiochemistry and Nuclear Chemistry (Fourth Edition), Academic Press, Oxford, 2013, pp. 513-544.
[3] K. Hashimoto, Y. Nagai, 8.14 - Radionuclide Production, in: A. Brahme (Ed.) Comprehensive Biomedical Physics, Elsevier, Oxford, 2014, pp. 219-227.
[4] M. Roeckerath, T. Heeg, J.M.J. Lopes, J. Schubert, S. Mantl, A. Besmehn, P. Myllymäki, L. Niinistö, Characterization of lanthanum lutetium oxide thin films grown by atomic layer deposition as an alternative gate dielectric, Thin Solid Films 517 (2008) 201-203.
[5] G. Scarel, C. Wiemer, G. Tallarida, S. Spiga, G. Seguini, E. Bonera, M. Fanciulli, Y. Lebedinskii, A. Zenkevich, G. Pavia, I.L. Fedushkin, G.K. Fukin, G.A. Domrachev, Atomic Layer Deposition of Lu Silicate Films Using $[(Me_3Si)_2N]_3Lu$, Journal of The Electrochemical Society 153 (2006) F271.
[6] H. Schumann, I.L. Fedushkin, M. Hummert, G. Scarel, E. Bonera, M. Fanciulli, Crystal and molecular structure of $[(n^5\text{-}C_5H_4SiMe_3)_2LuCl]_2$: A precursor for the procution of Lu_2O_3 films, Z. Naturforsch 59b (2004) 1035-1038.
[7] L.P. Roobol, A.v.d. Reijden, I.R. de Waard - Schaik, H. Bijwaard, Productie en gebruik van medische radio-isotopen in Nederland. Huidige situatie en toekomstverkenning, RIVM Rapport 2017-0063
[8] E. Kessels, Overview of all materials prepared by atomic layer deposition (ALD) - an up-to-date and colourfull periodic table, https://www.atomiclimits.com/2019/01/28/overview-of-all-materials-prepared-by-atomic-layer-deposition-ald-an-up-to-date-and-colorful-periodic-table-to-download/, Accessed on 7 October 2019

Acknowledgements

Even though only my name is on the cover, this work would not have finished if it was not for the help of a lot of people. Therefore, I would like to take this opportunity to express my gratitude.

Experimental research requires analysis and sometimes it is better to leave that to the expert. Therefore, I would like to thank Baukje Terpstra for the many INAA measurements she had to do on the many batches of Lu-particles I made and then had to deal with my impatience waiting on the results. Also many thanks to Willie Rook for taking the time to explain nitrogen adsorption and thinking along when the results were unexpected. Fatemeh Hashemi and Dominik Benz are thanks for XPS measurements. Huo van Bui and Damiano LaZara are thank for making the TEM – images.

Also I would like to thank a few students I had the pleasure of working with. Jordi Alkemade, Thomas Upcraft, Jeanine Frijns, Okker van Batenburg and Thomas Hardens thank you all for your input, thoughts, ideas and hard work.

Mojgan Talebi and Aris Goulas are thanked for their help with the ALD set ups I had to use and their willingness to share their experience and expertise on the set ups.

Tonny Schuit and the SBD are thanked for their input, view and expertise on working safely in conventional and radiological laboratories, respectively. That can be an ungrateful job at times.

Late Thea van Meerten is thanked for her explanation on how to use the specialised INAA-Ge detectors. Folkert Geurink, thank you for installing and explaining the software belonging to those Ge-detectors.

Baukje Terpsta, Astrid van der Meer, Adrie Laan and the HOR-operators are thanked for the many irradiations they carried out and had to pick up for me and my students.

Yvonne, Elly and Anouk, thank you for your kind words. I do not know how you do it, but you always somehow managed to get me an appointment with my three supervisors at the same time and at the same place despite their overflowing agendas.

Furthermore, I would like to thank Ruud van Ommen, Bert Wolterbeek and Antonia Denkova for allowing me this wonderful experience. I have learned a lot. I know I am not the average PhD-student, so thank you very much for your patients and guidance throughout the project.

Not only on a professional level I had help, also on the more personal level people deserve a thank you. Jose Buurman, thank you for your kind words. Information from physicians can only take you so far. Sometimes you just need someone with personal experience to tell you it is not the end of the world. Thank you Paul. I know I have not been the easiest person during the cause of the project to live with. Thank you for enduring me during my rants when things did not go as planned or hoped. Thank you for holding up the mirror, even though I did not always appreciate that.

To the people I forgot to mention, thank you as well. I have met a lot of people during the course of this project, and with my track record of forgetting names it does not mean I did not appreciate your kind words, friendly advice or help, I just misplaced your name in my head.

Curriculum Vitae

Josette Moret (3 July 1990, Zoetermeer, the Netherlands) got her BSc degree in Molecular Science and Technology at Technical University Delft in August 2012, after which she continued for her MSc degree in Chemical Engineering at Technical university Delft specialising in Nuclear Science and Engineering. This degree she received in August 2013. After a brief period working as a researcher, she started her PhD on the development of a high specific activity radionuclide generator in April 2014 as a joint project between Product and Process design, Technical university Delft and Applied radiation and Isotopes, Technical University Delft. Currently, she is working as radiological health expert at the Reactor Instituut Delft.

List of publications

Research articles

J.L.T.M. Moret, M.B.E. Griffiths, J.E.B.M. Frijns, B.E. Terpstra, H.T. Wolterbeek, S.T. Barry, A.G. Denkova, J.R. van Ommen; Journal of Vacuum Technology A **38**, 022414 (2020); https://doi.org/10.1116/1.513444

J.L.T.M. Moret, T.A. Hardens, O. van Batenburg, H.T. Wolterbeek, J.R. van Ommen, A.G. Denkova; Applied Radiation and Isotopes **160**; 109135 (2020); https://doi.org/10.1016/j.apradiso.2020.109135

Poster presentations

J.L.T.M. Moret, J.R. van Ommen, E. Oehlke, H.T. Wolterbeek, A.G. Denkova; Coating of high-surface area particles for medical applications, Separation of (chemically alike) isotopes; NPS 14 Utrecht

J.L.T.M. Moret, J. Alkemade, H.T. Wolterbeek, J.R. van Ommen, A.G. Denkova, E. Oehlke; Nano-structures as novel sorbent materials for radionuclide generators; Trace 'N Treat; Lisboa 2014

J.L.T.M. Moret, B.E. Terpstra, H.T. Wolterbeek, A.G. Denkova, J.R. van Ommen; Materials for nuclear medicine by atomic layer deposition; DPTI Rotterdam 2016

J.L.T.M. Moret, M. Griffiths, B.E. Terpstra, H.T. Wolterbeek, J.R. van Ommen, A.G. Denkova; Development of a radionuclide generator; NKRV Petten 2 June 2017

Oral presentations

J.L.T.M. Moret, B.E. Terpstra, H.T. Wolterbeek, A.G. Denkova, J.R. van Ommen; Lutetium nano-structures deposited using ALD; ALD2016 26 July 2016 Dublin

J.L.T.M. Moret, V. Garcia Cruz, J. Alkemade, E. Oehlke, H.T. Wolterbeek, J.R. van Ommen, A.G. Denkova; Nano-structures as possible sorbent materials for radionuclide generators; NRC9; 2 September 2016; Helsinki

J.L.T.M. Moret, B.E. Terpstra, H.V. Bui, R.M. de Kruijf, H.T. Wolterbeek, J.R. van Ommen, A.G. Denkova; Atomic layer deposition to aid the production of radionuclides having high specific activity; INCC 2017; 30 August 2017; Gothenburg